Development of a Protocol to Determine the Sorting Potential of Particulate Ore Material

By

Michael Graeme Duncan
B.Sc. Honours Geology (University of Johannesburg)

Thesis Presented for the Degree of
MASTER OF SCIENCE IN ENGINEERING

Department of Chemical Engineering
University of Cape Town
May 2016

Acknowledgments

I would like to thank my supervisor, Dave Deglon, for his support and guidance throughout the research.

I would like to thank the following institutions and people:

- Anglo American, for funding the research.
- Rados and Tomra for the ore sorting sensor response data.
- JKMRC for the assistance with the XMT analyses and data processing.
- My colleagues at Anglo American Technical Solutions who assisted with the research.
- My family, friends and girlfriend for their support.

Declaration

I know the meaning of plagiarism and declare that all the work in the document, save for that which is properly acknowledged, is my own.

_____

Michael Graeme Duncan

15 February 2016

Abstract

The objective of this research was to develop a protocol/ methodology to determine the potential for an ore to be sorted using sensor-based sorting. The research builds upon previous methodologies in literature to determine ore sortability. The first attempt to create a standard methodology to assess the amenability of an ore to sorting at a pilot-scale was developed by Fitzpatrick (2008). Tong (2012) developed a methodology to assess the amenability of an ore to sensor-based sorting on an ideal laboratory-scale. These methodologies focus on determining the upgrading potential of an ore based on ore sorting amenability tests. In order to gain further acceptance of sorting technology in the mining industry, Lessard *et al.* (2015) developed a method to determine the impact of ore sorting on an operation from an economic perspective.

The protocol, developed during the current research, is used to determine the potential ore sortability based, firstly, on intrinsic particle properties and, secondly, based on laboratory-scale sensor sortability tests using ideal and industrial sensor measurement parameters. The intrinsic sortability results represent the ideal/ best-case sortability if a perfect separator existed and are calculated based on particle-by-particle ore characterisation. Ore that is intrinsically sortable is further assessed based on ideal laboratory-scale sensor sortability tests using selected sensors. Ore sorting sensors that show potential based on the ideal sensor tests are further assessed by determining the sortability of the ore using sensor measurement parameters similar to those used on industrial-scale ore sorting machines.

At each stage of the protocol, the grade-recovery relationship is established based on the intrinsic/ measured particle properties. The grade-recovery results are used to determine the overall economic impact of implementing ore sorting on an operation based on plant throughput data and operational costs. The economic impact established in the protocol does not include the capital and operating expenditure required to implement ore sorting and is used to determine if there is any potential for sorting *i.e.* a positive economic impact indicates that there is potential. This provides

meaningful results to assist in the decision-making process as to whether or not to initiate further ore sorting test work. The protocol follows a stepwise process where the project only progresses to the next stage if the economic potential warrants it, therefore avoiding unnecessary test work.

The protocol was demonstrated using a case study from Anglo American's Los Bronces copper operation in Chile. The sample used for the case study is not representative of the Los Bronces ore as particles were hand-picked to incorporate a wide range of particle sizes and grades. Therefore the case study is used to demonstrate the protocol should a representative sample have been taken. The sorting duty identified was to remove hard, low-grade pebbles from the pebble crusher circuit allowing for increased throughput; the run-of-mine ore feed to the plant would increase to compensate for ore removed through sorting.

Ore characterisation was carried out using a statistically valid method to determine the surface grade of each pebble using the X-ray fluorescence technique. The intrinsic sortability results indicated that the ore had the potential to be sorted based on the positive economic impact for the operation. Sensors were selected for the laboratory-scale sensor amenability tests, including X-ray fluorescence (XRF), X-ray-transmission (XRT), near-infrared, electromagnetic and colour sensors, based on the geological descriptions of the Los Bronces ore. It was shown that the Los Bronces ore was amenable to sorting using the XRF and XRT sensors. The ideal laboratory-scale sensor sortability tests found that the ore had the potential for sorting using the XRF and, to a lesser extent, XRT sensor. The XRF sensor was selected for further investigation using industrial-scale measurement parameters. It was determined that the XRF sensor under industrial conditions would be ineffective for sorting as a net loss would be incurred for the operation if industrial-scale XRF sorting was to be implemented. Bulk sorting tests would therefore not be considered with the current sensor technology.

Future research should focus on improving the techniques, such as the XMT, available to characterise coarse (>10 mm) particles for the purpose of estimating ore sortability. Research into improving the sensitivity/ resolution of ore sorting sensors as well as the throughput of automated sorting machines will open up further opportunities to implement ore sorting.

Table of Contents

List of Figures

List of Tables

Chapter 1

Introduction

1.1 Background

Economically viable ore deposits form in the earth's crust when valuable minerals or elements are concentrated at accessible depths for extraction (Robb, 2005). The metals contained in these ore deposits are usually extracted using a combination of smelting (pyrometallurgy), solvent extraction (hydrometallurgy) and electrowinning (electrometallurgy). In order to make these processes profitable the minerals containing the valuable metals generally need to be enriched by physical separation through mineral processing operations (Wills *et al.*, 2006).

Mineral processing involves comminution (crushing and grinding), size classification and beneficiation of an ore to produce a portion enriched in value minerals (concentrate) and a discard containing mostly gangue minerals (tailings). The first stage of the process is comminution where particle size is reduced until sufficient liberation of value minerals from gangue is achieved. The fine grinding stage of comminution is generally the most costly stage in mineral processing accounting, on average, for ~40 % of the total energy costs for an operation (Lessard *et al.,* 2014). The ore then undergoes size classification to produce a feed with the correct particle size distribution for processing. Physical separation through various beneficiation techniques (flotation, magnetic separation *etc*.) is then carried out to produce a concentrate and tailings stream (Wills *et al.*, 2006).

Pre-concentration of ore material prior to fine grinding by separating barren/ or low grade material from ore is one of the means of optimizing energy consumption on an operation (Bamber, 2008). Commonly used pre-concentration techniques include hand sorting, size classification, gravity separation, dense medium separation, coarse flotation and automated sensor-based ore sorting. The current research focusses on pre-concentration using sensor-based ore sorting.

Sensor-based ore sorting uses electronic sensors to measure the physical properties of particles individually. Based on the sensor response, particles are either accepted into the concentrate or rejected into a waste stream. Commonly used ore sorting sensors include radiometric, X-ray transmission (XRT), X-ray fluorescence (XRF) near infrared (NIR), colour (CCD) and electromagnetic (EM) sensors (Tong, 2012). Ore sorting requires that the physical properties used to sort the ore correlate with the composition of the element/ or mineral of interest. A discernible difference between particles considered as value or gangue is also required for sorting and is referred to as the intrinsic heterogeneity of the ore. The higher the intrinsic heterogeneity between particles, the more likely it is that the ore can be sorted (Fitzpatrick, 2008). Sorting technologies are widely used in the recycling and food industries (Fitzpatrick, 2008) but has not been widely applied in hard-rock mining, with the exception of the diamond industry, due to the low throughput compared to typical stream throughputs in modern mineral processing operations. Improvements in computing power, resolution of detectors and sorter throughput has made sorting a more feasible option in the mining industry (Lessard *et al.*, 2015).

Ore separability in mineral processing is characterized by assessing the feed and products of laboratory-scale tests. Some of these standard tests include laboratory-scale batch flotation, sink-float analyses to assess separability based on gravity separation and Davis Tube tests to assess the potential for magnetic separation. Few attempts in literature to develop a standard methodology to assess the sortability of an ore for sensor-based sorting have been presented.

The first general methodology to assess the amenability of an ore to sorting at a pilot-scale was developed by Fitzpatrick (2008) using a multi-sensor approach (inductive and optical sensors). The methodology was validated using case studies from a nickel/ copper and an iron ore deposit. Tong (2012) developed a methodology to assess the amenability of an ore to sensor-based sorting on an ideal laboratory-scale as a means of assessing the ore sorting potential prior to pilot-scale test work. These studies focus on the upgrading potential of an ore using sorting. In order to gain further acceptance of sorting technology in the mining industry, Lessard *et al.* (2015) developed a method to determine the overall economic impact of ore sorting on an operation.

The objective of this study is to develop a protocol/ methodology for determining the sortability of an ore based on intrinsic particle properties as well as laboratory-scale

ore sorting sensor tests. The research includes two previous studies for assessing ore sortability by Fitzpatrick (2008) and Tong (2012).

The sortability will be established based on the economic impact of implementing sorting on an operation. The protocol will first determine the intrinsic sortability which is a measure of sorting potential if a perfect separator existed. Once it has been established that an ore is intrinsically sortable, further sortability test work, using multiple ore sorting sensors, can be carried out to assess the sorting potential using the methodologies present in literature (Tong, 2012; Fitzpatrick, 2008).

1.2 Introduction to the Los Bronces Case Study

The protocol to determine the sortability of an ore was developed using a case study from the Los Bronces copper operation owned by Anglo American, Chile. A description of the Los Bronces deposit is given in Section 2.1.

The sorting duty identified for the Los Bronces operation was the removal of hard, low-grade waste material from the pebble crusher stream in the comminution circuit (cf. Figure 1) at a cut-off grade of 0.4 % Cu. Removing these low-grade pebbles would enable the run-of-mine throughput to be increased thus increasing production. A set of one hundred Los Bronces SAG mill pebbles was selected for the case study from a previous ore sorting study conducted at Anglo American.

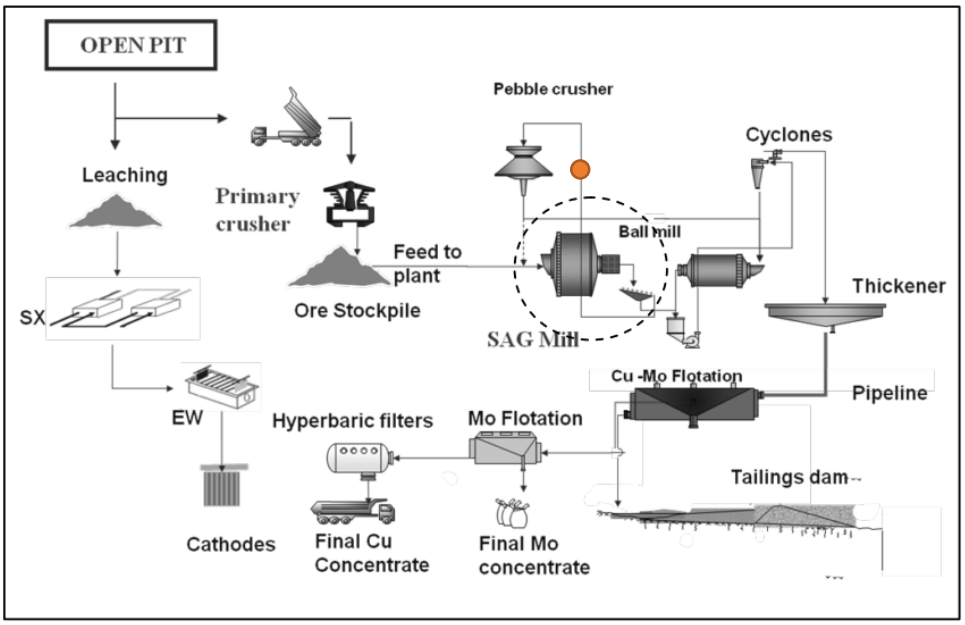

Figure 1: Flow diagram of the Los Bronces comminution circuit highlighting the stream identified for sorting (orange circle) (Agus, 2011).

1.3 Structure of Thesis

The thesis is divided into six chapters. Chapter 1 gives the background to the project, introduces the Los Bronces case study and discusses the scope and limitations. Chapter 2 presents a review of literature relevant to the current study as well as the research objectives. Chapter 3 presents the protocol methodology developed in this research. Chapter 4 details the materials and experimental methods that were used for the Los Bronces case study. Chapter 5 presents the results and discussion of the Los Bronces ore sorting case study. Chapter 6 provides conclusions and recommendations of the research.

1.4 Scope and Limitations

The Los Bronces case study was used to demonstrate the protocol developed during the current research and the results do not represent the actual sorting potential of the ore. Particles were hand-picked to incorporate a wide range of particle sizes and grades. Particles collected through hand-picking do not constitute a sample and are therefore not representative of the SAG-mill oversize screen material from Los Bronces.

The operational data used to determine the economic impact of sorting represents typical operational data from a copper operation similar to Los Bronces and does not reflect the actual economic potential for sorting of the Los Bronces ore.

The variability within an ore body may result in some sections being sortable whilst other sections not. The protocol was developed to determine the overall/ average sortability of an ore body.

Chapter 2

Literature Review

This chapter presents a review of the literature pertaining to the development of a protocol to determine ore sortability. The geology, mineralogy and metallurgy of the Los Bronces ore used as the case study is discussed in Section 2.1. Section 2.2 describes literature associated with sampling including particulate heterogeneity, Gy's Theory of Sampling and sampling for ore sorting amenability. Section 2.3 reviews the particle characterisation techniques applicable to this study as well as methods to statistically validate the characterisation data. Ore separation processes are discussed in Section 2.4 including gravity concentration, dense medium-, magnetic-, electrostatic separation, flotation and the section concludes with a detailed review of sensor-based ore sorting. The standard methodologies used in the characterisation of separation processes is described in Section 2.5 and concludes with a detailed review of methodologies present in literature to assess ore sortability. Section 2.6 summarises the reviewed literature and presents the research objectives and hypothesis.

2.1 Los Bronces Ore Geology, Mining and Processing

This section describes literature associated with the geology, mining and metallurgical processing of the Los Bronces copper porphyry deposit that will be used as a case study for the protocol development.

2.1.1 Los Bronces Copper Porphyry Deposit

The Los Bronces ore body is a brecciated copper porphyry deposit located ~69 km from Santiago, Chile as indicated in Figure 2. The geology is extensively described in literature by Warnaars (1985). The history of the Los Bronces deposit, geology, rock types and mineralogy as well as the mining and minerals processing of Los Bronces is described in a previous literature review by Dalm (2011).

The Los Bronces deposit comprises 7 breccia types as well as the host rock, quartz monzonite, that are extensively described by Warnaars (1985), a table of various characteristics of the breccia types is given in Table 1 and a geological map indicating the distribution of these breccias is presented in Figure 3.

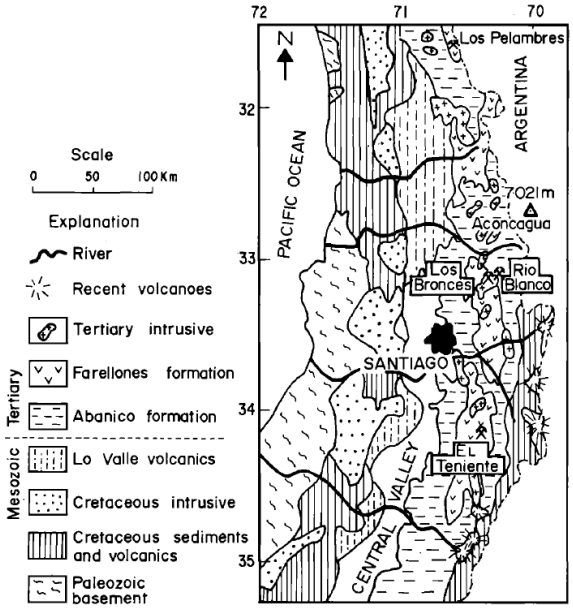

Figure 2: Simplified regional geological map indicating the position of the Los Bronces deposit (Warnaars, 1985).

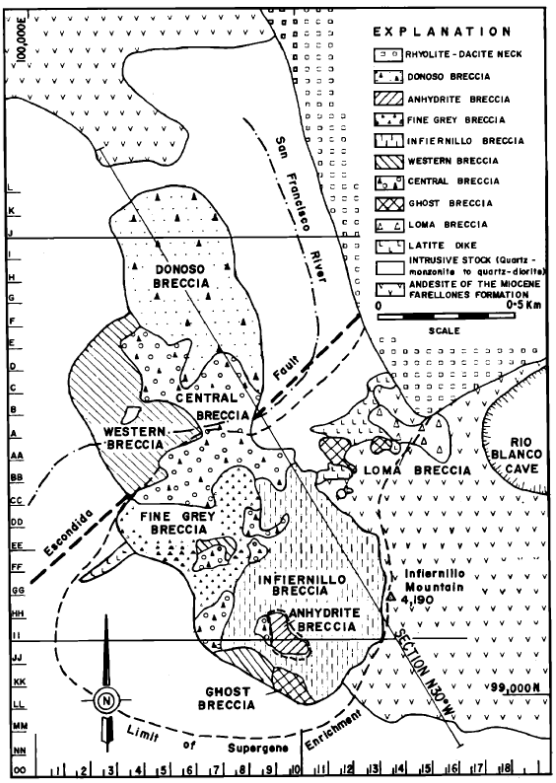

Figure 3: Geological map indicating the distribution of the breccia types at Los Bronces (Warnaars, 1985).

Table 1: Various characteristics of the breccias found at Los Bronces (Warnaars, 1985).

Breccia characteristic	Early tourmaline	Ghost	Central	Western	Infernillo	Anhydrite	Fine Grey	Donoso
Composition of matrix	tm, qtz	rfl, qtz, tm, spec, sulf	rfl, tm, spec, qtz, ser, sulf	rfl, chl, tm, ser, spec, sulf	qtz, chl, tm, spec, sulf	anh, tm, spec, qtz, sulf	qtz, rfl, ser, chl, spec, sulf	tm, spec, qtz, sulf, (rare rfl)
Percent matrix	5-15	5-30	15-90	10-30	5-15	5-60	10-40	5-25
Type of clast	QM	QM>SYE	QM (AND, SYE)	QM (AND)	AND > QM, LA	AND > QM	QM > AND, LA	QM (AND, SYE)
Alteration of clast	Strong silic	Weak to strong qtz-ser and chl	Strong qtz-ser and locally strong silic	Weak qtz-ser, strong chl	Strong chl, weak qtz-ser, mod-strong silic	Strong chl, mod silic	Strong qtz-ser, mod-strong silic	Weak to strong qtz-ser, strong chl
Size of clast (cm)	5-50	rfl-15	rfl-20	2-25	1-15			
Angularity of clasts	Angular and sub-rounded	Not definable	Sub rounded to sub angular	Sub angular	Angular to sub angular	Angular to sub angular	Sub angular	Angular to sub angular
Sulphide minerals (minor in parentheses)	Few (py, cpy)	py, cpy, cc, mo	py, cpy, cc, mo, (bn)	py, cpy, cc, mo, (bn)	py, cpy, cc, mo, (bn)	py, cpy, mo	py, cpy, cc	py, cpy, (cc, bn)
Approx. average grade of all drill hole intercepts %CuT/%MoT	?	?	0.74/0.024	0.66/0.024	0.86/0.025	0.47/0.051	1.08/0.025	0.92/0.008
Surface and subsurface area (m2)	Minor and erratic	24500	280000	160000	327000	16000	116000	297000
Contact relationship	Forms clasts in other breccias	Forms clasts in most other breccias	Forms clasts in most other breccias	Gradual contact with central bx	Contains clasts of central bx; at depth changes into Western bx	Contains Infernillo and Central bx clasts	Forms apophyses in Central and Western bx	Contains clasts of Ghost and Central bx

Abbreviations AND = andesite, anh = anhydrite, bn = bornite, bx = breccia, chl = chlorite, cc = chalcocite, cpy = chalcopyrite, LA = latite (porphyry), mo = molybdenite, mod = moderate, py = pyrite, QM = quartz monzonite, qtz = quartz, rfl = rock flour, ser = sericite, silic = silicification, spec = specularite, sulf = sulphide, SYE = syenite, tm = tourmaline

2.1.2 Los Bronces Mining and Processing

The Los Bronces mine is an open pit operation employing drilling and blasting mining techniques. Mining is not selective and the waste rock is removed to a separate waste dump.

The ore is separated into oxide and sulphide streams and these are processed separately. The oxide ore is transported to a leach bed where it is leached using sulphuric acid. Copper is concentrated using solvent extraction followed by electrowinning.

The sulphide ore is transported to the Los Bronces comminution circuit where it undergoes crushing and milling. After primary crushing, the ore is treated in two stages of milling, first through a semi-autogenous (SAG) mill followed by milling in a ball mill. Oversize pebbles from the SAG mill are redirected to a pebble crusher before being re-introduced into the SAG mill.

The resulting slurry from the comminution circuit goes through a thickener before being transported via a pipeline to the Las Tortolas flotation plant. The ore is first treated by flotation to produce a Cu-Mo concentrate. The Cu-Mo concentrate then undergoes further flotation to separate the material into a saleable Mo and Cu concentrates. The Mo concentrate is then sold to market. Some of the copper concentrate is sold directly to market whilst the rest is transported to Chagres smelter where Cu anodes and sulphuric acid are manufactured. A flow diagram of the operations at Los Bronces is presented in Figure 1 (Dalm *et al.*, 2014; Agus, 2011). As a result of using non-selective mining techniques, the ore comprises a large proportion of barren waste rock that dilutes the Cu grade.

2.2 Sampling

The first, and most important, step in any mineralogical or metallurgical test work is to collect a representative sample of the material of interest. Sampling involves removing a representative portion from a much larger mass of material that is referred to as the *lot*. The sample must represent the lot as accurately as possible to assure valid metal accounting as well as to assist in process control. Plant performance is assessed

based on the results of a few small samples, emphasising the importance of correct sampling (Afewu *et al.*, 1998).

Gy's Theory of Sampling as well as a method of sampling for ore sorting amenability are discussed in Sections 2.2.1 and 2.2.2 respectively.

2.2.1 Gy's Theory of Sampling

The Theory of Sampling (TOS), first developed by Pierre Gy (1979), describes all the theories and methods to quantify the different sampling errors encountered during the extraction of a sample of particulate material. Gy's theory is the only general theory of sampling and is well described in literature (Esbensen, 2004; Gerlach *et al.*, 2003; Lyman, 1986; Minkkinen, 2004).

The two categories of sampling errors are random and systematic errors. Random errors occur as a result of the intrinsic heterogeneity (IH) of the material. The random errors introduced as a result of particle heterogeneity are the fundamental sampling error (FSE), grouping/segregation error (GSE) as well as the in-situ nugget effect (NE). FSE cannot be eliminated but only minimized by decreasing particle size and/or increasing sample mass. Systematic errors (bias) are introduced due to poor physical sampling procedures where each particle does not have the same probability of being selected from a population (Lyman *et al.*, 2013).

Sampling errors are described in Section 2.2.1.1 whilst Gy's sampling equation is discussed in Section 2.2.1.2

2.2.1.1 Sampling Errors

This section describes the various random and systematic errors described by TOS as well as how to minimize or eliminate them. The various sampling errors are listed in Table 2 and described in Sections 2.2.1.1.1 to 2.2.1.1.4.

The total sampling error (TSE) when sampling particulate materials comprises three main categories: random errors, systematic errors as well as errors that comprise both random/systematic errors.

Table 2: Sampling errors (Assibey-bonsu, 1996; Minnitt et al.*, 2007a; Petersen* et al.*, 2005).*

	Error category	Sampling errors
Intrinsic errors	Random	In-situ nugget effect (NE)
	Random	Fundamental sampling error (FSE)
	Random	Grouping/segregation error (GSE)
Handling errors	Systematic	Delimitation errors (DE)
	Systematic	Extraction errors (EE)
	Systematic	Weighting errors (WE)
	Systematic/Random	Preparation errors (PE)
Analytical error	Systematic/Random	Analytical error (AE)
Processing errors	Systematic/Random	Short-range heterogeneity (SQE)
	Systematic/Random	Long-range heterogeneity (LQE)

Random errors are introduced as a result of the materials intrinsic heterogeneity and cannot be completely eliminated.

Systematic errors, or bias, are sampling errors generated from the process of sampling itself and are grouped into process, handling and analytical errors. The errors can be mostly eliminated by following correct sampling procedure (Assibey-bonsu, 1996; Minnitt *et al.,* 2007b; Petersen *et al.*, 2005). However, there is still a component of random error associated with SQE, LQE, AE and PE that cannot be completely eliminated. Figure 4 highlights the difference between random and systematic errors.

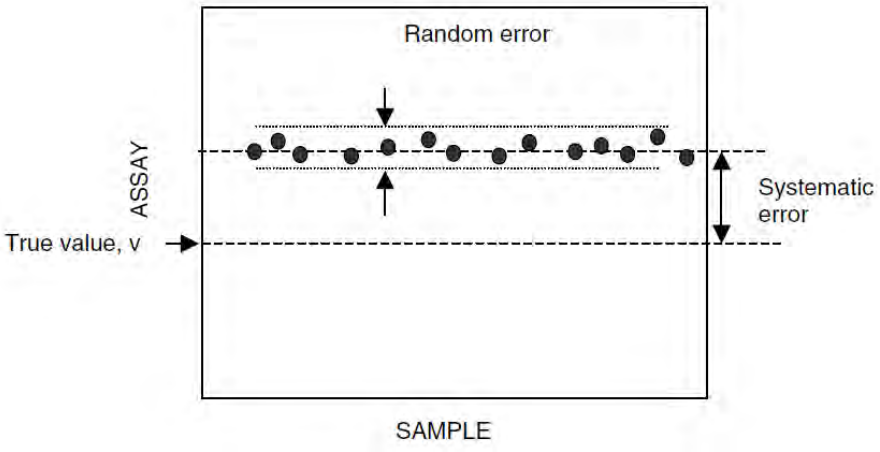

Figure 4: Random errors vs. systematic errors when sampling for chemical assay. The true value (v) represents the actual chemical composition of a material. Random errors are fluctuations in the composition of subsamples that are introduced due to the IH of the material. Systematic errors are deviations in composition away from the true value that are introduced as a result of incorrect sampling (Gupta, et al. *2006).*

2.2.1.1.1 Intrinsic Errors

Intrinsic sampling errors include the in-situ nugget effect (NE), the fundamental sampling error (FSE) as well as the grouping and segregation error (GSE). These errors are introduced when sampling as a result of the heterogeneity between particles in a population.

The NE is a geostatistical phenomenon where small-scale variations in grade are present across an ore body. This is often referred to as a “chaotic component” in literature (François-Bongarçon, 2004). Although the in-situ heterogeneity can relate to the particulate heterogeneity, there is no quantitative link between in-situ and particulate heterogeneity. Particulate heterogeneity is a function of its state of comminution (Lyman, 2012).

The FSE is an error that manifests as a result of the intrinsic heterogeneity of the material being sampled. The IH of particulate material is a measure of the variation in each particles intrinsic properties (grade, mass, density *etc.*) compared to the mean properties of the population. The degree of variation between the compositions of individual particles is directly proportional to the IH (Petersen *et al.*, 2005). It usually makes up the largest proportion of the total sampling error (TSE). FSE can only be minimized by increasing the sample mass or by comminution of the material. FSE generally decreases with a decrease in particle size (Lyman *et al.*, 2013; Petersen *et al.*, 2005; Gy, 1995).

The grouping and segregation error (GSE) is introduced when sampling as a result of distribution heterogeneity (DH) in a population of particles. DH occurs when particles of varying density and/or size become segregated or stratified into regions of varying density and/or size. Thorough mixing of the lot prior to sampling helps to minimize the grouping and segregation error (Petersen *et al.*, 2005).

The GSE occurs as a result of the combination of material heterogeneity and the sampling process. Particulate ore material is complex and the differences between high and low grade particles are subtle thus the heterogeneity is generally lower. This presents a unique challenge in upgrading complex particulate ores unless a high degree of liberation is achievable.

2.2.1.1.2 Process Errors

Processing errors are introduced due to quality variations in the ore stream and are termed short-term quality errors (SQE) or long-term quality errors (LQE). An example of SQE is sampling material from a conveyer belt where mass and/or grade have periodic fluctuations referred to as short-range heterogeneity. The second type is caused by changes in grade of the material being sampled over the life-of-mine called long-range heterogeneity (Petersen *et al.*, 2005).

2.2.1.1.3 Handling Errors

Handling errors are introduced during physical extraction and/or sample preparation. The handling errors include the delimitation, extraction, weighting and preparation errors (Petersen *et al.*, 2005).

Figure 5 describes sample delimitation and extraction. The delimitation error is introduced due to poor sample cutter design and/or the incorrect operation of the sample cutter. As a result the geometrically delimited sample increment differs from the actual sample shape. The extraction error occurs when particles within/ or on the edge of the correctly delimited sample increment are not correctly extracted to the sample. The 'centre of gravity' rule applies to the particles that lie on the edge of the delimited sample increment. The rule states that particles should be retained in the final sample if their centre of gravity lies within the delimited sample increment.

The weighting error occurs due to the sampling increments having different masses as a result of flow rate fluctuations. The error is introduced when calculating the mean of quality characteristics (*e.g.* grade) of the lot without considering the differences in sample mass. The error can be eliminated by either stabilising the flow rate or to calculate a weighted mean of the quality characteristics (Petersen *et al.*, 2005).

The sample preparation error (PE) is introduced after the sample has been extracted due to human error, spillage, loss of material that adheres to packaging *etc.* Strict control of sample preparation procedures is the only way to minimize these errors as they cannot be statistically determined (Petersen *et al.*, 2005).

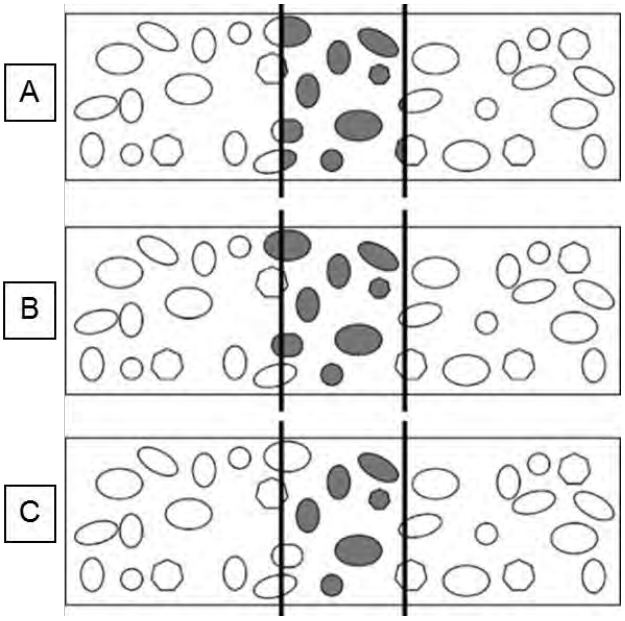

Figure 5: Schematic illustration of a cross stream sampler. (A) Indicates a correctly delimited sample increment, particles whose centre of gravity lie within the delimited sampling increment must be retained in the sample. (B) Shows the correct extraction of particles in the sampling increment (grey particles) to the sample. (C) Incorrectly extracted sampling increment where particles on the edge of the delimited sampling increment are not retained in the sample (Petersen et al., 2005).

2.2.1.1.4 Analytical Errors

Analytical techniques, such as chemical assaying, require a small portion of sampled material for analysis. The aliquot is extracted using appropriate size-mass reduction procedures to minimize the sampling error (cf. Figure 6). If aliquots of the same material are identically prepared and analysed for chemical composition, the results may still differ from one sample to the next. This difference between the repeat results is the analytical error. Analytical errors comprise systematic and random errors that are described as accuracy and precision respectively.

The precision is influenced by random fluctuations about the mean and are introduced as a result of the intrinsic heterogeneity of the material *i.e.* the fundamental sampling error as described in Section 2.2.1.1.1. The material undergoes a considerable amount of size reduction before analytical analysis, usually down to 80 % passing 75 µm, to minimize the FSE.

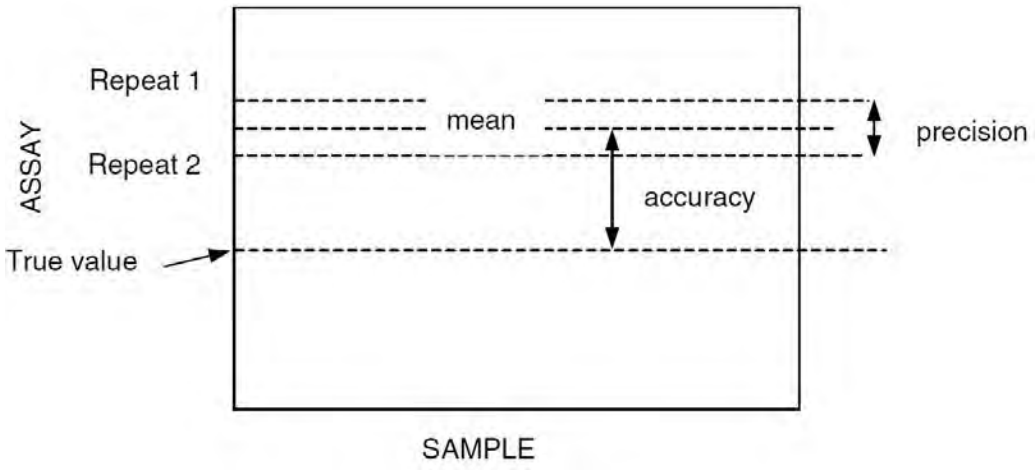

Figure 6: Accuracy and precision for assaying of repeat samples (Gupta, et al. *2006).*

The accuracy is the difference between the average assay results and the true value for a sample and is introduced by the analytical instrument. For instance, if an instrument has not been calibrated correctly then all of the repeat aliquots for a single sample will deviate from the true value.

TSE is generally much greater than analytical error (AE) as modern assay laboratories have strict quality control/quality assurance (QA/QC) procedures (Petersen *et al.*, 2005; AMIRA P754, 2007).

2.2.1.2 Gy's Sampling Equation

Gy's equation (Equation 1) can be used to determine the minimum sample mass required at a specific confidence and *vice versa.* Gy's sampling equation is used to determine the variance on the fundamental error (σ^2_{FE}).

$$\sigma^2{}_{FE} = \frac{K d_N^{\alpha}}{M_S} \qquad [1]$$

The components of σ^2_{FE} are the sampling constant *(K)*, the nominal top size *(d_N)* with its exponent (α) and the sample mass *(M_s)*. The exponent α was originally a cubic function as proposed by Gy but empirical work carried out around α led to the realisation that the exponent on the nominal top size was dependent on the ore type

and must be calibrated in order to decouple the sampling constant from the nominal top size (Minnit *et al.*, 2007b).

More recently, a 'sampling constant' computer programme was developed to automatically calculate the components of Gy's equation based on mineralogical data collected from mineralogical techniques that are reviewed in Section 2.3.1. The results from the programme are automatically reported into a spread sheet including a sampling nomogram as presented in Figure 9 (Lyman *et al.*, 2013).

The two components that must be calibrated in order to use Gy's sampling equation are K and *α.*The sampling tree experiment, the 100 particle heterogeneity test and a technique to determine the sampling constant based on intrinsic particle properties are described in Sections 2.2.1.2.1 to 2.2.2.1.3.

2.2.1.2.1 Sampling Tree Experiment

An approach to estimating K and *α* is presented in literature as the sampling tree experiment (or duplicate series analysis). The procedure involves collecting a sample of run-of-mine ore and crushing it into progressively finer portions (generally 4 nominal top sizes). Each nominal top size is split into 32 sub-samples and the entire series of all 4 top sizes is chemically analysed to determine the relative variance per series for the elements of interest. Equation 2 is derived from Equation 1 to produce a linear function and is used to plot the calibration line for K and α. The values for $Ln(\sigma^2 x M_S)$ and $Ln(D_N)$ for each series are calculated and plotted as in Figure 7. The slope of the line is α and the intercept at the Y-axis determines Ln(K) (Minnitt *et al.*, 2010; Minnitt *et al.*, 2007b).

$$Ln\left(\sigma^2 \times M_s\right) = \alpha Ln(d_N) + Ln(K) \quad [2]$$

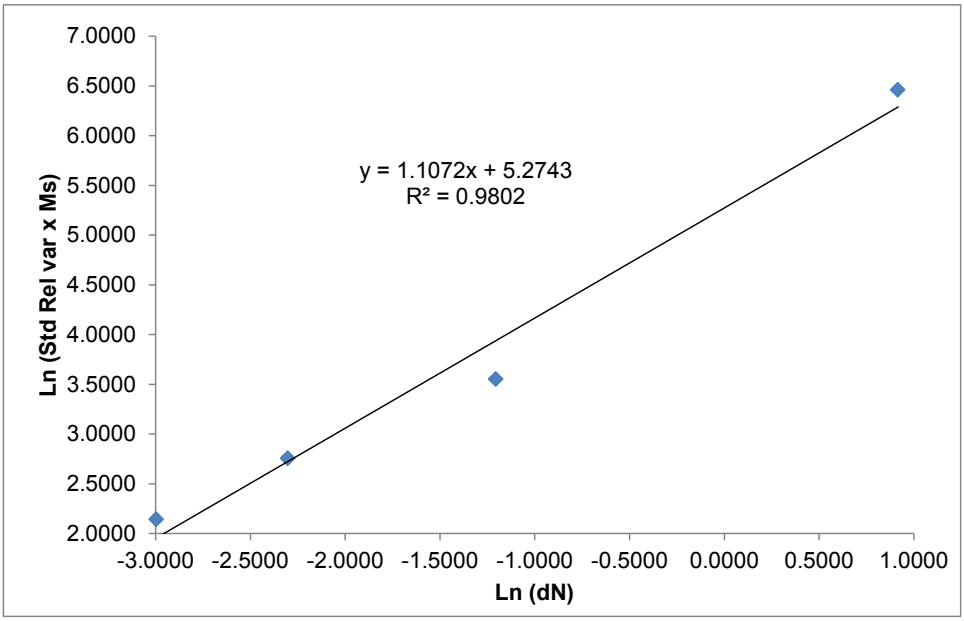

Figure 7: Calibration curve for K and α (Minnitt et. al.*, 2007b).*

Once K and α are known for an ore, based on the sampling tree experiment, they can be used to design a sampling protocol with the use of the sampling nomogram that plots the standard relative variance *vs.* sample mass. The nomogram is used to design a sampling protocol where size and/or mass reductions can be plotted to ensure that they lie within a certain confidence interval (c.f. Figure 8).

The mineralogical characterisation of particulates requires that the particle size is not altered during the sampling of the material under investigation. A sampling nomogram can be plotted, as in the example from Lyman *et al.,* (2013) (c.f. Figure 9), to determine the minimum sample mass required for mineralogical analysis. Size reduction cannot be used in the sample preparation. This is to preserve the mineralogical texture.

Gy's equation relates the variance on the fundamental error directly with the material fragment size and inversely with the sample mass. The variance on the fundamental error decreases with an increase in sample mass and increases with an increase in particle size.

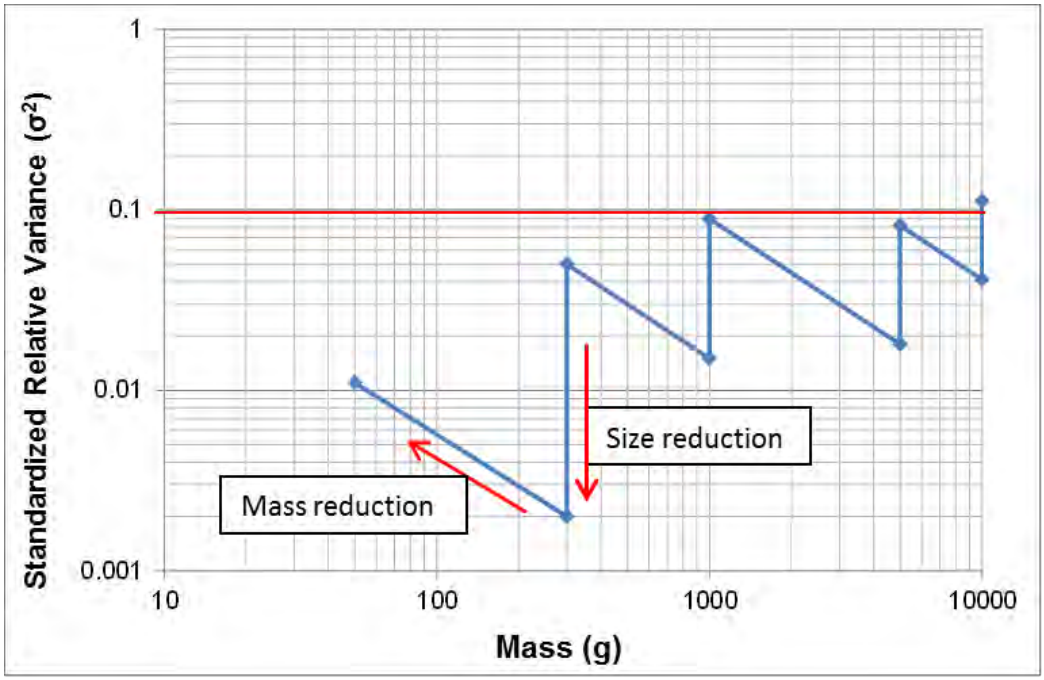

Figure 8: Sampling nomogram for size mass-reduction sampling (Minnitt et al., *2007b).*

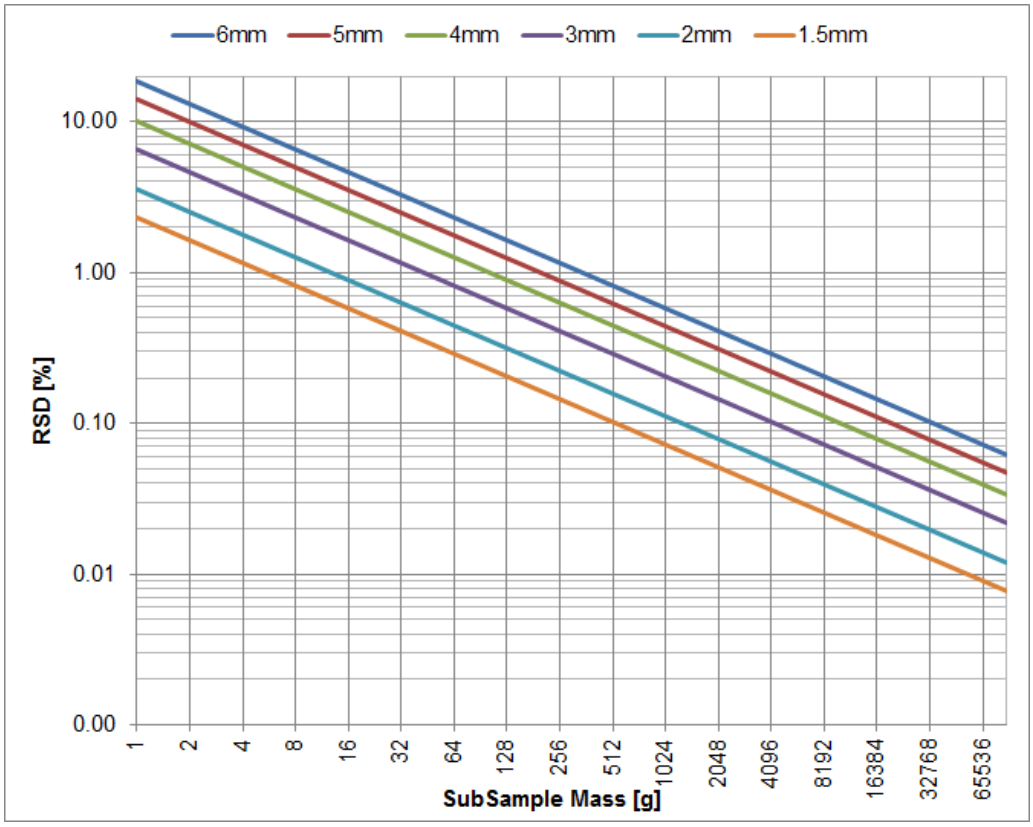

Figure 9: Sampling nomogram for a fine grained sample analysed on QEMSCAN (Lyman et al.*, 2013).*

2.2.1.2.2 100 Particle Heterogeneity Test

The 100 particle heterogeneity test can be used to determine the sampling constant which in turn can be used to determine σ^2_{FE} using Gy's sampling equation. The exponent on the nominal top size α, as presented in Equation 1, is not estimated using this technique and therefore a cubic function is used in place of α as Gy first proposed. Equation 3 is used to calculate the sampling constant based on the particle properties of 100 particles.

$$K = fgcl \quad [3]$$

The shape factor *f* is the deviation of the shape of particles from a cube. A cube has a shape factor of *f*=1 and needle-like grains have a value of *f*=~0.1. Practically, the shape factor lies between 0.2 and 0.5 and a value of 0.5 is generally used (Minnitt *et. al.*, 2007a). The granulometric or size distribution factor *g* is the average particle volume divided by the nominal particle volume. The ratio of metal density to the grade of the lot is known as the mineralogical composition factor *c*. The liberation factor *l* is a number between 0 and 1 where a liberation factor of 0 is indicative of no liberation and a liberation factor of 1 demonstrates complete liberation, (R. C. A. Minnitt et al., 2007a).

The 100 piece heterogeneity test has its limitations as the number of samples used may not be representative. For example, the heterogeneity may be completely incorrect in a veined deposit where the chances of sampling adequate veined material are low (Lyman, 2012). The incorrect estimation of the components in Equation 4 has a dramatic effect on the sampling variance (Geelhoed, 2011; Lyman *et al.* 2013).

2.2.1.2.3 Determining K Based on Intrinsic Particle Properties

A methodology to determine the sampling constant based on intrinsic particle properties was developed by Lyman and Schouwstra (2011). This methodology is also described in AMIRA P754 (2007). Herein, the sample population is divided into size (Ns) and composition (Nc) classes as shown in Figure 10. The variance on the IH is equal to the sampling constant (K_S) divided by the sample mass (M_s) (cf. Equation 4). The sampling constant K_S is a measure of the materials intrinsic heterogeneity and is

determined on an overall and size-by-size basis using Equation 5. The sampling constant can be calculated for individual elements or minerals of interest on a size-by-size and overall basis.

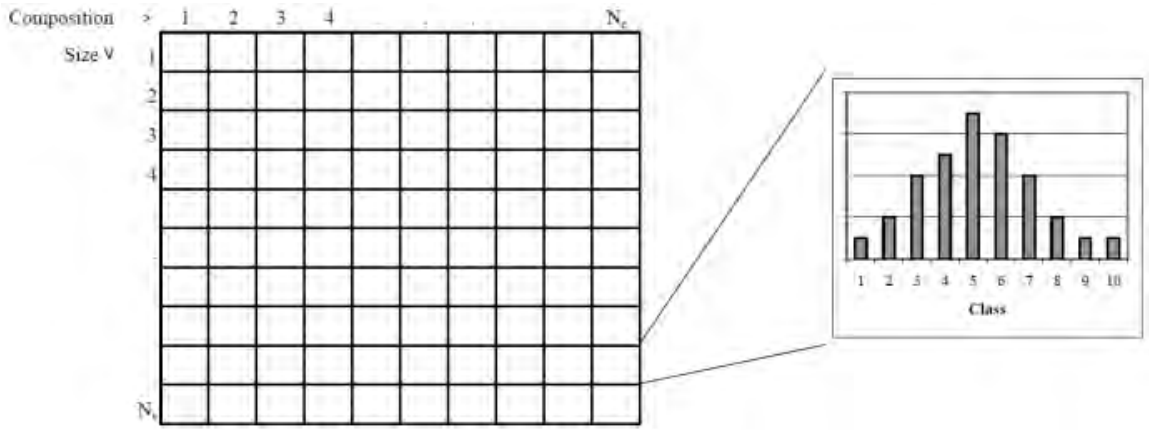

Figure 10: Size and composition classes used to determine the sampling constant (AMIRA P754, 2007).

$$Var\left\{\frac{a_S}{a_L}\right\}_{IH} = \frac{K_s}{M_S} \quad [4]$$

where

$$K_s = \sum_{i=1}^{N_s} X_i V_i \sum_{j=1}^{N_c} Y_{ij} \rho_{ij} \left(\frac{a_{ij} - a_L}{a_L}\right)^2 \quad [5]$$

Where:

X_i = mass fraction of particles in i^{th} size fraction

V_i = mean particle volume in i^{th} size fraction

γ_{ij} = mass fraction of particles in j^{th} composition class within i^{th} size fraction

ρ_{ij} = mean particle density in j^{th} composition class within the i^{th} size fraction

a_{ij} = analyte content in j^{th} composition class within $^{the\ ith}$ size fraction

as = analyte content in the sample as a whole

The use of this methodology requires the mineralogical composition of a large number of particles across closely spaced screen fractions in order to be valid. The method is useful when particle-by-particle mineralogical data is available.

2.2.2 Sampling for Ore Sorting Amenability

When determining the amenability of an ore to different electronic ore sorting sensors, the results of the test work should be completed within a reasonable turnaround time.

The numbers of particles required as well as the duration of data collection for each particle are the two factors contributing to the time taken to collect data for ore sorting amenability. The sample for the amenability test work should only be large enough to include all of the identifiable rock types in the material under investigation to minimize time taken to complete the test work (Fitzpatrick, 2008).

As ore sorting requires that the material to be sorted is as coarse as possible, some of the more commonly used sampling techniques, such as Gy's sampling equation, may result in an exorbitantly high number of particles required for a sample to be representative. It may not be practically possible to use Gy's equation in some cases depending on the ore type, nominal top size and confidence level required for amenability test work. However, to determine the economic impact of beneficiation for an ore stream, the sample mass determined by Gy's equation should be used.

The method by Fitzpatrick (2008) uses binomial distribution to calculate the probability of a number of successes in a sequence of independent events i.e. the probability of a particle being accepted or rejected into the sample during individual sampling events as described by Equation 6.

$$P(r) = \binom{n}{r} (p)^r (1-p)^{n-r} \quad \text{for } x = 0, 1, 2 \ldots n \qquad [6]$$

Probability of *r* successful outcomes in a sequence of *n* individual events is a factor of the probability (*p*) of succeeding *r* times and failing *n-r* times

Fitzpatrick (2008) decided the number of particles of the least abundant rock type should include at least 3 particles at 95 % confidence to calculate the number of particles (*n*) required to be collected. Figure 11 presents a log-log chart that was calculated using Equation 6 for a multitude of relative abundances and confidence intervals. The chart indicates how many particles are required to be randomly selected to obtain at least three particles of the least abundant rock type (Fitzpatrick, 2008).

In an example highlighting the differences in the sampling methods presented, Gy's equation was used to calculate the minimum sample mass required for a lead ore with a nominal top size of 25 mm to achieve a variance of 0.1 % at a confidence level of 99 %. The minimum mass required to achieve this would be 176.6 kg for the lead ore which equates to approximately 5400 particles. The sample preparation and analysis

time would be both too costly and time-consuming if *only* amenability is to be determined.

The method determines the minimum number of particles required at a certain confidence level using binomial distribution. The technique indicates that the number of randomly selected particles required to represent all the identifiable rock/particle types for the amenability test work is only 124 particles at a confidence level of 95 % for the Pb ore.

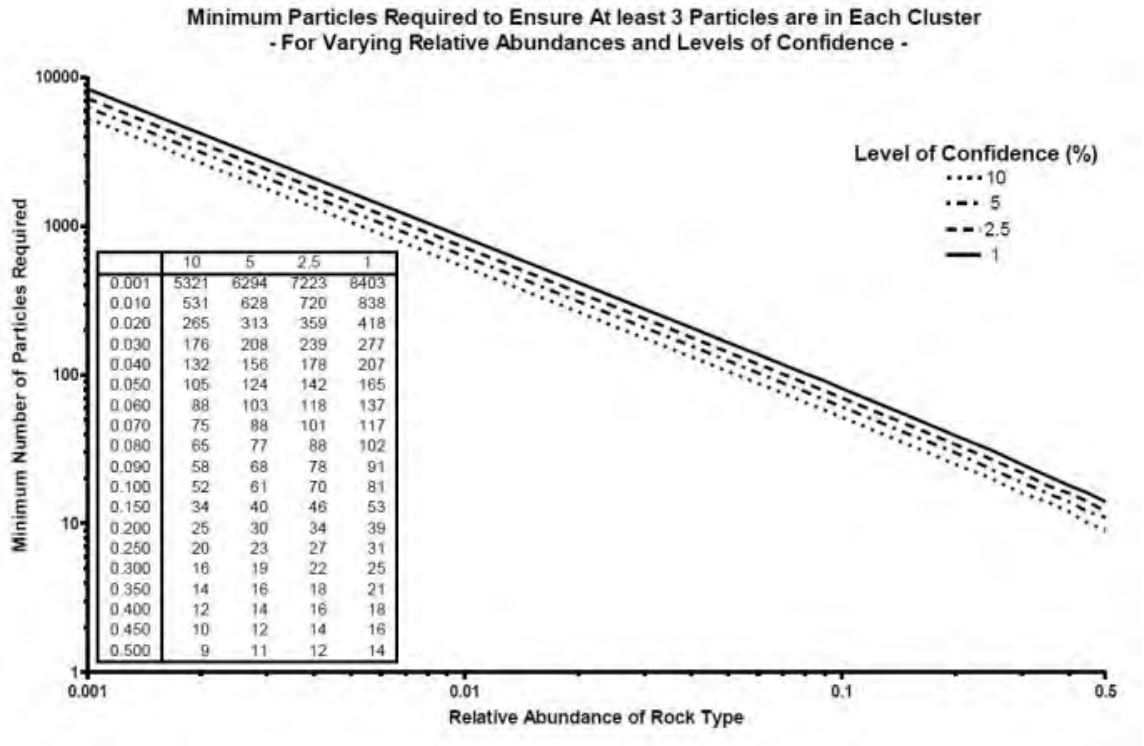

	10	5	2.5	1
0.001	5321	6294	7223	8403
0.010	531	628	720	838
0.020	265	313	359	418
0.030	176	208	239	277
0.040	132	156	178	207
0.050	105	124	142	165
0.060	88	103	118	137
0.070	75	88	101	117
0.080	65	77	88	102
0.090	58	68	78	91
0.100	52	61	70	81
0.150	34	40	46	53
0.200	25	30	34	39
0.250	20	23	27	31
0.300	16	19	22	25
0.350	14	16	18	21
0.400	12	14	16	18
0.450	10	12	14	16
0.500	9	11	12	14

Figure 11: Log-log chart of the minimum number of particles vs. the relative abundance of rock types at different confidence intervals (Fitzpatrick, 2008).

2.3 Ore Characterisation

The results of ore characterisation can be used to predict the beneficiation potential of an ore. The gangue and value minerals can be assessed in order to assist in deciding the best way to process an ore.

Ore characterisation can be accomplished by numerous techniques that are available. The rapid development of automated mineralogical techniques over the last twenty years has greatly improved the quality and turnaround time of mineralogical data (Schouwstra *et al.*, 2011). The focus of this section is to describe the mineralogical and chemical techniques available to characterise particulate ore material in the

context of this research including two-dimensional automated SEM-based systems (aSEM), X-ray Micro-tomography (XMT), hand-held X-ray fluorescence (XRF) and hyperspectral imaging. Recent advances in on-line ore characterisation are also reviewed.

2.3.1 Two-Dimensional aSEM Mineralogical Characterisation

The most frequently used techniques for mineralogical analysis are aSEM systems such as the Mineral Liberation Analyser (MLA) and QEMSCAN technique (Fandrich *et al.*, 2007; Hoal *et al.*, 2009; Pascoe *et al.*, 2007). The aSEM techniques analyse 2-dimensional polished sections of particulate samples; these techniques combine backscattered electron (BSE) images of the mineral grains with Energy-dispersive X-ray spectroscopy (EDS) information to produce mineral maps. The BSE images and EDS spectra collected from the sections are used to classify the minerals present by comparing them to a set of mineral standards. The use of XRD and chemical assay is employed to validate these results. Once the particles have been classified the resulting pixel information for each particle is extracted into a database. The database contains all the relevant pixel information used to calculate liberation, particle size, grain size, mineralogical composition, chemical composition, shape, association and density.

The aSEM techniques are well developed and can collect data from thousands of particles in a relatively short period of time. The advantage of the techniques is that X-rays can be collected directly from the sample during analysis and a high degree of automation is possible (Schouwstra *et al.*, 2011).

The drawback of using 2D particle section data is that liberation is almost always overestimated. Some form of stereological correction needs to be applied to the 2D data in order to get a better estimate of liberation (Miller *et al.*, 2009).

2.3.2 Three-Dimensional X-ray Tomography

X-rays have the ability to penetrate materials in varying degrees depending on the composition. This property is utilised extensively in medical and security applications to produce 2-dimensional radiographs or projections of internal structures of specimens. The 2-dimensional projections lose depth information making interpretation more challenging. A technique was developed in the 1970's called

Computerised Transverse Axial Tomography (CT) that could reconstruct 3-dimensional images by combining multiple projections of an object taken at different directions. Instruments were developed to automatically collect high resolution X-ray projections of specimens at multiple directions. XMT has the ability to produce projections with a resolution of less than one micron. An extensive review on X-ray tomography can be found in literature that discusses the history, principles and applications of the technology in geosciences (Cnudde *et al.*, 2013)

The XMT (cf. Figure 12) uses a cone-beam X-ray source that transmits X-rays through a sample. The X-rays lose energy as they move through the sample; the X-ray attenuation co-efficient determines how much energy is lost for different phases based on their average effective atomic mass. The attenuated X-rays are then converted to light energy using a scintillator screen. The light is then focussed using detector optics into the CCD camera to produce a single projection, the process is repeated until the sample has rotated through 360° at user defined intervals (Hsieh, 2012).

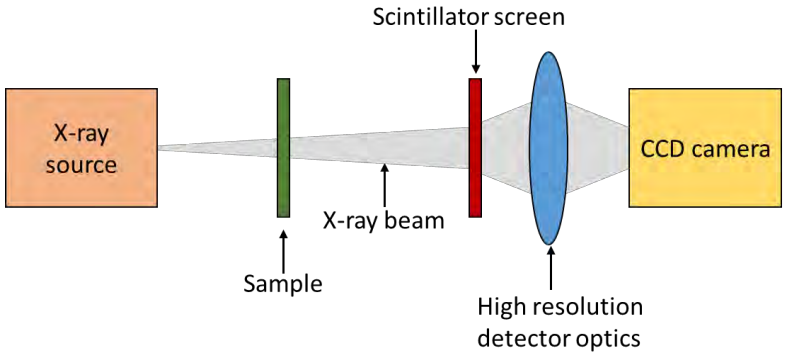

Figure 12: Components and layout used for high resolution X-ray micro-CT analysis (after Hsieh, 2012).

The advantage of XMT is that 3-dimensional images can be generated non-destructively. This allows multiple analyses of the same sample under different conditions (*e.g.* environmental changes, mechanical stress); even allowing the analysis of live specimens. Data that can be generated from the 3D volume include: ore component volume fractions, texture (surface/volumetric), particle/pore size and morphology to name a few.

The disadvantages of the technique include X-ray image noise, discretization effects, operator dependency and imaging artefacts. The obtainable resolution is directly proportional to the size of the sample. The resolution is represented by voxel size, features that are smaller than this voxel size cannot be fully resolved. Voxels at the

grain boundaries of minerals may not be fully resolved resulting in voxels of intermediate grey level between two phases. The accuracy of data analysis on reconstructed 3D volumes is therefore a function of the resolution.

A set of procedures and analysis techniques using high-resolution XMT is presented in a thesis by Hsieh (2012) and gives a comprehensive guide on the use of XMT for quantitative analysis including sampling, sample preparation, image analysis and data processing.

Mineralogical analysis can be carried out using XMT provided that there is sufficient contrast between the X-ray attenuation co-efficient of the minerals under investigation. Recently, the use of dual energy XMT (DE-XMT) has been used to increase the sensitivity of the technique to distinguish between minerals of similar atomic number (Ghorbani *et al.*, 2011). Samples are measured at low and high X-ray energies (kV). X-ray scattering occurs in two ways namely photoelectric and Compton scattering. The X-ray scattering at lower kV is dominated by photoelectric scattering and the higher kV by Compton scattering (Lin *et al.*, 2013). The resulting pixel information from the low and high kV analyses is combined to produce data with a higher contrast between phases with similar composition but different densities and *vice versa.*

2.3.3 Particle Surface Characterisation

Many of the ore sorting sensor technologies rely on surface analysis (XRF, NIR, and Colour sensors). Therefore, an important step is to assess the correlation between the surface grade and the total volumetric grade of each particle in a sample. The results will determine if the ore can be sorted based on surface properties (Tong, 2012). The literature associated with estimating the surface grade, including hand-held X-ray fluorescence and hyperspectral imaging, are discussed.

Many surface characterisation techniques exist for the analysis of particulate materials but the focus of this review is to assess surface characterisation techniques applicable to the current research on coarse particulate ore.

2.3.3.1 X-ray Fluorescence

X-ray fluorescence (XRF) works on the principle of beam interaction with a sample, effectively displacing electrons of fixed specific energies which are characteristic of

each element. It is a non-destructive technique, requiring little /no sample preparation. It provides bulk chemical real time analysis.

Previous estimates of surface grade of pebbles had used an average grade derived from 5 to 10 randomly selected points on each pebble (Tong, 2012). However, with a spot size of ~5 μm, this was not representative of the entire surface of the pebble. Measurement of the surface grade of any particulate is also complicated if the particle has irregular surfaces.

2.3.3.2 Hyperspectral Imaging

Hyperspectral imaging measures the reflectance of materials and classifies the information into very narrow bands of the electromagnetic spectrum (Agus, 2011).

The use of hyperspectral imaging (Gallie *et al.*, 2002) as well as thermal infra-red reflectance (Feng *et al.*, 2006) have been described in literature as a new way to determine the total sulphide content of broken ores. Results showed that the chalcopyrite grade could be determined at ±15 % chalcopyrite content at a 95 % confidence level. Further development is required to lower the errors in estimating chalcopyrite content based on hyperspectral imaging.

Agus (2011) mineralogically characterised pebbles generated from the SAG mill at Los Bronces using hyperspectral imaging focussing on the mica content. The study showed that the spatial distribution of minerals, including sulphides, can be characterized across a 2-dimensional section using hyperspectral imaging.

2.3.4 On-line Ore Characterisation

The use of on-line characterisation techniques to determine ore particle size distribution (PSD) has shown success using a machine vision approach. The technique captures grey-scale images of the particulates on conveyer belts and automatically calculates the PSD using image analysis software. It was noted that the position of the camera about the conveyor belt as well as the selection of size parameter, such as equivalent area diameter, had a major influence on the estimation of grain size (Al-Thyabat *et al.*, 2007; Tessier *et al.*, 2007).

Efforts towards estimating the on-line ore composition on conveyor belts is presented in literature. The approach uses colour images of ore particles and the colour and

textural features are used to identify different rock types; the abundance of each rock type is estimated based on the distribution within an image. The approach is limited by the position where images can be taken on a plant and the size and type of ore; there must also be a visual difference between rock types. Results may also be inaccurate if the ore is wet or dry when photographed; wet ore may reflect more light. The technique can be used to sort ore into different processing streams based on the abundance of different rock types. Softer ore can be separated and processed differently to harder ore types (Tessier *et al.*, 2007).

The use of magnetic resonance to determine the mineral phase concentration of copper ore has been investigated with the aim of producing rapid on-line ore characterisation to determine the composition of ore on conveyor belts. The technique uses Nuclear Quadrupole Resonance (NQR) or antiferromagnetic Nuclear Magnetic resonance (NMR) to estimate mineral abundance. Minerals are subjected to radio frequencies where the resulting echo is diagnostic of the mineral under excitation. The determination of copper mineralogy can be determined down to very low concentrations (~0.1%) depending on the size of the copper minerals (Bennett *et al.*, 2007, 2009). The technique has been used to determine the chalcopyrite content in rocks and slurries with compositions as low as 0.1%; the technique was validated using QXRD (Bennett *et al.*, 2009).

2.3.5 Statistical Validation

The data generated from the various mineralogical techniques can be used to estimate the error of the analysis. A statistical method based on bootstrap resampling can be used to determine if the number of particles measured is sufficient at a desired confidence level (Evans *et al.*, 2013). More particles can be analysed if the required confidence level is not achieved. The bootstrap resampling procedure is discussed in Section 2.3.5.1. Analytical methods to determine the complete sampling distribution have been published in literature in order to understand the heterogeneity of particulate material which is very useful if the particulate samples cannot be mineralogically studied *i.e.* too large for analysis. Mineralogical data by size can be used to determine the sampling distribution using bootstrapping (Lyman, 2014).

Another approach to determine the error based on the number of particles and proportion of mineral phase in question from polished section data is also discussed in Section 2.3.5.2 (Jones, 1987).

2.3.5.1 Bootstrap resampling

The mineralogical data determined from the techniques described in Section 2.3 need to be statistically validated. The use of a statistical validation tool based on bootstrap resampling can be used to determine the error of mineralogical data.

The technique involves resampling a population of mineral particles; *M* random subsets of *N* particles are taken from the population and the mean, variance and standard deviation is determined for the parameter of interest. The coefficient of variation (also referred to as the relative standard deviation (RSD)) is determined by dividing the standard deviation by the mean of the parameter of interest and multiplying it by 100. The lower the RSD, the more statistically valid the results will be (Evans *et al.*, 2013).

The statistical variation can be determined for a number of mineralogical characteristics. An example of a chart showing the coefficient of variation for chalcopyrite grain size *vs.* the area of particles measured is presented in Figure 13. The results can be used to determine whether more particles need to be collected and added to the data set in order to achieve the desired RSD using regression analysis.

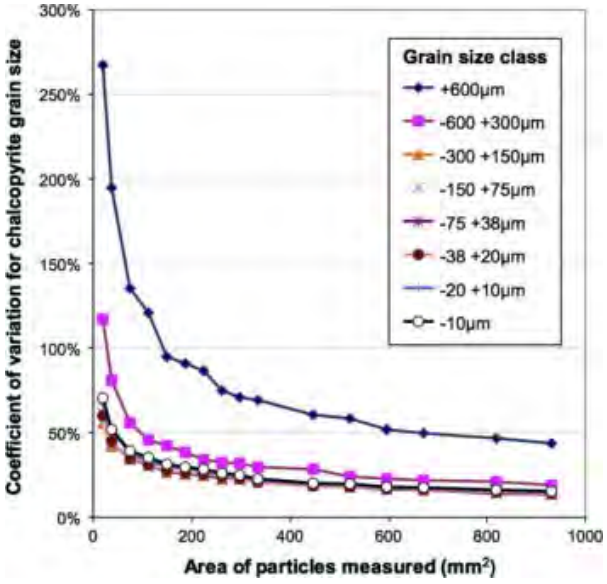

Figure 13: Relationship of the coefficient of variation vs. area of particles measured (Evans et al.*, 2013).*

A resampling spreadsheet created by Wood (2011) can be used to perform bootstrap resampling on any component of interest. The spread sheet is used to produce *M* random subsets of *N* particles taken from the population and the mean, variance and standard deviation is determined for the parameter of interest. The relative standard deviation when taking samples with different numbers of particles is plotted as presented in Figure 13 and a regression curve can be calculated. The slope of the curve can be used to predict the number of particles required to collect a representative data set.

2.3.5.2 Estimating error in mineral content

A statistical method to estimate the error in mineralogical data from polished sections was developed by Jones (1987). If the proportion of the mineral is known in the sample then the number of particles required to obtain a desired error can be determined. The absolute and relative error in mineral content is calculated using the formulae in Equation 7 and 8 respectively:

$$e = 2\sqrt{\frac{pq}{n}} \quad [7]$$

$$E = \frac{e}{p} \quad [8]$$

Where:

p = proportion of selected mineral

q = (1-p)

N = number of measured particles

e = absolute error

E = relative error

2.4 Separation Processes

This section describes the physical separation processes used in mineral processing including gravity concentration, dense medium-, magnetic- and electrostatic separation in Section 2.4.1. These physical separation techniques can be applied as pre-concentration techniques similarly to sensor-based ore sorting. The section concludes with a detailed review of electronic sensor-based ore sorting in Section

2.4.2. A summary of the various processing techniques available, as well as the ideal size range where the techniques can be applied, are presented in Figure 14 (Kelly *et al.,* 1982).

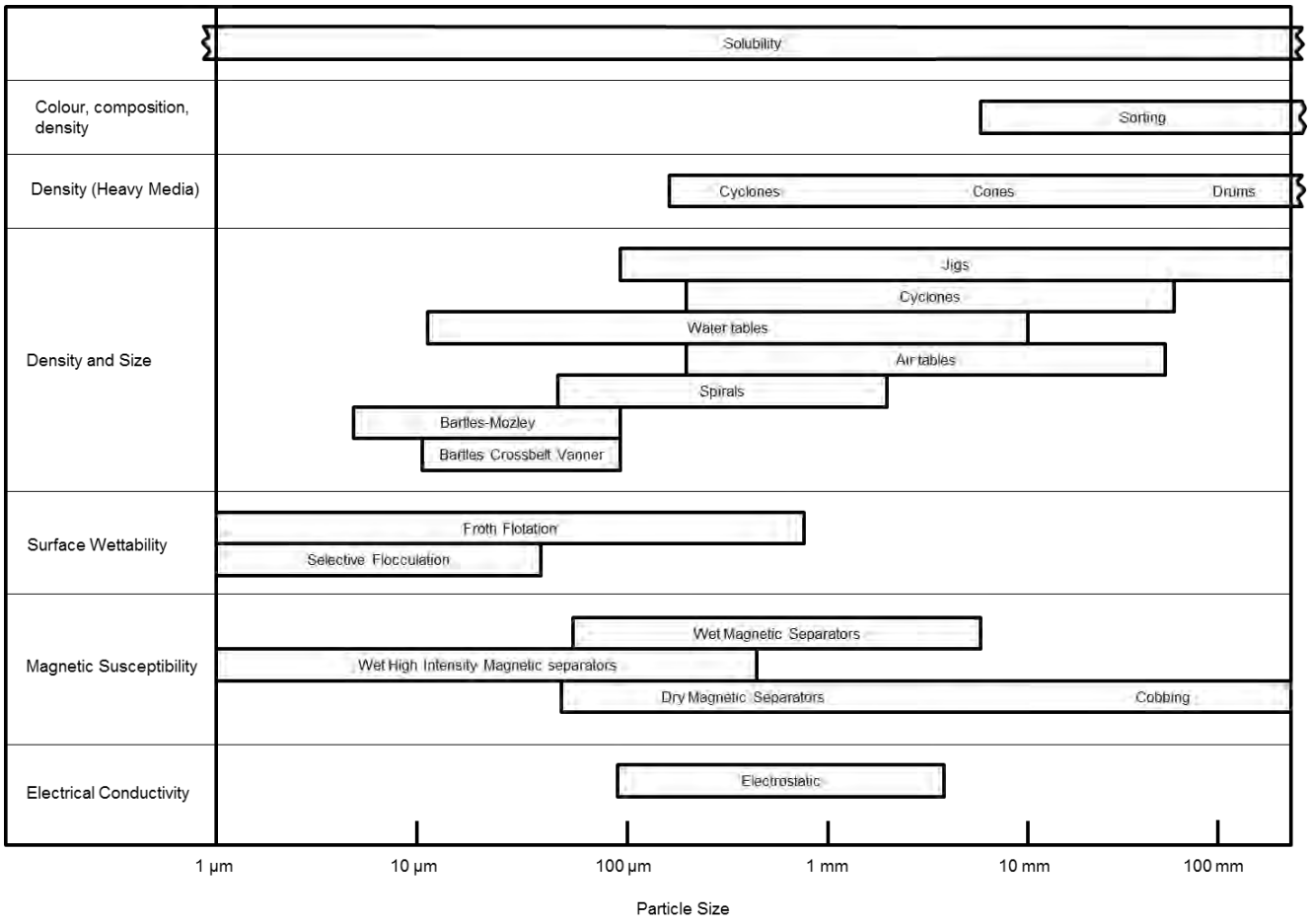

Figure 14: Separation techniques and their optimal size range (Kelly et al.*, 1982).*

2.4.1 Physical Separation Processes

Pre-concentration of ore is generally applied to particles above 1 mm in size and achieved through coarse physical separation processes as well as electronic sensor-based ore sorting. The physical separation processes that can be applied as a pre-concentration technique are discussed.

2.4.1.1 Gravity Concentration

Gravity separation is achieved due to the differences in density between particulates. This section describes the gravity separation processes where the separation medium is *less* dense than the material being processed. There are four main mechanisms that are used to separate particles by gravity concentration and at least two need to

be used in combination. The mechanisms include density, stratification, flowing film and horizontal shear (Burt, 1999).

Gravity separation works by separating particles from each other by an applied force and then allowing differential settling to occur to separate particles based on their density and size. Processes can be grouped into three categories based on the direction of the particle separation process. The categories include jigging (vertical motion), shaking concentration (horizontal motion) and flowing film concentrators (motion on an inclined surface). The medium used for gravity separation is most commonly water which is less dense than the material being sorted.

Not all ore types can be processed using gravity separation; one commonly used technique to assess the amenability of an ore to these processing techniques is the concentration criterion (CC). The CC is defined by Equation 9 where SG represents the specific gravity:

$$Concentration\ criterion = \frac{SG\ of\ heavymineral - SG\ of\ fluid}{SG\ of\ lightmineral - SG\ of\ fluid} \quad [9]$$

The concentration criterion for gravity separation for particulates of varying size is graphically presented in Figure 15 highlighting where gravity separation is possible.

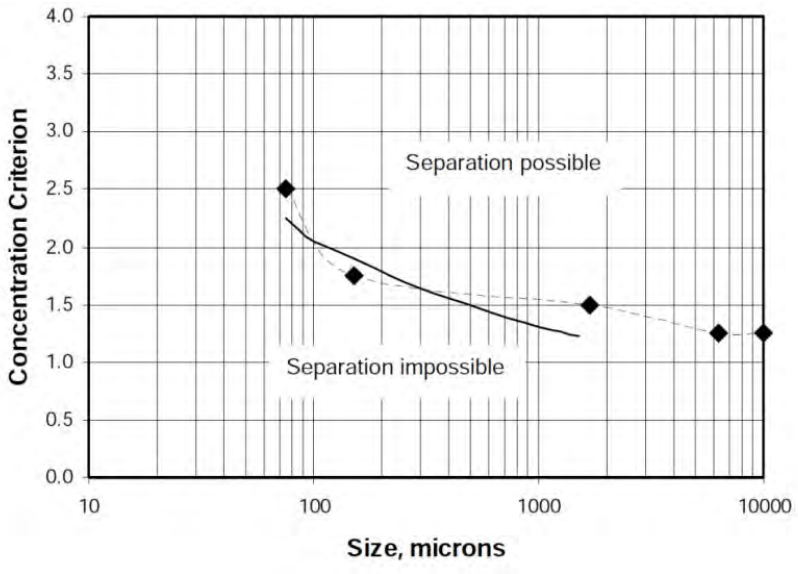

*Figure 15: Concentration criterion per vs. particle size (*Gupta et al., 2006*).*

The particle size and shape in all particulate ores are heterogeneous in nature and separation by gravity may not be possible and is highlighted in an example of a mixture of gold and arsenopyrite (FeAsS) which have SG values of 19.3 and 6.1 respectively is presented in Figure 16.

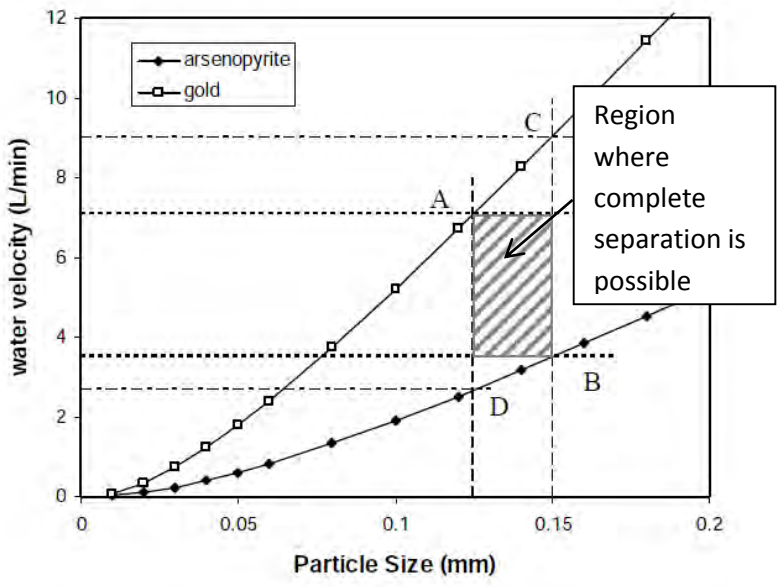

Figure 16: Settling curve for a mixture of pyrite and chalcopyrite where the CC is 1.275. A represents the intersection of the lower size and higher density curves and vice versa at B. Flow rates above C will results in all particles floating and below D where particles will all sink. Complete seperation is only possible in the highlighted region (Gupta et al*., 2006).*

2.4.1.1.1 Vertical Motion Separation (Jigging)

Jigging is the separation of particles based on their differences in acceleration of minerals in a moving fluid due to density differences between minerals (Wills, 2006).

The process involves moving water or air using a piston moving up and down in a vertical direction as indicated in Figure 17. Particle stratification initially occurs due to differential acceleration during the upward movement of the piston (pulsation). Particles then undergo hindered settling during the downward motion of the piston (suction). Consolidated trickling then allows the heavy finer particles to move down through the bed and concentrate below the light particles; the process is repeatedly continuously.

Jigging uses screens at the base of the particle bed to separate the material into heavy and light fractions as indicated in Figure 18. The light fraction is removed from above the screen whilst the heavy fraction sinks to the bottom of the jig. Ragging, which is made up of particles that are coarser than the screen apertures but less dense than the heavy particles are used to close off the screen to feed material prior to pulsation. The heavy particles sink below the ragging and through the screen during hindered settling ensuring efficient separation of heavy and light fractions (Gupta *et al.*, 2006).

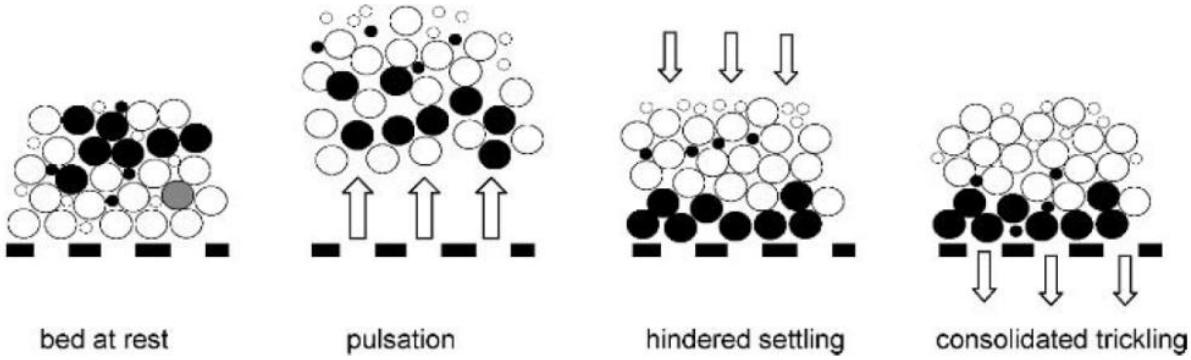

Figure 17: The process of jigging involves pulsation of the separation fluid (Gupta et al.*, 2006) .*

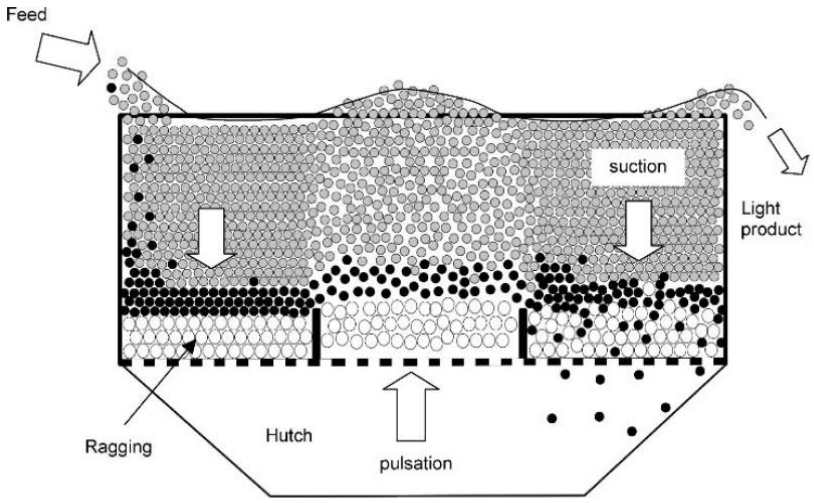

Figure 18: Cross section through a typical jig (Gupta et al.*, 2006).*

The types of jigs available and there applications is well documented in the literature (Gupta *et al.*, 2006; Wills *et al.*, 2006).

2.4.1.1.2 Horizontal Motion Separation

Horizontal motion separators subject particles in a flowing film to horizontal shaking. The particles are segregated based on differences in size and density to produce a light and heavy particle fraction as indicated in Figure 19.

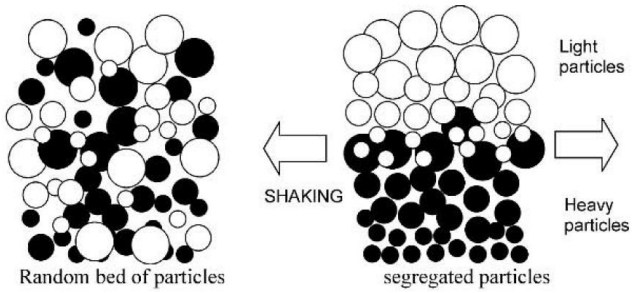

Figure 19: Segregation of particles due to horizontal motion (Gupta et al.*, 2006).*

Table separators, like the Wilfley table, use slightly inclined decks comprising riffles as indicated in Figure 20. Particles are segregated into light particle fractions on top of the particle bed and heavy particle fractions at the bottom. Lighter particles are washed over the riffles whilst heavy particles move along the table in the direction of the shaking.

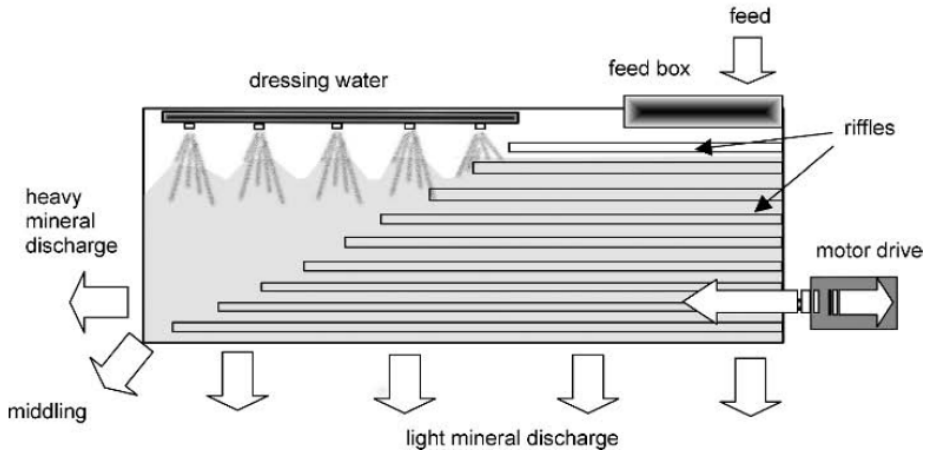

Figure 20: Basic design of shaking tables. Lighter particles are washed over the riffles leaving behind heavier particles. Heavy particles are conveyed down the table in the direction of the shaking (Gupta et al.*, 2006).*

2.4.1.1.3 Flowing Film Separation

Inclined surface or flowing film concentrators separate particles as they interact with a fluid flowing down a slope. In the case of sluicing, heavier particles settle to the bottom of the flowing fluid faster than the lighter particles. Heavy particles are trapped using either riffles or cloth whilst lighter particles are washed over the top as shown in Figure 21 (Gupta *et al.*, 2006).

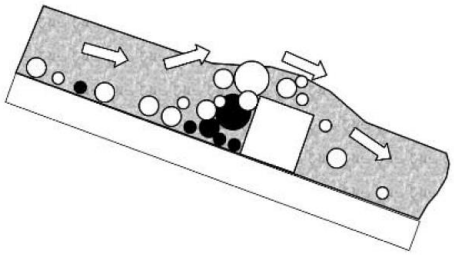

Figure 21: Basic operation of a sluice. Heavy particles are trapped behind riffles whilst lighter particles wash over (Gupta et al.*, 2006).*

2.4.1.2 Dense Medium Separation

Dense media separation (DMS) utilises a medium with a density that lies between the density of the light and heavy particles; light particles float and heavy particles sink.

The processes require that there is a sufficient difference between light and heavy particles *i.e.* sufficient intrinsic heterogeneity.

The use of dense organic compounds, on the industrial and laboratory scale, is on the decline due to the high toxicity (Burt, 1999) of the compounds and are therefore not mentioned in this review.

Dense medium separators aim to produce a float (light particle) and sink (heavy particle) product and the two main types include bath/trough (gravity DMS) separators as well as centrifugal separators.

Gravity DMS involves adding the feed as well as the separation medium into a vessel (drum or cone) producing sink and float product under the influence of gravity. The float fraction is removed by fluid flow out of the vessel with or without the assistance of paddles. Centrifugal DMS or cyclones are used to separate particles in a dense medium using an applied centrifugal force. Cyclones are used where separation of finer particles is required such as in the treatment of coal (Wills *et al.*, 2006).

2.4.1.3 Magnetic Separation

Magnetic separation has seen much success in the recycling of ferrous metals from non-ferrous and non-metallic material (Cui *et al.*, 2003). Magnetic separation has also been successfully utilised in the recycling of construction waste and waste electronic scrap (Cui *et al.*, 2003; Huang *et al.*, 2002).

Magnetic separation is widely used in the minerals industry to separate magnetic/paramagnetic minerals from gangue minerals. The three major categories of magnetic separators are low, medium and high intensity separators.

Minerals generally fall into three categories based on their magnetic properties including diamagnetic, paramagnetic and ferromagnetic. Magnetic separation requires that there must be discernible difference between the magnetic susceptibilities of the minerals present in the material.

Low intensity separators (LIMS) are generally wet separators used to separate magnetic minerals from gangue including magnetite and ferro-silicon. The separators work by utilising a revolving drum that lifts magnetic particles away from gangue minerals and are then scraped off the drum into a magnetic concentrate fraction.

Medium intensity magnetic separators (MIMS) are utilised to separate highly paramagnetic minerals from gangue; usually a dry process. It is used in the processing of ilmenite, chromite and garnet ores (Dobbins *et.al,* 2007).

High intensity magnetic separation can be used either as a dry or wet process and is utilised to separate minerals that are poorly paramagnetic from gangue. It is commonly used to beneficiate ilmenite and hematite ores as well as to upgrade gold and uranium concentrates (Corrans, 1979).

2.4.1.4 Electrostatic Separation

High tension or electric separation occurs as a result of the interaction of electrically charged particles within an electrical field (Drzymala, 2007). Minerals have differing conductivities and can be separated based on these difference.

Advantages are that all minerals have different electrostatic conductivities and the process could be applied to many different mineral assemblages. The disadvantage is that the throughput is very low and is difficult to use on an industrial scale.

2.4.2 Automated Sensor-Based Ore Sorting

Sensor-based ore sorting is a pre-upgrading method that uses electronic sensing technologies to discriminate ore based on measurable physical properties. The aim of ore sorting is to improve the grade and/or to remove unwanted contaminants from an ore processing stream (Death, 2005).

Sensor based sorting has been widely applied in the recycling and food industries whilst the application of sorting in minerals processing has had limited success with the exception of diamond sorting (Cutmore *et al.*, 1998). Diamond sorting has achieved success as a result of the unique mineralogical composition of the material that results in a high degree of heterogeneity between value (diamond-bearing) and waste material. The various methods used in diamond sorting include neutron sorting, gamma spectroscopy, X-ray induced luminescence, Raman spectroscopy, thermal and microwave techniques (Death, 2005).

The use of automated ore sorting in underground operations is described in literature for narrow veined mining operations. The removal of gangue/waste material as early as possible in a mining operation will have many benefits for downstream processing.

Removing waste before material is hauled to surface will results in cost reduction as less material, at higher grades, will be processed further downstream resulting in lower energy consumption (Murphy *et al.*, 2012).

Material can either be sorted particle-by-particle or an entire portion of the ore stream can be removed where higher grade particles are detected (recovery mode), the two techniques are presented in Figure 22.

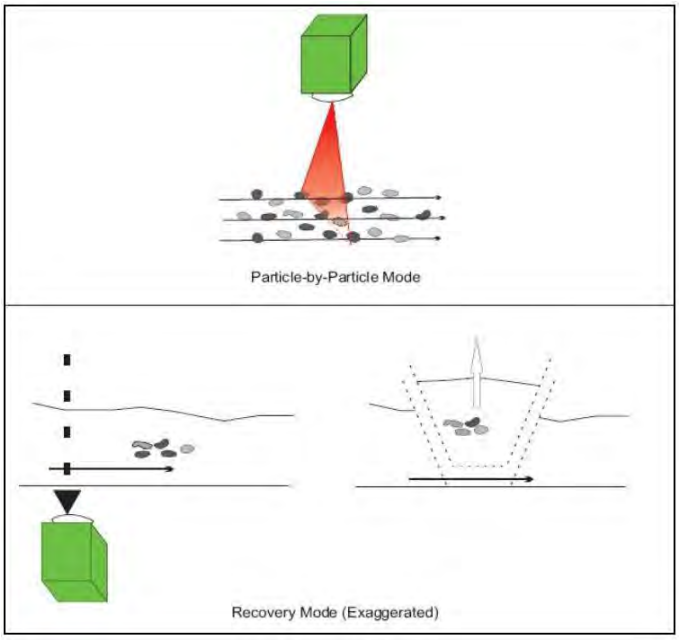

Figure 22: Ejection modes of ore sorting (Tong, 2012).

Ore sorting machines operate based on five unit operations that are extensively described in literature (Dalm, 2011; Death, 2005; Tong, 2012). These unit operations include material preparation, presentation, sensing, data processing and material separation and these operations are reviewed in this section.

2.4.2.1 Material Preparation and Presentation

Material preparation is required for some materials prior to sorting and includes sizing, washing, feed rate control, particle alignment, wetting, acceleration and stabilisation (Fitzpatrick, 2008). One or more of these preparation processes can be applied to the feed prior to sorting to optimise the process.

Material is presented to ore sorting systems either on conveyers (A) or as free falling material (B) as shown in Figure 23.

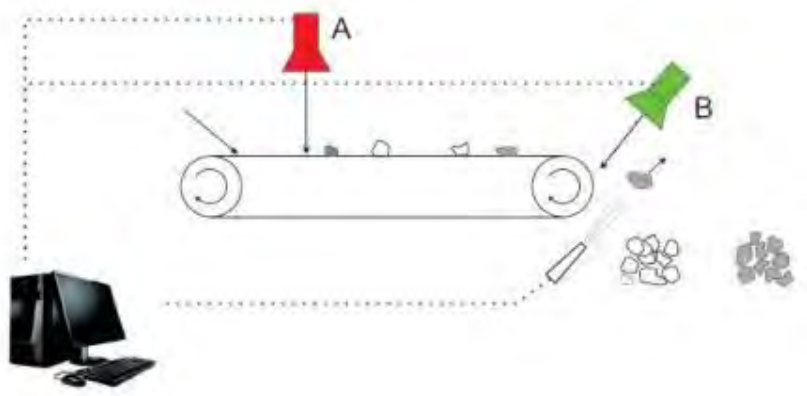

Figure 23: Material presentation to ore sorting sensors (Tong, 2012).

Sizing of the feed material is important prior to sorting as the ideal top to bottom size range for sorting should be less than 4:1 *i.e.* the size of the coarsest particles should not be more than 4 time the size of the finest particles in the material to be sorted. The ejection process may not be effective if bottom to top size ratio is above 4:1 (Death, 2005). Washing may be required where the particles surface is to be analysed by the sensors *e.g.* XRF, NIR and optical sensors. For optical sensors it may be necessary to wet the particle surface just before image capture as this will accentuate the colours on the surface of the particle. Particles can be accelerated as to stabilise their trajectory when free falling particles are analysed. Feed rate control is adjusted so that the sensing and data analysis is optimised. Particles may be lined up prior to presentation to the sensors if the sensors only have a narrow field of view.

2.4.2.2 Material Sensing and Data Processing

The sorting technologies that are currently available for ore sorting as well as those still under development are presented in Table 3 (Tong, 2012). Advances in data processing have helped to increase the throughput of ore sorters as more analyses can be processed per second. This section describes the operation and application of the various electronic ore sorting sensors.

Table 3: Ore sorting sensor technologies, physical properties detected and applications (Tong, 2012).

Sensing Technologies	Physical Properties Detected	Applications
Radiometric	Natural Gamma Radiation	Uranium, Precious Metals
X-ray Transmission - Single Energy (SE-XRT)	Atomic Density	Base/Precious Metals, Coal, Diamonds etc.
X-ray Transmission - Dual Energy (DE-XRT)	Atomic Density, Thickness	Base/Precious Metals, Coal, Diamonds etc.
X-ray Fluorescence (XRF)	Visible Fluorescence under X-rays	Diamonds
X-ray Fluorescence Spectroscopy (XRF-S)	Elemental composition	Base/Precious Metals
Near Infra-Red (NIR)	Reflection, Absorption	Industrial Minerals, Base Metals
Colour (CCD)	Colour, Reflection, Brightness, Transparency	Base/Precious Metals, Industrial Minerals, Gemstones
Photometric (EM)	Monochromatic Reflection, Absorption and Transmission	Industrial Minerals, Diamonds
Electromagnetic (EM)	Conductivity/Magnetic Susceptibility	Base Metals
Under Development		
Microwave-Infrared (MW/IR)	Microwave Absorption, Heat Conductivity	Base Metals, Carbonaceous Material
Laser-Induced Fluorescence (LIF)		
Laser-Induced Breakdown Spectrometry (LIBS)		

2.4.2.2.1 Single and Dual Energy X-Ray Transmission Sensors

The X-ray transmission (XRT) through particles depends upon the densities of its components. XRT sensors measure the transmission of X-rays across the entire volume of the particle and projection images are collected in grey-scale. The grey level intensity is indicative of its density. The grey level images are converted to binary images and the amount of low-density and high-density material is calculated (Strydom, 2010).

XRT sensors using a single X-ray energy (monochromatic imaging) may give incorrect results due to the varying thicknesses of material analysed; the amount of high density material may be overestimated in thicker particles due to lower X-ray attenuation. The use of dual-energy XRT (DE-XRT) uses two X-ray energy levels, low and high, to determine the density as well as the effective atomic number, thus the thickness is taken into account. The result is a much more accurate measure of the amount of high and low density material in a particle (Strydom, 2010; Tong, 2012).

Laboratory scale sorting optimisation test work has also been conducted to determine the sortability of torbanite from coal using DE-XRT sensors. The laboratory scale test work was conducted to determine the optimal pilot-scale sorting conditions. A bulk sample was processed using these optimal sorting conditions and a good separation of torbanite from coal was achieved (Strydom, 2010).

2.4.2.2.2 X-Ray Fluorescence Sensors

X-ray fluorescence (XRF) ore sorting sensors measure the elemental composition on the surface of particles by measuring characteristic secondary X-rays emitted from a sample whilst interacting with primary X-rays. The advantage of this method is that it can measure surface grade directly. The disadvantage is that in order for the sensor to be able to sort particles there must be a correlation between the grade of value, or proxy, elements on the surface and the grade of the total particle volume (Tong, 2012). XRF sorting sensors often only measure the composition of one side of each particle; this is problematic when the elements of interest are concentrated on one side of the particle.

2.4.2.2.3 Optical Sensors

Optical sorting relies on the analysis of surface images of particles using a CCD camera. The cameras either collect grey-scale or colour images and separation can only be achieved if there is a significant visual difference between ore and waste particles (Fitzpatrick, 2008).

Optical sorting is widely used in the food and recycling industries (Blasco *et al.*, 2007) but is not as widely used in ore sorting (AMIRA P902, 2005).

2.4.2.2.4 Electromagnetic Sensors

Electromagnetic (EM) sensors comprise transmitter and receiver coils. The transmitter coils produce a magnetic field that interacts with particles to be sorted. Magnetic minerals produce eddy currents resulting in secondary magnetic fields that are detected by the receiver coils. Sorting of the particles can be achieved based on the strength of the electromagnetic response of the particles. The advantages of the technique are that the entire volume of the particles can be measured for magnetic mineral content. The drawback of this technique is that the particles to be sorted must

contain magnetic minerals, the contents of these minerals must also correlate with the grade of the value element being targeted. Another advantage is that this method measures the full volume of the particle.

2.4.2.2.5 Spectral Based Near-Infrared Sensors

The near-infrared (NIR) sensor measures the absorbance of infrared light on the surface of particles. The result is a spectrum that is unique to different minerals. The disadvantage of this technique is that only certain minerals respond to NIR such as minerals with the following bonds: OH, H_2O, CO_3 and NH_4. It is therefore not suitable for direct detection of value minerals such as sulphides and will only succeed if there is a proxy mineral comprising one of the bond types that correlates with grade (Dalm, *et al.*, 2014).

The applicability of NIR sensors to sorting of Los Bronces SAG mill pebbles was investigated by Dalm (2011). The results indicated that NIR response does not correlate with the grade of the pebbles and is not a viable sensor type for Los Bronces.

2.4.2.2.6 Microwave-Infrared Sensors

Minerals that are subjected to microwave radiation exhibit differences in their heating rates. Particles that have been heated can be analysed using IR thermography and the mineral particles that heat up faster can be discriminated from particles with slower heating rates based on their temperature profiles (Ghosh *et al.*, 2013).

The technique is non-invasive and does not require any special sample preparation prior to analysis. The heating rates of many major ore minerals such as chalcopyrite, molybdenite (MoS_2) and sphalerite ((Zn,Fe)S) respond well to MW heating whist gangue minerals such as quartz and carbonates are poor heaters. The use of MW/IR for ore sorting applications shows much promise but further research is required to determine the potential for ore sorting on an industrial scale (Tong, 2012).

2.4.2.3 Physical Separation in Automated Sorting Machines

Once the particles have been analysed and the sensor data processed, the particle is either accepted or rejected depending on the sorting criteria. Particles are physically separated either using a blast of compressed air or by mechanical ejectors (Tong, 2012).

2.4.2.4 Economic Considerations for Ore Sorting

Ore sorting has become more economically viable in recent times as a result of improved throughput. In the coal industry the throughput has increased over the past decade to 10 times the original capacity. The viability of implementing of ore sorting must be established by assessing the economic impact on an operation (Lessard *et al.*, 2015).

An approach was developed by Lessard *et al.* (2015) to assess the economic impact of ore sorting using a case study from an operating copper mine in south-western USA. Operational data from the mine along with typical commercial scale sorter performance data was used to estimate the overall economic impact of sorting on an operation. The driver to implement ore sorting was to increase ROM throughput; additional ROM feed would replace the mass rejected by ore sorting. The additional profit was calculated at different levels of sorter performance (amount of mass rejection). These results can be used to motivate for ore sorting based on the potential economic impact.

2.5 Characterisation of Separation Processes

Separability in the minerals industry is characterized by assessing the feed and products of separation techniques and the results are generally presented in separability curves that are described in (Wills, 2006). The feed and products of metallurgical processing are assessed in terms of grade, recovery and yield (Drzymala, 2007). This section presents the standard laboratory separability tests and grade-recovery curves used to analyse separability in Section 2.5.1. The section then concludes with a description of methodologies present in literature for determining ore sortability using electronic sensor-based ore sorting in Section 2.5.2.

2.5.1 Separability and Grade-Recovery Tests

The standard laboratory tests to assess physical separability as well as the grade recovery curves produced from the standard test work are discussed. The methodologies are well established in mineral processing but few methodologies are widely used for ore sorting.

2.5.1.1 Standard Physical Separability Tests

The standard test used to assess the separability of particulates by gravity and DMS is conducted on a laboratory scale using sink-float tests that are performed by using heavy liquids covering a wide range of densities. Material is added to the highest density liquid first and the floats are successively removed and added to the next highest density liquid as presented in Figure 24. The sink fractions together with the final float are chemically assayed for the elements of interest and the results are used to assess the amenability of the material to gravity concentration. (Wills, 2006).

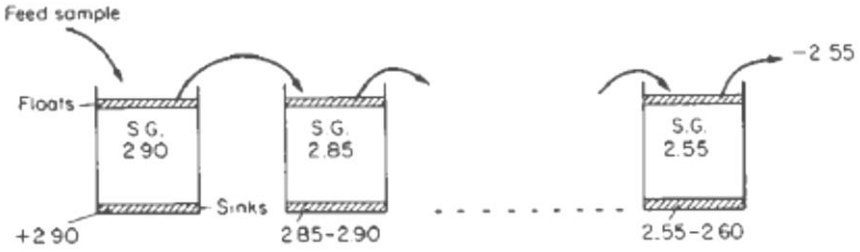

Figure 24: Diagram indicating the procedure for dense medium separation (DMS) (Wills, 2006).

Amenability of an ore to magnetic separation is determined by first assessing the ferromagnetic content using techniques such as SATMAGAN. Samples containing significant amounts ferromagnetic material (such as magnetite Fe_3O_4) are subjected to Davis Tube separation tests in order to assess the separability of value minerals from waste. Flotation response is determined on a laboratory-scale using batch flotation cells. The concentrate is collected at specific time intervals and submitted for chemical assay.

2.5.1.2 Grade-Recovery Curves

Separation is the process of splitting material into two or more products through the application of ordering and splitting forces as indicated in Figure 25 (Drzymala, 2007).

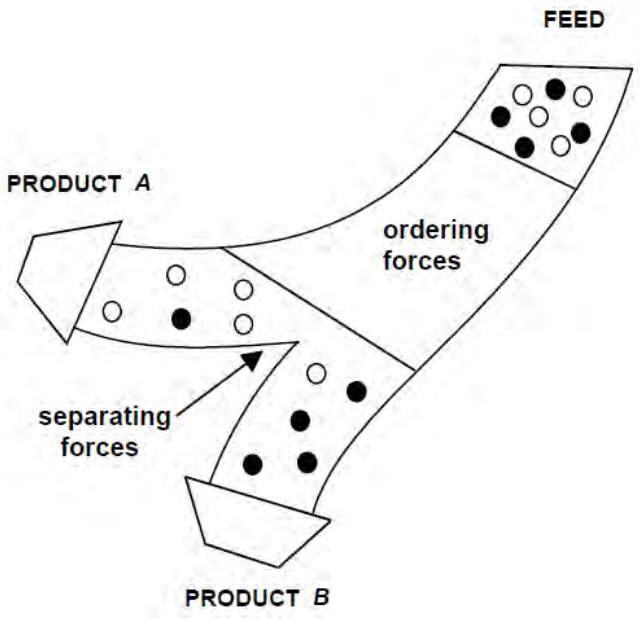

Figure 25: Ordering and separation forces required for separation where product A differs from product B (Drzymala, 2007).

A widely accepted means of assessing metallurgical performance is the grade-recovery curve (Drzymala *et al.*, 2013; Wills, 2006) that compares the quantity of material recovered with the quality of the product. This section discusses the grade-recovery curves that can be determined based on mineralogy, laboratory-scale separation tests as well as industrial-scale separation.

The physical separation of particulates in any separation process is limited by the liberation of the value minerals. The liberation data determined from mineralogical techniques such as aSEM can be used to produce liberation-limited grade-recovery curves as presented in Figure 26 (Miller *et al.*, 2009). These curves are theoretical grade-recovery curves and represent the best-case separation achievable. Drzymala (2003) discusses a similar method, referred to as ‘sorting’, to evaluate upgrading processes based on mineralogical information. Both techniques involve assigning particles into groups based on particle properties *e.g.* 10 % liberation categories of a specific mineral.

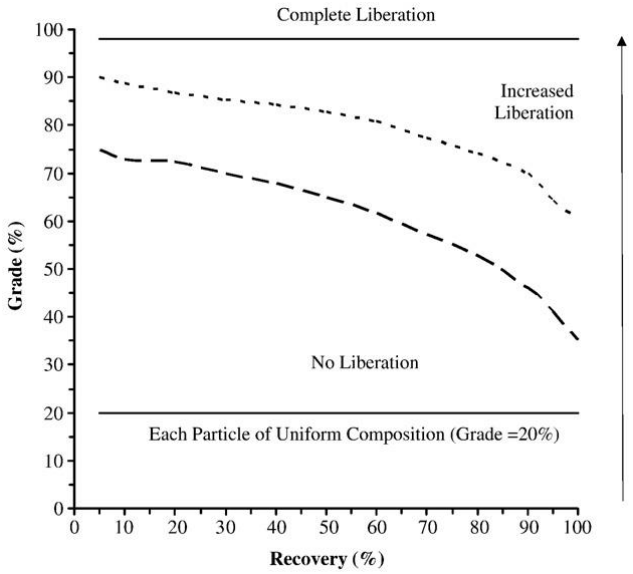

Figure 26: An illustration of the liberation-limited grade and recovery curve (Miller et al.*, 2009).*

The grade of the separation products from laboratory- and industrial-scale separation are determined to assess the grade-recovery relationship. The grade is plotted *vs.* the recovery (cf. Figure 27) to assess the separation potential.

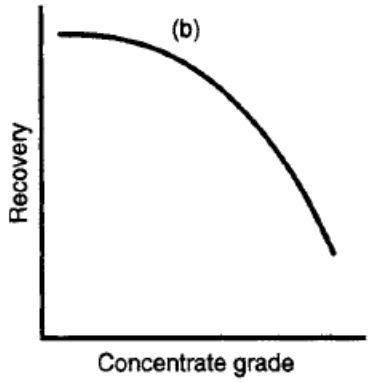

Figure 27: Grade-recovery curve used to assess laboratory- and industrial-scale separation (Wills, 2006).

2.5.1.3 Partition Curves

The laboratory-scale tests are performed under ideal conditions allowing sufficient time for separation of material based on density. In an industrial setting the separation conditions are from ideal and the efficiency of the separation process must be assessed. The efficiency of separation is determined by calculating the partition co-efficient *i.e.* the percentage of material in a specific density category that reports to the sink/ float products depending on the commodity. The separation becomes less efficient as the amount of near-dense (densities close to the separation density)

material increases. The partition co-efficient is plotted against the density in the example of a partition curve in Figure 28. The probable error of separation (E_p) is defined by Equation 10 where A is the density where 75 % of material is recovered to sinks and B is where 25 % is recovered to sinks. The lower the E_p the more efficient the separation process.

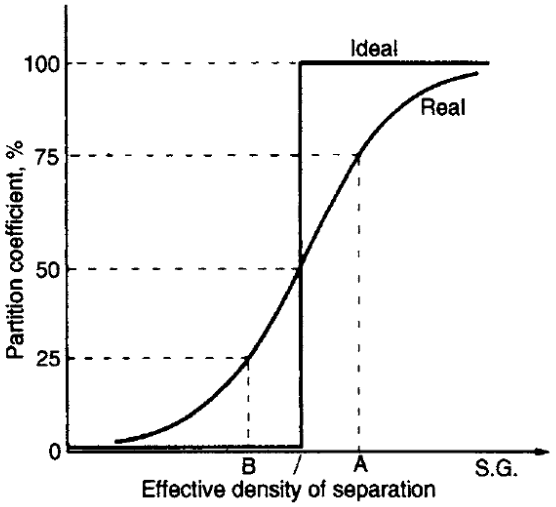

Figure 28: Partition curve for gravity separation (Wills, 2006).

$$E_p = (A - B)/2 \quad [10]$$

2.5.2 Methodologies for Ore Sortability

Standard tests for physical separation are well established in the mining industry including sink-float and bench-scale flotation tests. Methodologies for determining ore sortability are not commonly practiced. This section describes the current methodologies available in literature.

Currently there are two methodologies that exist in literature to assess the potential sortability of an ore using electronic sensor technologies. Fitzpatrick (2008) presents a methodology for automated sorting in an attempt to create a standard methodology for the minerals industry. Tong (2012) presents a methodology to determine ore sortability on a laboratory scale using an example of a Mississippi Valley type lead-zinc ore. The methodologies described comprise similar steps and are compared in this review. The general steps used for the methodologies are summarised in Table 4 for both methods and includes: sampling, sample preparation, ore characterisation, sensor selection, determining sensor potential, optimisation of the ore sorter,

determination of rejection criteria, grade-recovery relationship, impact evaluation and bulk sample sorting tests. A detatiled description follows for each step.

Table 4: Comparison of Fitzpatrick (2008) and Tong (2012) ore sorting methodologies.

Steps in the Methodologies	**Methodologies**	
	Fitzpatrick (2008) Methodology	**Tong (2012) Methodology**
Sampling	Binomial distribution so that all rock types are represented – non-representative	Hand picked to collect a wide range of grades and sizes – non-representative
Sample preparation	Cleaning of particle surface, wetting of particles for optical sensors	Cleaning of particle surface, wetting of particles for optical sensors
Ore characterisation	Literature review of ore/ mine under investigation	Qualitative mineralogical and chemical analysis on a sub-sample of material under investigation
Sensor selection	Only optical and inductive sensors selected as they are commonly used	Sensors with previous base metal application, selection not completely justified based on ore characterisation
Determining sensor potential	Sensor response recorded followed by destructive chemical analysis, sensor response compared to grade to determine any correlation	Sensor response recorded under ideal laboratory scale conditions, destructive chemical analysis. Grade-recovery relationship determined
Impact evaluation	-	Product and waste bond-work index (BWI) calculated to asssess any improvements in energy consumption. Laboratory-scale flotation on products to assess metallurgical performance.
Industrial-scale sorting tests	Pilot-scale tests conducted on a portion of material to assess product streams to determine upgrading potential	-

2.5.2.1 Sampling and Sample Preparation

In the methodology by Fitzpatrick the number of particles required to be sampled for ore sorting sensor amenability need only represent all of the rock types present in the material under investigation as the aim of the methodology is to establish whether it is physically possible to separate an ore using electronic sensors. The case studies where the methodology was applied include an iron ore sample from the Marandoo deposit and a copper/nickel sample from the Raglan mine. In both cases, an 18 kg sample was collected. The methodology to determine the minimum number of particles for ore sorting amenability (as described in Section 2.2.2) was applied to the samples in order to include at least 3 particles of the least abundant rock types. The number of particles required for the analysis of the iron ore and copper/nickel samples was 56 and 19 respectively. The methodology does discuss that bulk sample test work would need to be carried out to confirm that the ore is sortable and what the ecomic impact would be. A procedure for bulk sampling is not discussed for the two case studies.

The sample used by Tong (2012) is a Mississippi Valley type zinc-lead ore from Pend Oreille Mine that was hand sorted to include particles with visible sulphide and were within the correct size range for the study. The sample is therefore not representative of the run-of-mine ore. The number of particles selected for each sensor test were done at random. A statistical method to determine the minimum number of particles required to achieve a known degree of error is not discussed as the methodology describes a quick laboratory-scale amenability test to be performed prior to pilot-scale tests.

For sample preparation, both of the methodologies highlight the importance of screening prior to any ore sorting test work. Sorting requires that the particles lie within a narrow size range to improve the accuracy of particle rejection. As well as screening, sample preparation in both the iron and nickel-copper ore case studies in Fitzpatrick (2008) and the the surface sensors in Tong (2012) (XRF and optical) also include cleaning and drying prior to testing. Fitzpatrick also wetted the particles prior to image analysis using optical sensors to improve image resolution. Particles analysed using XRT and MW/IR (Tong, 2012) did not need any further sample preparation as surface contamination would not influence the sensor response.

2.5.2.2 Ore characterisation

Ore characterization in the methodology by Fitzpatrick (2008) is conducted by reviewing literature of the ore deposit under investigation as the first stage of his methodology. Qualitative information about the geology, mineralogy and metallurgy is collected in order to gain an understanding of the ore types and minerals present in the ore body as well as their relative abundances. The information will guide the investigators as to which separation method may be used as well as whether the ore will be sorted to upgrade or remove unwanted components within the ore. The ore characterisation in this methodology is flawed if there is insufficient information about the ore body in literature or the stream identified for sorting has a different composition compared to the run-of-mine ore.

Tong (2012) chooses to conduct ore characterization after initial sampling using a sub-sample of the material. The results are therefore more useful than the information gathered by Fitzpatrick (2008) as the mineralogy is determined on the same material that is to be analysed with the sensors. The subsample is however analysed destructively and cannot be used in the sensor tests which would be ideal.

2.5.2.3 Sensor selection

The methodology by Fitzpatrick (2008) discusses the use of many different types of sensors to determine if they can be used to sort an ore but the the methodology was developed using an automated ore sorting machine equipped with only optical and inductive sensors.

Tong (2012) selected sensors that have previously shown applicability to base metal ores including XRT, XRF, Optical and MW/IR. Sensor selection has not been completely justified based on the ore characterisation results.

2.5.2.4 Determining of Sensor Potential

The procedure to determine sensor potential for optical and non-optical sensors is described by Fitzpatrick (2008). Training and optimisation of the ore sorting sensors was conducted to determine the optimal sensor response to separate product from waste. In both cases the sensor response is recorded for each particle and the particles are then destructively analysed to determine the bulk chemistry. The assay

results of product and waste are compared to determine if any significant upgrading has taken place. Fitzpatrick uses two case studies where the potential for electromagnetic and optical sensors on an iron ore and nickel/copper ore was investigated. The iron ore case study indicated that the optical sensor could distinguish between ore particles of different grade; it was however found that the ore was not intrinsically separable. The Ni/Cu ore showed interesting results in that a multiple sensor approach was used. An optical sensor was first used to separate out sulphide rich particles. The sulphide rich stream was then separated into conductive and non-conductive products resulting in significant upgrading of Ni with a good recovery.

The sensor potential for XRF, XRT Optical and MW/IR sorting is described by Tong (2012). Similarly, the method also relies on chemical analysis to assess the sensor potential. Many sensors measure a particles surface and an important step in the determining sensor potential was to compare the surface grade with the particles total grade. If there is a correlation between surface and volume grade then the sensor can potentially be used for sorting.

The method by Tong (2012) also involves assessing the sensor potential in terms of grade and recovery event though the sample is not representative; the example used here presents the procedure that was used to assess the XRF sensor potential. Particles are grouped by sensor response (Zn content in this case) into five cut-off grade thresholds for Tests 1 to 5. The particles in each concentrate (Concentrates 1-5 as well as the final discard) category are pulverized, combined and weighed. A representative split of each test concentrate and final discard was submitted for chemical assay and, together with the masses, the potential grade-recovery relationship is determined. The results are plotted on grade-recovery curves as presented in Figure 29.

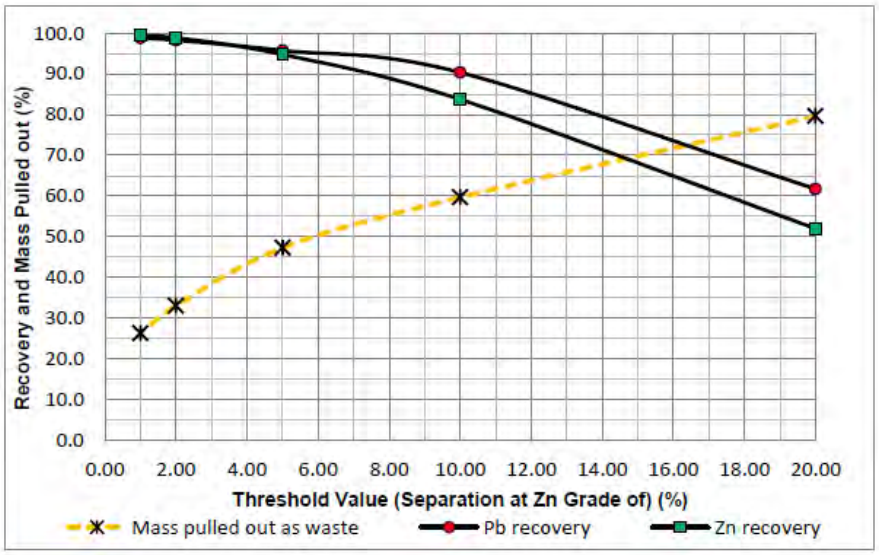

Figure 29: Pb and Zn grade recovery curves as well as mass pulled out as waste per grade class. Results indicate that 45 % of waste can be removed whilst 95 % of metals can be recovered (Tong, 2012).

The results from both methodologies are not representative of the actual grade-recovery that can be achieved but do give insight as to the sensor potential.

2.5.2.5 Impact evaluation

The downstream impact of removing particles by ore sorting is investigated by Tong (2012). The Bond work index is calculated for the sorting product and waste in order to determine if there are any significant differences in the overall ore hardness of each stream. It would benefit the metallurgical processing if the ore reporting to the concentrate sorting stream is softer than the unsorted feed to the plant. The material was also processed on a laboratory scale flotation cell to assess the metallurgical performance of the pre-concentrated material.

Potential uses for the waste material are also investigated *i.e.* utilizing waste material as backfill in the mine.

2.5.2.6 Industrial-scale sorting tests

Tong (2012) does not include the procedure to assess the sortability of an ore on an industrial scale as the aim of both the methodologies is to assess the amenability of an ore to sensor based sorting. Fitzpatrick (2008) conducts industrial scale tests on a small portion of material and determines the composition of the concentrate and waste streams to determine the amount of upgrading achieved.

2.6 Research Objectives

2.6.1 Literature Review Summary

The literature relevant to the development of a protocol to determine the separation potential of an ore has been reviewed in this chapter.

The Los Bronces ore geology as well as the mining and processing operations was reviewed highlighting the complexity of the Los Bronces deposit. The ore comprises many different breccia types that all have their own distinct mineralogy which presents a unique challenge in the mining and processing of the ore. The ore is not selectively mined and therefore the feed to the comminution plant may contain a large proportion of barren or low grade host rock. This presented an ore sorting opportunity in the comminution circuit to remove hard low grade pebbles discharged from the SAG mill prior to pebble crushing. The removal of the barren host rock early on in the process would have a positive impact on downstream processes in terms of energy consumption and sustainability of the mine.

The sampling section discussed the techniques in literature used to collect a representative sample. It was highlighted that the heterogeneity of particulates has the biggest impact on the error introduced during sampling. A sampling method based on binomial distribution was discussed which can be used to collect a sample that represents all identifiable rock types present in a material. A sample that represents all the rock types is useful when determining the amenability of an ore to sorting. Gy's Theory of Sampling is reviewed and is useful when samples must be representative of an ore stream within a processing plant. TOS describes all of the errors introduced during a sampling procedure as well as ways to mitigate these errors. The sampling equation, first developed by Gy, is reviewed and various methods to calculate the components of the sampling equation were presented. It was found that all of the techniques can be useful depending on the mineralogical and physical properties of the material to be sorted.

The ore characterisation techniques relevant to the protocol including 2-dimensional aSEM techniques, 3-dimensional XMT as well as surface characterisation techniques were reviewed. The aSEM techniques are well established compared to XMT which is still in the early developmental stage; the XMT is advantageous as it is a non-

destructive technique. Other techniques that are reviewed include non-destructive HH-XRF and hyperspectral imaging techniques.

The section on ore characterisation includes a procedure to statistically validate results using bootstrap resampling techniques. A technique to determine the absolute and relative error on individual minerals from aSEM techniques was also presented.

The various physical separation processes were reviewed and highlighted which physical properties each process exploits to sort an ore into two or more streams. Sensor based ore sorting techniques were then reviewed in detail.

The various standard laboratory tests to assess the amenability of an ore to physical separation were reviewed including laboratory-scale sink-float, batch flotation and magnetic separation techniques. The characterisation of ore separability tests using grade-recovery curves was discussed. The section concluded with a review of the methodologies present in literature to determine sensor-based ore sorting potential. It was found that the only general methodology for sensor based sortability was developed by Fitzpatrick (2008).

2.6.2 Objectives

A general methodology to assess the amenability of an ore to sorting at a pilot-scale was developed by Fitzpatrick (2008) using a multi-sensor approach (inductive and optical sensors). The methodology was validated using case studies from a nickel/ copper and an iron ore deposit. Tong (2012) developed a methodology to assess the amenability of an ore to sensor-based sorting on an ideal laboratory-scale as a means of assessing the ore sorting potential prior to pilot-scale test work.

The objective of this study is to develop a protocol/ methodology for determining the sortability of an ore based on intrinsic particle properties as well as laboratory-scale ore sorting sensor tests. The intrinsic sortability is a measure of sorting potential if a perfect separator existed. Once it has been established that an ore is intrinsically sortable, further sortability test work can be carried out to assess the sorting potential using similar methodologies present in literature (Tong, 2012; Fitzpatrick, 2008).

The overall objective of the research is to produce a protocol for ore sortability in order to:

- Give guidelines to samplers in terms of understanding how to take a representative sample with a known error at a particular level of confidence.
- Assess the grade and recovery based on intrinsic particle properties.
- Assess the grade and recovery based on laboratory-scale sorting tests using ideal and industrial ore sorting sensor measurement parameters.
- Assess the potential economic impact of ore sorting on an existing flow sheet.

2.6.3 Hypothesis

A standard methodology/ protocol to assess the separation of ore particulates based on intrinsic particle properties for a wide variety of separation techniques, including physical separation and electronic sensor-based ore sorting, can be developed in order to assess the feasibility of separating an ore into two or more streams.

Chapter 3

Protocol Methodology

This chapter presents the protocol methodology developed during the current research using the Los Bronces case study. The protocol was developed as a set of standard procedures to assess the sorting potential of a particulate ore. The protocol is divided into six stages, a simple flow diagram of the protocol is presented in Figure 30; section numbers are shown in brackets.

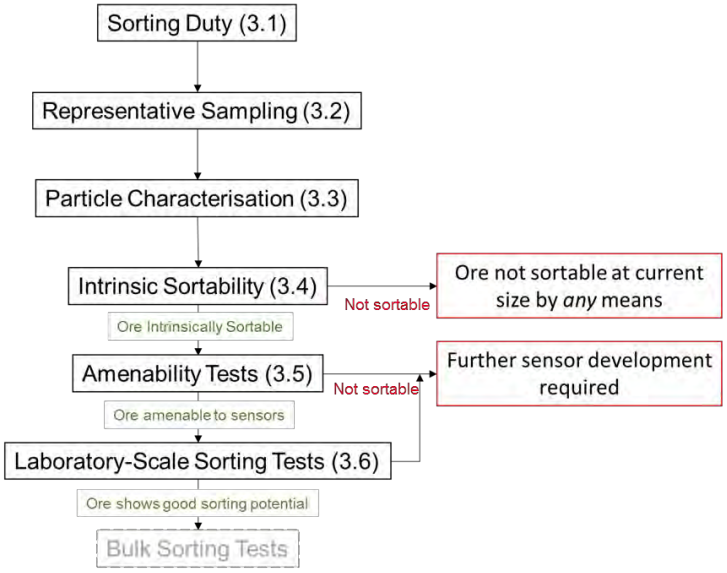

Figure 30: Flow diagram presenting the protocol methodology (section numbers in brackets), the final stage of the protocol is the laboratory-scale sorting tests as bulk sorting tests are beyond the scope of the current research.

The first stage of the protocol is to identify a potential sorting duty (Section 3.1) based on plant information and ore mineralogy. The next stage of the protocol is to collect a representative sample (Section 3.2) of the material identified for the potential sorting duty. The individual particles of the representative sample are mineralogically and chemically characterised in the next stage (Section 3.3). The intrinsic sortability is then calculated based on the particle characterisation data (Section 3.4); the results represent the sortability if a perfect separator existed. The potential economic impact of sorting based on the intrinsic sortability is determined at this stage to assess the feasibility of applying ore sorting. If it is determined that applying ore sorting is

economically feasible then the amenability of the ore to various sorting techniques is assessed in the next stage (Section 3.5). The sorting techniques that show potential to be used for sorting are then assessed further by conducting laboratory-scale sorting tests (Section 3.6) to determine the potential sortability based on the ore sorting sensor responses. The economic impact of sorting using varying sorting criteria is then calculated to assess if ore sorting is economically feasible.

3.1 Sorting Duty

The first stage of the protocol is to identify a sorting duty. For example, the sorting duty for the Los Bronces case study was the removal of hard, low-grade SAG mill oversize pebbles from the pebble crusher stream (cf. Figure 1) at a cut-off grade of 0.4 % Cu. The aim of sorting was to increase run-of-mine throughput which would, in turn, increase the revenue.

The identification of a sorting duty will initiate the use of the protocol. Potential sorting duties can be broken down into three categories depending on the desired result:

- Upgrading of value minerals/ elements (*e.g.* increase Cu grade by removing waste rock).
- Removing penalty minerals/ elements (*e.g.* removing phosphorus from an iron ore stream).
- Splitting material into two or more processing streams (*e.g.* splitting an ore into hard and soft components for separate treatment).

Existing information about mining techniques, ore mineralogy and mineral processing techniques is gathered at this stage to assist in identifying potential sorting duties. The information is gathered through literature surveys and communication with site personnel.

3.2 Representative Sampling

Once a potential ore sorting duty has been identified, the next stage in the protocol is to collect a representative sample of the material. A simplified flow diagram of the sampling procedure is presented in Figure 31 and described in Sections 3.2.1 to 3.2.3.

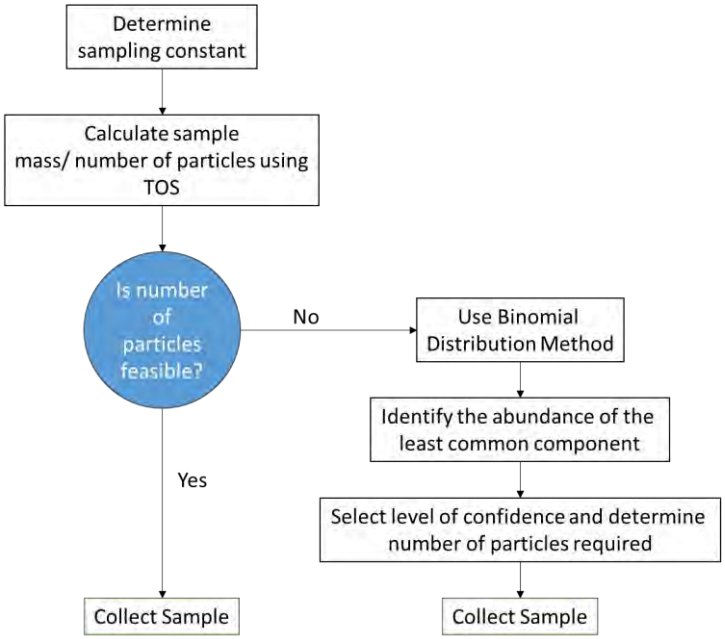

Figure 31: Flow diagram of the procedure to collect a representative sample.

3.2.1 Determining the Sampling Constant

Ideally, a sample is collected for the protocol using Gy's theory of sampling as to minimise the error introduced due to the heterogeneity of the particles. Therefore the first step in collecting a representative sample is to determine the sampling constant (K_S) for the elements of interest. K_S can be calculated using the techniques described in Section 2.2.1.2.

3.2.2 Minimum Sample Mass/ or Number of Particles

Gy's sampling equation (Equation 1, Section 2.2.1.2) is used to determine the minimum sample mass required for a sample to be representative. According to TOS, the relative variance on the mineral/ element of interest should not exceed more than 10 % at each stage of sampling. For example, when a copper ore with a grade of 1 % Cu is sampled for chemical assay and a confidence interval of 95 % is required, the assay results of each aliquot should be within 0.1 % Cu for at least 95 out of 100 aliquots. The number of particles required can be estimated based on the sample mass and the average particle size.

It may not be feasible to analyse the number of particles determined using Gy's equation depending on the ore type and element of interest. The binomial distribution method, as described in Section 2.2.2, can be used to as an alternative to collect a

sample that represents the different components/ rock types within the ore. The sample collected with this method may not be wholly representative for the purposes of determining the sorting potential as the variability in particle size and composition is not taken into account. However, the results will give a good indication of sorting potential.

3.2.3 Sample Collection

Irrespective of the method used to determine the number of particles required, the sample must be collected as to minimize the sampling errors as described in Section 2.2.1.1.

3.3 Particle Characterisation

The next phase of the protocol is the characterisation of the sampled ore particles on an overall and size-by-size basis. A flow diagram of the particle characterisation phase is presented in Figure 32 and the procedures are explained in Section 3.3.1 to 3.3.4.

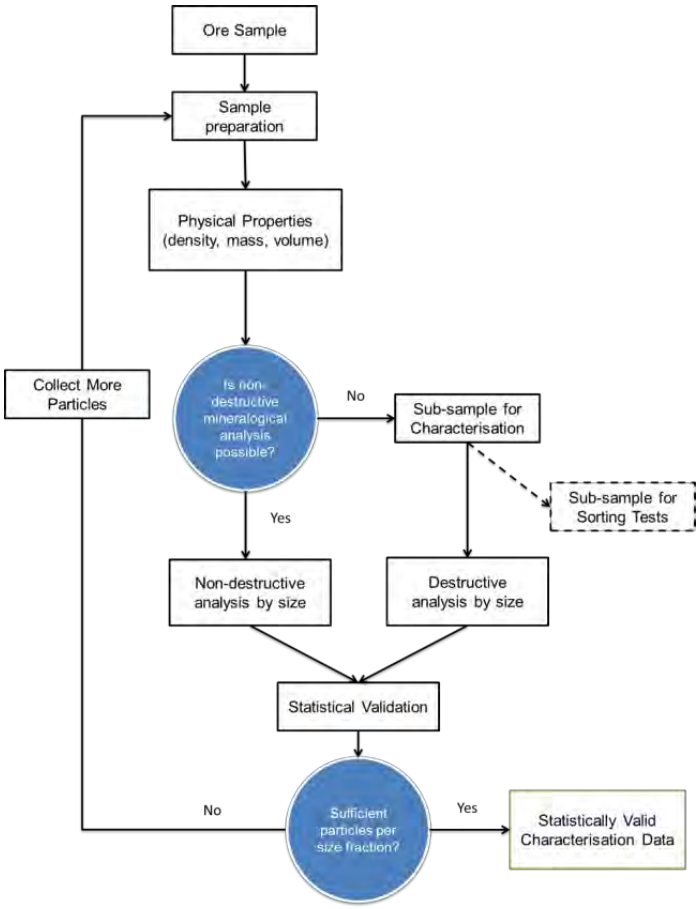

Figure 32: Flow diagram for the particle characterisation phase of the protocol.

3.3.1 Sample Preparation

The material should be characterised on a size-by-size basis to determine if the ore is sortable at a specific size range. Ore sorting can only work efficiently within a certain size range depending on the material being sorted as well as the sorting machine limits. Therefore the first step is to remove material that is too coarse or fine for efficient sorting. For example, Fitzpatrick (2008) used an optical sensor with a resolution of 2 mm; particles below 2 mm could not be accurately measured. The ore sorting machine used in the investigations also had a size limit of ~100 mm; coarser particles could not be ejected into the waste stream efficiently. The oversize and undersize material was removed prior to screening.

The material can then be screened into appropriate size fractions for analysis. The screen sizes are selected to ensure that the top to bottom size ratio does not exceed 3:1 for particles less than 40 mm and 2:1 for particles greater than 40 mm. In the optical sensor example by Fitzpatrick (2008) the screen sizes selected for sorting are presented in Table 5.

Table 5: Screen sizes selected for optical sorting and their top to bottom size ratios (Fitzpatrick, 2008).

Screen size (mm)	Ratio of sizes
2	
	3:1
6	
	3:1
18	
	2.78:1
50	
	2:1
100	

Further sample preparation may be required for destructive mineralogical analysis depending on the technique used. Many of the mineralogical and chemical techniques require the material to be crushed, milled and/ or split into representative aliquots for analysis.

3.3.2 Measurement of Physical Properties

The next step is to measure the physical properties on a particle-by-particle basis to determine the density, size and mass. The physical properties are measured first as further non-destructive characterisation may not be possible.

3.3.3 Mineralogical and Chemical Characterisation

The samples need to be analysed to determine the mineralogical and/ or chemical composition of individual particles on a size-by-size basis. Techniques relevant to the protocol are described in Section 2.3. The bulk modal mineralogy and chemistry data can be assessed at this stage to determine if there are any proxy minerals and/ or elements that correlate with minerals/ elements of interest. This will help in identifying potential ore sorting sensors.

Many of the ore sorting sensor technologies rely on surface analysis (XRF, NIR, and Colour sensors). Therefore, an important step is to assess the correlation between the surface composition and the total volumetric composition based on a statistically valid number of particles as determined using the sampling methods described in Section 3.2. The results will determine if the ore can be sorted based on surface properties.

3.3.4 Statistical validation

In order to ensure that the characterisation results are representative in terms of the mineral/ or element of interest, further statistical validation is required to check the representivity of the initial sample collected.

A method based on bootstrap resampling, as described in Section 2.3.5.1, is used to assess whether sufficient particles have been analysed. The end result is a regression curve, as presented in Figure 33, which can be used to determine how many particles are required to achieve an acceptable level of error. For example, when characterising a copper ore comprising ~2.8 % Cu where Cu occurs mostly in chalcopyrite, the maximum allowable error on chalcopyrite content is 10 % RSD (Evans, *et al.* 2013).

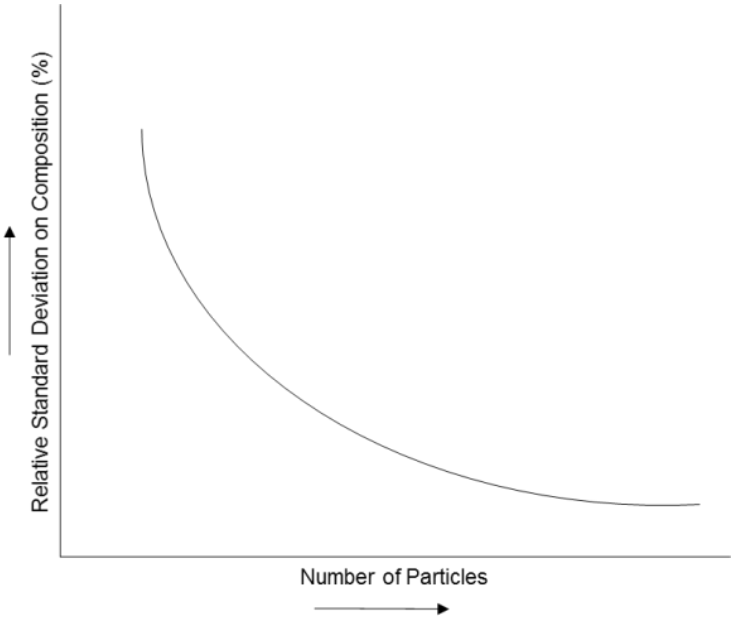

Figure 33: Example of a regression curve determined using resampling.

For mineralogical analysis using the aSEM techniques, the estimation of error in mineral content can be assessed using the methods described in Section 2.3.5.2. In general, less than 1 % relative error is acceptable for mineralogical analysis.

3.4 Intrinsic Sortability

The grade-recovery relationship of a particulate ore undergoing a separation process is influenced by plant design and operation as well as the particle properties. In order to determine the ideal or intrinsic sortability, only the particle compositions are considered and it is assumed that the separation process is 100 % efficient *i.e.* if a perfect separator existed. The methods to determine the grade-recovery relationship based intrinsic particle properties is discussed in Section 3.4.1. Figure 34 presents a flow diagram of the procedures to determine the intrinsic sortability.

Ore sorting is implemented to improve the economic potential of a mineral processing operation. A technique to establish the impact of ore sorting on the profitability of an operation is presented in Section 3.4.2

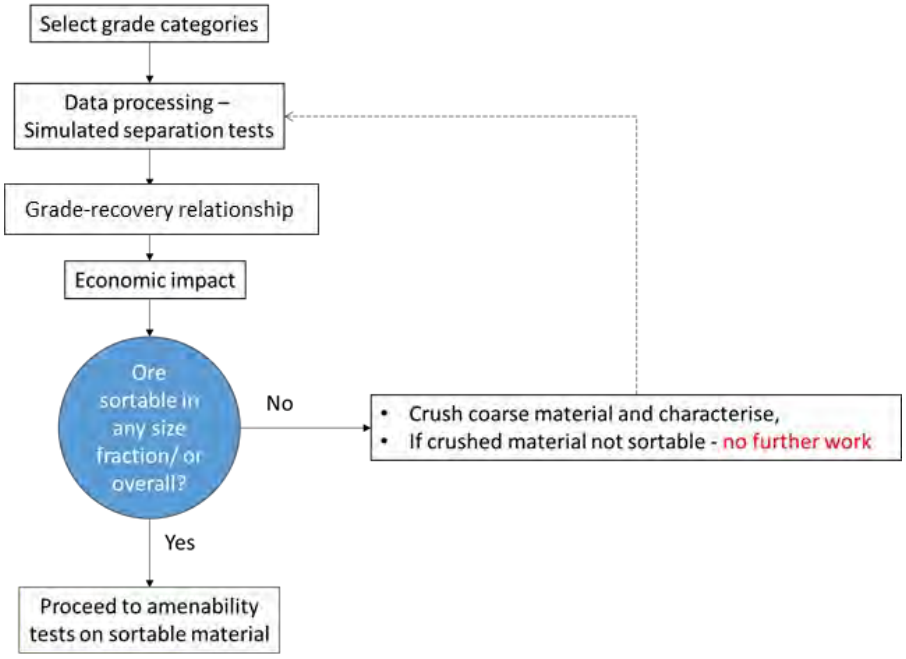

Figure 34: Flow-diagram of the procedure to determine the intrinsic sortability.

3.4.1 Grade-Recovery Relationship

The intrinsic sortability of the ore is determined using the particle characterisation data to assess whether the ore can be sorted by any means. The sortability is calculated on a size-by-size basis to determine if the sorting potential varies with size.

The grade-recovery relationship is calculated using a similar technique developed by Tong (2012), as described in 2.5.1.4, to assess ore sorting sensor amenability. The method in the protocol differs from the approach by Tong (2012) in that the grade-recovery relationship is determined based on the properties of individual particles *i.e.* the grade and mass of each particle in the sample.

The particles are grouped into appropriate grade categories (grade x_1, x_2, x_3…*etc.*). These grade categories represent the separation criteria that will be used in a simulated separation process. Using the selected categories, successive simulated separation tests are carried out (cf. Figure 35).

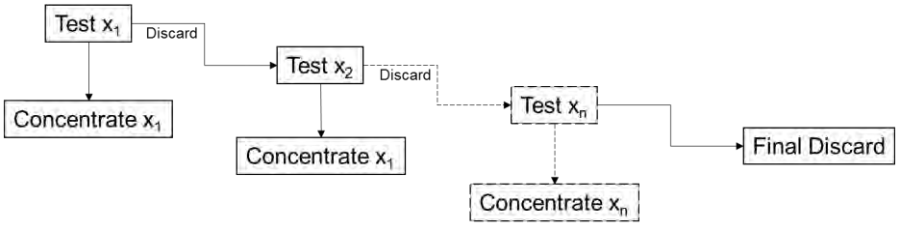

Figure 35: Simulated separation tests.

All of the particles form the feed to Test x_1 (cf. Figure 36). Particles that are more than/ or equal to the grade category for Test x_1 are removed to form Concentrate x_1. The remaining particles then form the feed to Test x_2. Tests x_1 to x_n are carried out and the remaining particles form the final discard.

The cumulative grade, recovery and mass rejection data is compared on an overall and size-by-size basis to assess the sorting potential of the ore based on intrinsic particle properties as presented in an example in Figure 36.

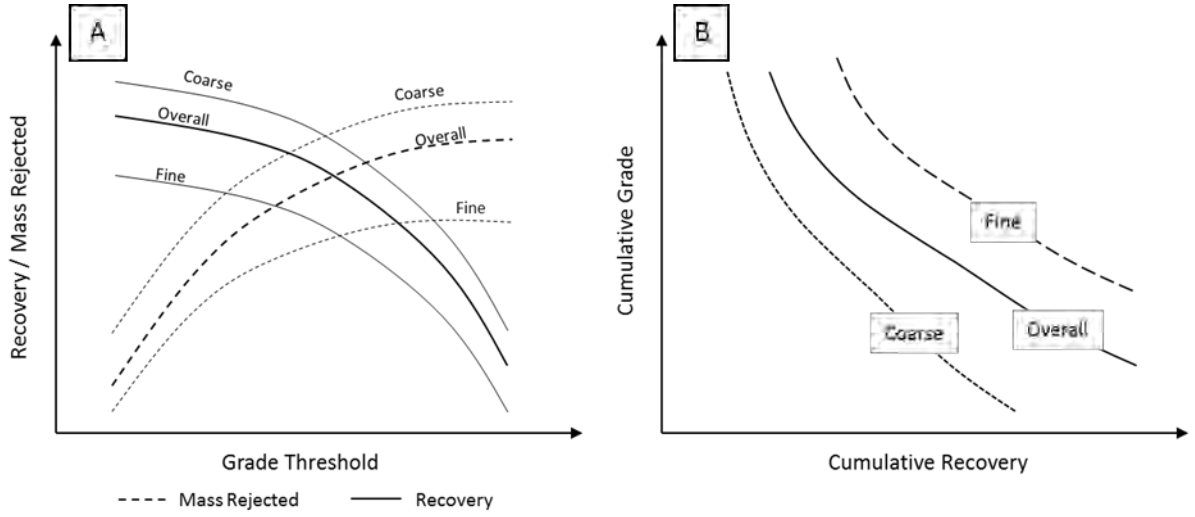

Figure 36: Example of a plot of the recovery and mass rejection per grade threshold (A) and cumulative grade-recovery curves (B).

The grade-recovery and mass rejection results are used to assess the potential economic impact of ore sorting as described in Section 3.4.2. If the ore shows good potential to be sorted at a specific size/ or overall then the next phase in the protocol (amenability test work) can commence. If the sorting potential is low at all sizes analysed then the ore cannot be effectively sorted at the current size.

Reducing the size of the material through comminution could result in improved sorting potential due to improved liberation; however, the size reduction may result in particles that are too fine for ore sorting techniques. In order to determine if changing the particle size would improve the sortability for the purposes of the protocol, the coarser size fractions can be reduced in size until the PSD is similar to the finer fractions. The sortability of material can then be assessed after reducing the particle size and comparing it with the sortability of the original fine material. It can then be concluded whether particle size reduction results in improved sortability.

3.4.2 Economic Impact of Implementing Ore Sorting

Ore sorting is implemented to either save on costs by decreasing throughput of low grade material or to increase revenue of the operation by increasing throughput. The economic impact of ore sorting will therefore be used in the protocol to quantify the ore sorting potential. The profitability of implementing ore sorting at varying cut-off grades will be calculated based on the intrinsic sortability results at this stage of the protocol. The decision to continue with the next stage of the protocol will be made based on the economic impact.

A method was developed by Lessard *et al.* (2015), as described in Section 2.4.2.4, to assess the economic impact of ore sorting. The method requires plant operational data and operating costs, this information is first used to create a baseline for the operation without ore sorting. The impact of implementing ore sorting, using varying ore sorter performance criteria (mass rejection or cut-off grades), on the existing operation is calculated based on ore sorting operational data and costs.

Many established economic analysis techniques are available in literature, the method developed by Lessard (2015) is used as an example of how to integrate an economic analysis into the protocol. The choice of economic analysis technique is dependent on the user of the protocol.

3.5 Amenability Tests

The next phase in the protocol is to determine which particle properties (sensor responses) correlate with the grade (surface/ volume). A flow diagram is presented in Figure 37 and the procedures are described in Section 3.5.1 to 3.5.3. The aim is to assess whether a sensor can accurately measure physical properties that correspond with the composition. Only a small selection of particles with varying compositions is required to assess the amenability.

The amenability of the ore to physical separation procedures can be assessed using the characterisation data that has already been collected for each particle (density, size *etc.*).

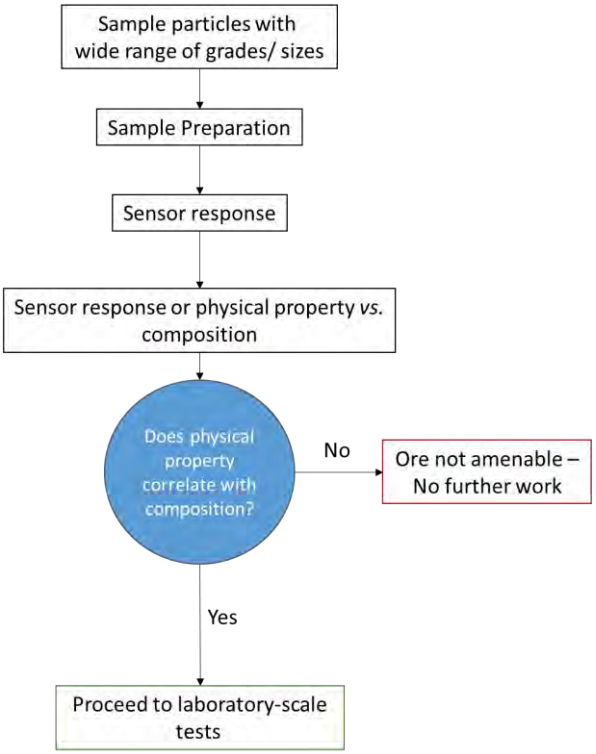

Figure 37: Flow diagram for the amenability tests. The amenability tests can be repeated if sensor technology improves for the selected sensors.

3.5.1 Sampling and Sample Preparation

Using the ore characterisation data, a selection of particles that cover a wide range of compositions are selected to assess the amenability of the ore to various ore sorting sensors. Samples may require specific sample preparation procedures depending on the sensor selected.

3.5.2 Sensor Selection and Response Tests

Appropriate sensors are selected based on the physical, mineralogical and/ or chemical data that have the potential to measure appropriate physical properties. Table 3 presents the uses of each sensor and ore types and where they are applicable. For example, electromagnetic sensors would not be tested unless there is a magnetic component within the material.

The sensor response tests are to be carried out on a laboratory-scale using ideal measurement settings for each sensor. The aim is to assess the amenability without considering the throughput required for industrial-scale ore sorting machines.

3.5.3 Particle Property-Grade Comparison

The intrinsic and measured particle properties (sensor response) are compared with the composition of each particle as indicated in an example in Figure 38. The aim is to determine which sensors can discriminate between particles of varying composition based on intrinsic or measured physical properties. Only the physical properties and sensors that show a positive, or negative, correlation with the composition will be further assessed in the laboratory-scale sorting tests (Section 3.6).

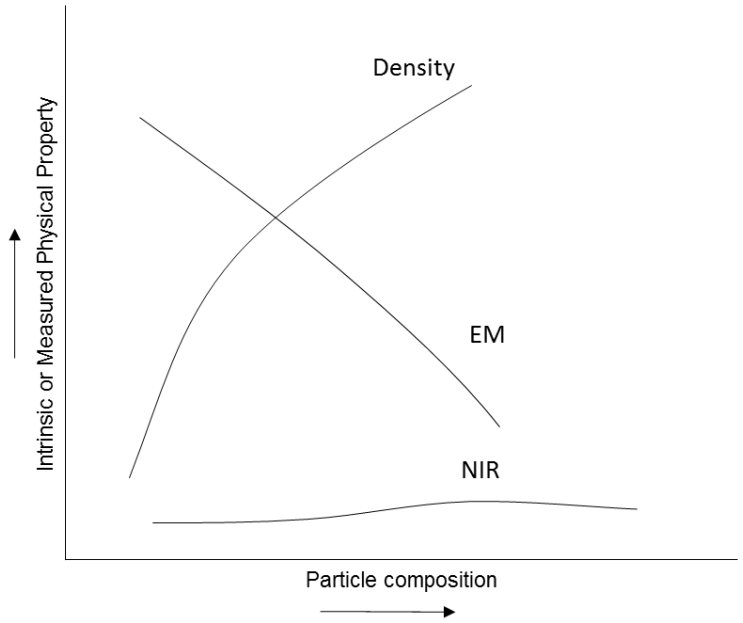

Figure 38: Particle composition vs. *intrinsic or measured (sensor response) particle properties. The NIR sensor is not applicable in this example as the sensor response does not correlate with the composition of the element/ or mineral of interest. Density and EM show a correlation between particle property and composition.*

3.6 Laboratory-Scale Sensor Sorting Tests

This section presents the methodology to determine the sorting potential of the ore on a laboratory-scale. The sensors that showed good amenability to sorting are assessed further to determine the sorting potential of the ore by analysing all of the particles in the representative sample with the selected sensor/s.

Figure 39 presents a flow diagram of the laboratory-scale sorting test procedures. The sorting tests are divided into two stages that both follow a similar procedure. In the first stage, the particles are analysed using ideal sensor measurement settings to maximise the sensor response. The aim is to determine if the sorting potential without taking into account the throughput required for actual ore sorting. If the results of the

ideal sensor tests are successful for any of the sensors then the procedure is repeated using the industrial measurement settings used during actual ore sorting.

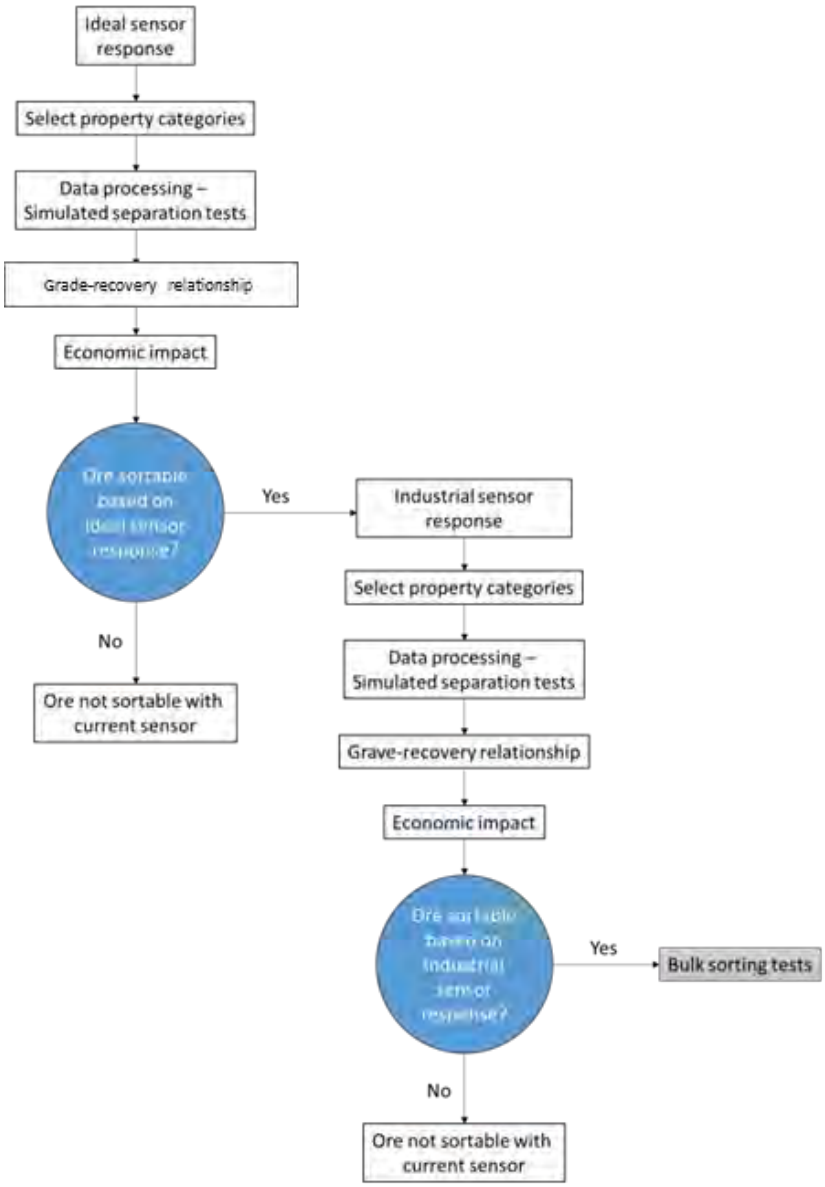

Figure 39: Flow diagram of the laboratory-scale sorting tests.

3.6.1 Sensor Response

The sample is analysed on a particle-by-particle basis using selected ore sorting sensors on a laboratory scale using both ideal responses as well as sensors using measurement parameters similar to those used on industrial ore sorting machines. For the ‘industrial’ sensor response it may be necessary to develop an algorithm that estimates the grade of the particles based on the sensor response.

3.6.2 Data Processing and Grade-Recovery Relationship

The particle data is grouped into sensor response categories for each sensor for the ideal/ industrial sensor tests. Using a similar method as in Section 3.4, the grade and recovery relationship is calculated for the elements of interest based on the sensor response categories instead of grade. The cumulative grade, recovery and mass rejection data is calculated and can be plotted for comparison (cf. Figure 40). The cumulative grade, recovery and mass rejection data is then used to assess economic impact of sorting based on the intrinsic, ideal sensor and industrial sensor response data as presented in Section 3.6.3.

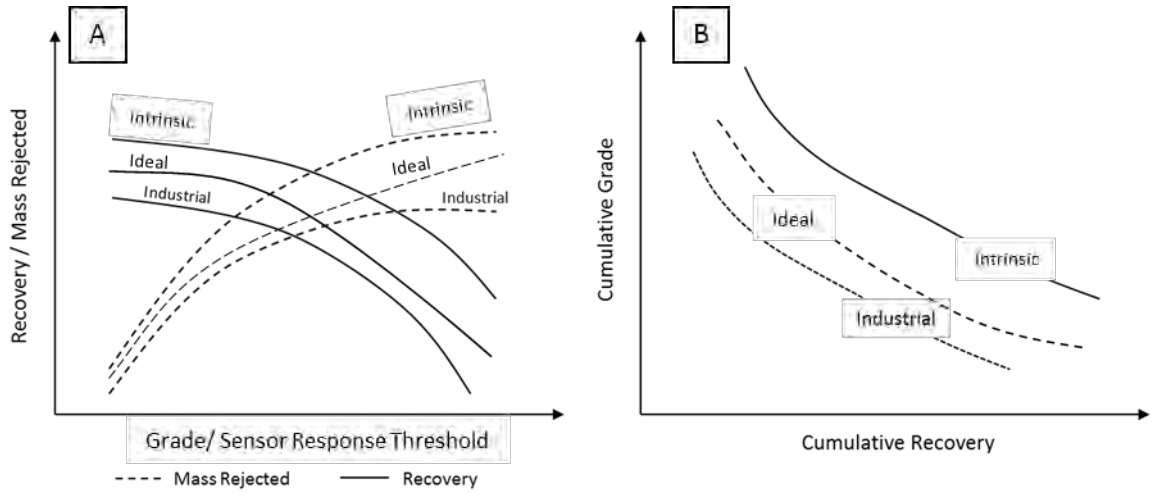

Figure 40: Example of a plot of the recovery and mass rejection per sensor response threshold (A) and cumulative grade-recovery curves (B) for the intrinsic and laboratory-scale sorting tests using both ideal and industrial sensor response data.

3.6.3 Economic impact

The economic impact based on the ideal laboratory-scale sensor response tests is quantified to determine the ore sorting potential using the methods described in Section 3.4.2. The results are calculated based on the different sorting criteria for each sensor and not the cut-off grades as used for the intrinsic sortability.

If sorting is economically feasible using ideal sensor responses then the industrial sensor response is assessed in terms of the economic impact. The economic impact will be used to motivate for further bulk sorting tests, this stage is beyond the scope of the current research.

3.7 Protocol Summary

The protocol methodology to assess the ore sorting potential of a particulate ore has been detailed in this chapter.

The number of particles required is first established using TOS or the binomial distribution method. Ideally, a sample should be collected using TOS as the intrinsic heterogeneity of particles is taken into account allowing for more accurate grade-recovery data. The binomial distribution method can be used if it is not feasible to analyse the number of particles using TOS; this will give an indication of the amenability of the ore to sorting.

The ore sample is characterised and the ideal grade-recovery relationship is established if a perfect separator existed *i.e.* the intrinsic sortability. The potential economic impact of sorting based on the intrinsic sortability is determined at this stage to assess the feasibility of applying ore sorting.

If the ore shows good economic potential based on intrinsic sortability then the amenability of the ore to various ore sorting sensors will be assessed. A smaller selection of particles with varying composition are analysed and the sensor response is compared with the composition of each particle.

Sensors that show good amenability will be further tested by analysing the entire representative sample with the selected sensors on a laboratory scale. The particles are first analysed by the selected sensors using ideal measurement parameters to maximise the sensor response and the grade-recovery relationship is established. The sensors that show good sorting potential based on the ideal sensor response will be further assessed by analysing the sample using industrial sensor measurement parameters on a laboratory-scale and the grade-recovery relationship is determined.

The economic impact will be determined based on the laboratory-scale sorting tests to determine the potential financial benefits of ore sorting. These results will be used to assess the feasibility of conducting bulk ore sorting tests using automated sorting machines.

Chapter 4

Experimental

The sortability of the Los Bronces ore was assessed using the protocol developed during the current research. This chapter describes the experimental procedures used for the Los Bronces case study. The sorting duty was described previously in Section 1.2. The ore sample is discussed in Section 4.1. Particle characterisation using the XMT and XRF are discussed in Section 4.2 as well as the statistical validation methods used to assess the results. The procedures to determine the intrinsic sortability of the Los Bronces sample is presented in Section 4.3. The laboratory-scale ore sorting test procedure is discussed in Section 4.4.

4.1 Ore Sampling

Previous ore sorting test work was conducted at Anglo American on a 316 kg sample of Los Bronces SAG mill oversize pebbles. The sample was screened at 20 mm for the original test work. The -20 mm material was discarded as it was considered too fine for efficient ore sorting.

Only the +20 mm size range of the material was considered for the protocol development. The particles were visually inspected and one hundred pebbles were collected for the case study; each particle was labelled for identification. The aim was to have a wide range of copper grades and particle sizes.

4.2 Particle Characterisation

Particle characterisation was carried out on the Los Bronces 100 pebble sample. The pebbles were characterised in terms of their physical properties (density, mass and volume), bulk mineralogy and surface chemical composition.

The methods used to determine the physical properties of each particle are presented in Section 4.2.1. The development of the XMT to determine the mineralogy of the Los Bronces pebbles is discussed in Section 4.2.2. The procedures to determine the

surface chemical composition by XRF are presented in Section 4.2.3. Statistical validation methods are described in Section 4.2.4.

4.2.1 Measurement of Physical Properties

The density of each of the 100 pebbles was determined using Archimedes' Method where the mass of each pebble was determined in air and in water. The density was determined using Equation 11 and the volume was then calculated using Equation 12. The total mass of the 100 pebble sample was ~8.6 kg. The density of the particles ranged from 2.48 to 3.28 g/cm^3.

$$\frac{Density\ of\ object}{Density\ of\ fluid} = \frac{Weight\ of\ object}{Weight\ of\ displaced\ fluid} \quad [11]$$

$$Density = \frac{Mass}{Volume} \quad [12]$$

The equivalent spherical diameter (ESD) was used in the case study as a measure of the particle size. Equation 7 was used to determine the diameter (d_V) based on the pebble volume (V) calculated using Equation 13. The ESD for the 100 pebbles ranged from 27 mm to 49 mm.

$$d_V = \sqrt[3]{\frac{6V}{\pi}} \quad [13]$$

4.2.2 Development of the XMT for Mineralogical Characterisation

X-ray Micro-tomography (XMT) is an analysis technique that produces 3-dimensional images of the internal structures of multiphase solid objects. The technique measures the X-ray attenuation coefficients of the irradiated object to produce 2-dimensional projections. Multiple projections are reconstructed into 3-dimensonal images that are analysed using image analysis techniques. The technique can be used to quantify both the volumetric and surface mineral composition.

During the initial test work on the Los Bronces ore sorting project at Anglo American, the XMT technique was selected to be developed in an attempt to determine the

pebble mineralogy. The method development was based on the work of Hsieh (2012) which describes the procedures and analysis using the XMT.

The XMT was chosen for development as it is a non-destructive technique. The pebbles could not be destroyed for the characterisation as they needed to be kept for future ore sorting sensor test work. This section describes the method developed to analyse the pebbles on the XMT along with the results and conclusions on the technique.

The pebble sample and sample preparation is described in Section 4.2.2.1. The XMT data collection is discussed in Section 4.2.2.2. The data processing techniques are presented in Section 4.2.2.3. A discussion and conclusions on the XMT technique are given in Section 4.2.2.4.

4.2.2.1 Sample and Preparation

A set of 34 Los Bronces SAG-mill oversize pebbles was used for the development of the XMT to estimate the volumetric and surface modal mineralogy. Only 34 pebbles were analysed within the time frame allowed. Pebbles were selected to include as many distinguishable rock types as possible. The XMT requires little sample preparation and is a non-destructive technique. Pebbles were placed in a plastic container and were held in position with polystyrene as not to allow movement of the pebble during the analyses as shown in Figure 41. The plastic components were removed as background during image analysis.

4.2.2.2 Data Collection

The pebbles were analysed using an Xradia Versa 520 X-ray microscope, Figure 41 shows the instrument configuration used for the Los Bronces pebbles. A summary of the analysis parameters are given in Table 6 and the methods to determine these parameters are discussed.

Table 6: XMT analysis parameters.

Power		Filter	Exposure time (s)	Number of projections per analysis	Objective lens	Source WD (mm)	Detector WD (mm)	Resolution (µm)
kV	W							
160	10	2mm Pb-glass	6.0	3601	0.4X	215.9	47.7	60

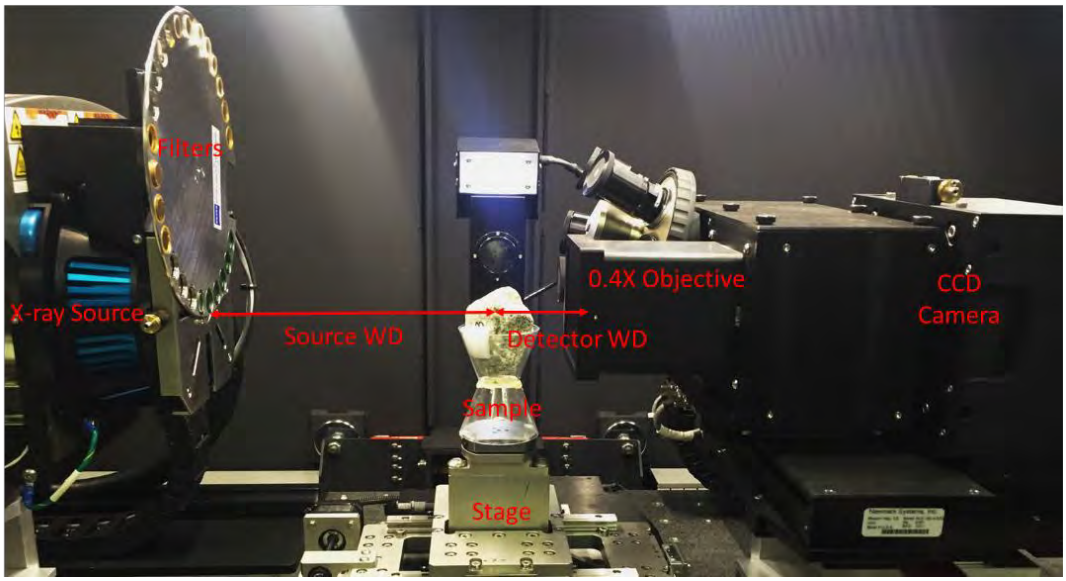

Figure 41: XMT instrument configuration for Los Bronces pebble analysis.

The objective lens with the lowest magnification (0.4X) was used for the analyses due to the pebble size. The sample was first centred by adjusting the stage along the x, y and z axes. The working distance (WD) of the X-ray source and detector was then adjusted so that the pebbles would fit into the field of view (FOV) as shown in Figure 42. It was found that pebbles did not always fit into the field of view along one of the axes. Some of the pebbles therefore required two tomographic analyses that were stitched into a single image during reconstruction.

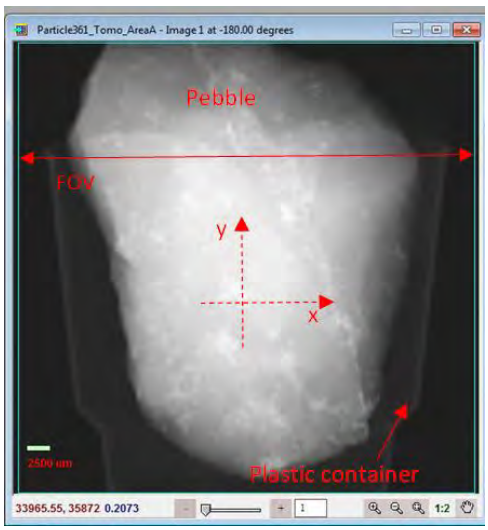

Figure 42: X-ray projection of a pebble indicating the field of view (FOV) and the direction of the stage axes.

The next step was to determine the power settings and filter to be used in order to optimize the X-ray transmission without overexposure of the detector. The X-ray transmission was initially determined using power settings of 140 kV and 10 W (Hsieh,

2012). The sample was first moved out of the FOV and projections were taken of air using different exposure times until the X-ray counts were sufficient without overexposure of the detector (~5000 counts). Overexposure for 0.4X detector is ~30,000 X-ray counts. The sample was then placed in the FOV and a projection was taken using the same settings as for air. The X-ray transmission was determined by dividing the X-ray counts of the sample projection with the counts of the air projection. The X-ray transmission through the sample was calculated to be ~15 %. A 2 mm lead glass filter was selected using the standard procedures (Xradia, 2010) to determine the filter required. The kV was then adjusted with the filter in place until sufficient X-ray transmission through the sample was achieved (~20 %).

The number of projections was selected to minimize the noise of the tomographic images whilst allowing the analyses to be completed within a reasonable turnaround time. The analyses took 6-12 hours per pebble depending on the number of tomographies required.

4.2.2.3 Data Processing

The raw X-ray projection data was submitted to the Julius Kruttschnitt Mineral Research Centre (JKMRC) where it was used to develop an automated data processing application for the pebble analysis. The processing steps include calculating the centre-shift, beam hardening correction factors and image analysis procedures are presented in Sections 4.2.2.3.1 to 4.2.2.3.3. Using these correction factors, tomographic reconstruction was done on all the pebbles using the same parameters to produce 16-bit grey-scale tomographic images. The image analysis procedures are presented in 4.2.2.3.3.

4.2.2.3.1 Centre Shift Correction

The FOV is not always centred on the object during analysis and a centre shift correction must be calculated. A single slice of a pebble is reconstructed using a range of centre shift step sizes and a reconstructed image is generated for each one (cf. Figure 43). The step size is equivalent to the voxel resolution. Each of the images is examined to determine which one is the most focussed and the centre shift of that image is used during reconstruction. A centre shift of ~0.6 was calculated.

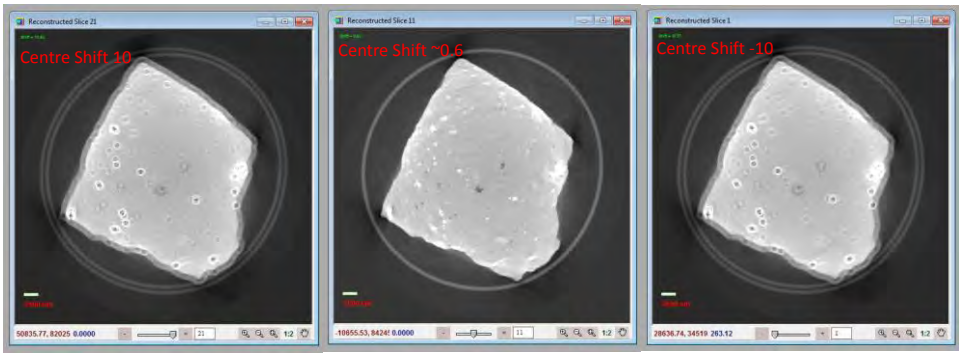

Figure 43: Determination of the centre-shift correction factor.

4.2.2.3.2 Beam Hardening Correction

The beam hardening correction factor is calculated to ensure that the grey level is uniform across the reconstructed slices. A slice of the pebble was reconstructed using different beam hardening constants. The X-ray attenuation is plotted across the slice as shown in Figure 44. The images are assessed to determine which beam hardening constant results in uniform attenuation across the slice. This number is then used for reconstruction of the tomographic image. The beam hardening constant was determined to be 0.2 for the pebbles.

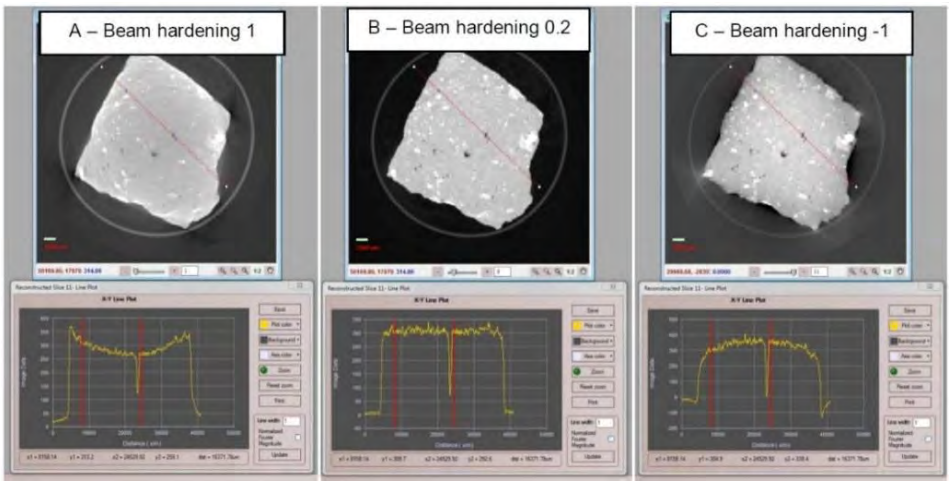

Figure 44: Determining the beam hardening correction factor.

4.2.2.3.3 Image Analysis

Using the reconstructed data, image analysis to determine the mineralogical composition was done using a software application that automatically filters and calculates the mineral content. The image is first smoothed using a non-local means filtering algorithm that reduces noise allowing for better discrimination between areas of differing grey level.

It was found by visual inspection of the pebbles and the reconstructed images that the grey levels of some of the minerals were very similar and could not be resolved using image analysis. All of the identified base-metal sulphides, including pyrite (FeS_2) and chalcopyrite ($CuFeS_2$), as well as iron oxides had similar grey levels. This is as a result of the minerals having a similar attenuation co-efficient. The results are therefore reported as mineral (BMS + Fe-oxide) and gangue (silicate) content.

The images were divided into grey level bands (cf. Table 7) that represent the background, mineral and gangue composition respectively. The software was also able to estimate the area per cent mineral content exposed on surface. The volumetric and surface mineral content was compared to determine if surface mineralisation was similar to bulk mineralisation of the pebbles.

Table 7: Grey level bands representing different mineral phases

Grey-level Band Range	Likely mineral type
<7000	Background
≥7000<15000	Gangue (quartz, feldspar *etc.*)
≥15000	Mineral (BMS/Fe-oxides)

4.2.2.4 Results, Discussion and Conclusions

The results of the volumetric and surface mineral content are compared in Figure 45. It was found that the volume and surface area percent of BMS/Fe-oxide mineralisation showed a good correlation. The correlation between the surface and volumetric composition indicates that the mineralisation is evenly distributed/ disseminated. Based on these results it was decided that the pebbles would be characterised in terms of the surface composition as described in Section 4.2.3 using XRF.

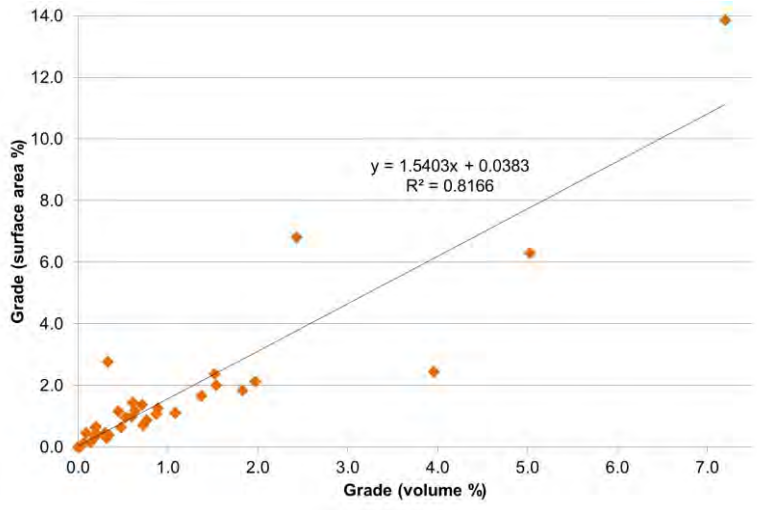

Figure 45: Volumetric vs. surface mineralisation as determined by XMT.

4.2.3 XRF Methodology

The XRF technique was used to determine the surface composition/ grade of each pebble. The average surface chemical composition was determined by analysing a statistically valid number of points on the surface. It was found that the copper grade ranged between ~0.1 % and ~2.2 % copper. The overall grade of the sample was 0.44 % Cu.

The experimental procedures included the calibration of the XRF instrument, as described in Section 4.2.3.1, to minimize matrix effects during analysis. Section 4.2.3.2 discusses the methods used to determine the minimum analysis period per XRF point to achieve accurate results. Section 4.2.3.3 discusses how the minimum required number of XRF points per pebble was determined to estimate the average surface composition. Section 4.2.3.4 presents the statistical validation and Section 4.2.3.5 discusses the determination of proxy elements for copper based on the XRF results.

4.2.3.1 XRF Calibration

Matrix effects are introduced when analysing ore material using the XRF unless a sample preparation technique is used where the material is homogenised. The fusion glass bead method is one such technique (Demir *et al*., 2006). Matrix effects are introduced due to differences in mineral grain size, particle heterogeneity and mineralogical effects. Mineralogical effects occur as a result of elements occurring in different minerals, the sensitivity of the XRF to these elements may be different depending what mineral phase they occur in. The XRF must therefore be calibrated to minimise the matrix effects.

Ten samples of varying composition from the Los Bronces operation were selected to use for the calibration. The samples were originally collected as part of a circuit survey at the Las Tortolas flotation plant. These samples were selected as they had a wide range of chemical compositions as determined by chemical assay. A representative portion of each sample was prepared into a pressed powder pellet using an automated sample preparation instrument that mills, binds and presses the material into steel sample holders. The samples were first analysed by HH-XRF using the standard factory calibration; these factory calibrations do not consider any matrix effects.

Scatter plots comparing the XRF and chemical assay results for the elements of interest are presented in Figure 46, the calibration factor was calculated for Cu, Fe, Si, Al, and S. The slope and intercept of the trend lines represent the calibration factors. These factors are recorded on the XRF and are used to correct for matrix effects during analysis.

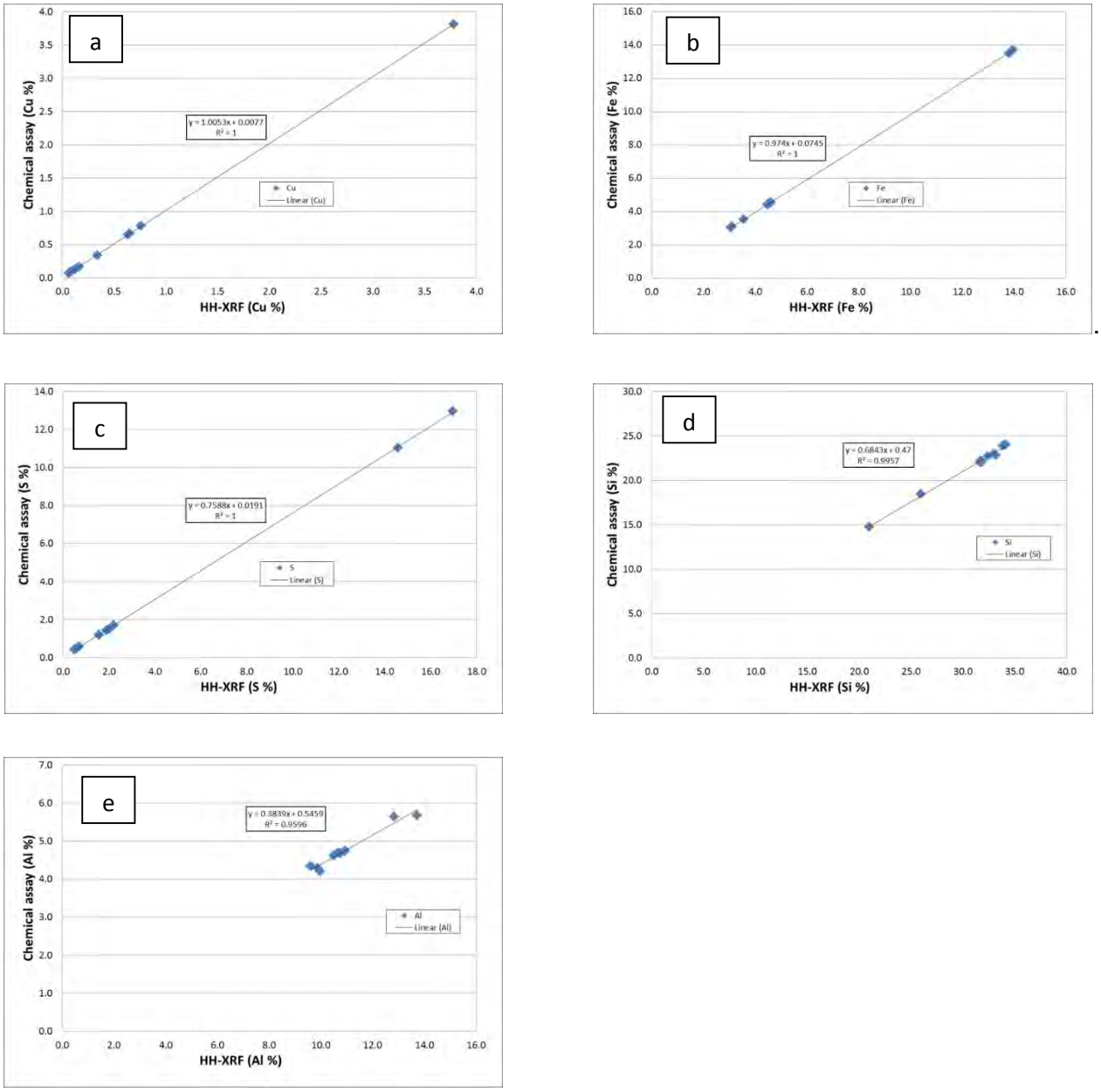

Figure 46: Calibration curves for Cu, Fe, S, Si and Al (a, b, c, d, and e respectively).

4.2.3.2 Minimum Analysis Period

It was necessary to determine the minimum analysis period required in order to optimize the data collection process. The same Los Bronces sample was analysed three times each at different time intervals; the intervals included 30, 60, 90, 120, 180, 225, 270 and 360 seconds. The analysis period determined here focusses on Cu and Fe content as the mineral of interest in the pebbles is chalcopyrite ($CuFeS_2$).

The average grade determined at the varying time intervals for Cu and Fe is plotted in Figure 47. The grade determined after 90 seconds had reached an acceptable level of error. The relative standard deviation for Cu and Fe was 0.13 % and 0.38 % respectively for the 90 second analyses.

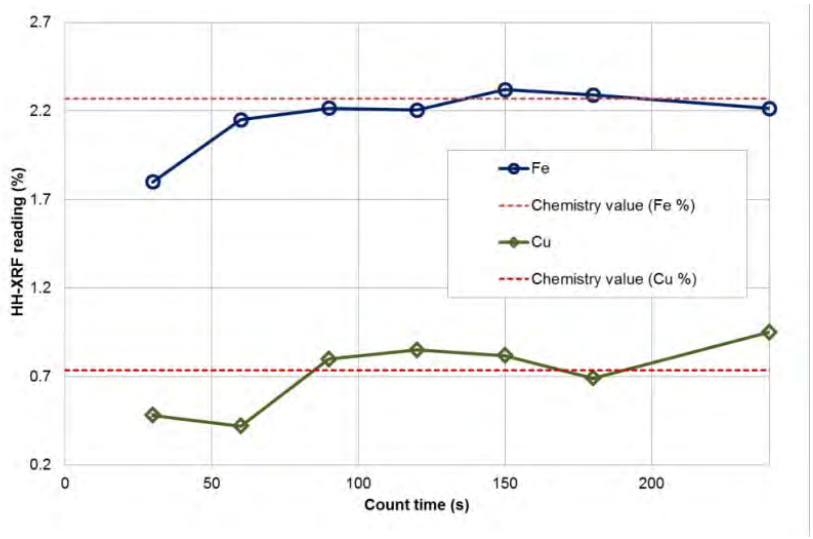

Figure 47: HH-XRF Fe and Cu reading at varying analysis periods.

4.2.3.3 Minimum Analysis Points

The number of analysis points required to determine the surface chemistry of the pebbles was statistically validated using a method based on bootstrap resampling. In the case study, the number of analyses used to determine the surface chemistry was validated based on the copper grade determined for each analysis point. The copper grade of hundreds of points from one pebble was entered into the resampling spread sheet created by Wood (2011); the method is described in Section 2.3.5.1. The number of analyses required was determined to be between 30 and 50 analyses (depending on size) to achieve an RSD of 10 % that was considered acceptable for the case study.

4.2.3.4 Statistical validation

The statistical validation of the copper content was determined using a method based on bootstrap resampling as described in Section 2.3.5.1 (Evans *et al.,* 2013). The relative standard deviation (RSD) for copper content was determined based on 200 resamples using resample sizes of 10, 20, 30, 40, 50, 60, 70 and 80 particles. The RSD% for the various resample sizes are plotted in Figure 48.

The results indicate that the RSD for the copper content in the pebbles is below 10 % when ~40 random particles are analysed. Based on the regression curve the error on the copper content when analysing 100 pebbles was ~5 % RSD.

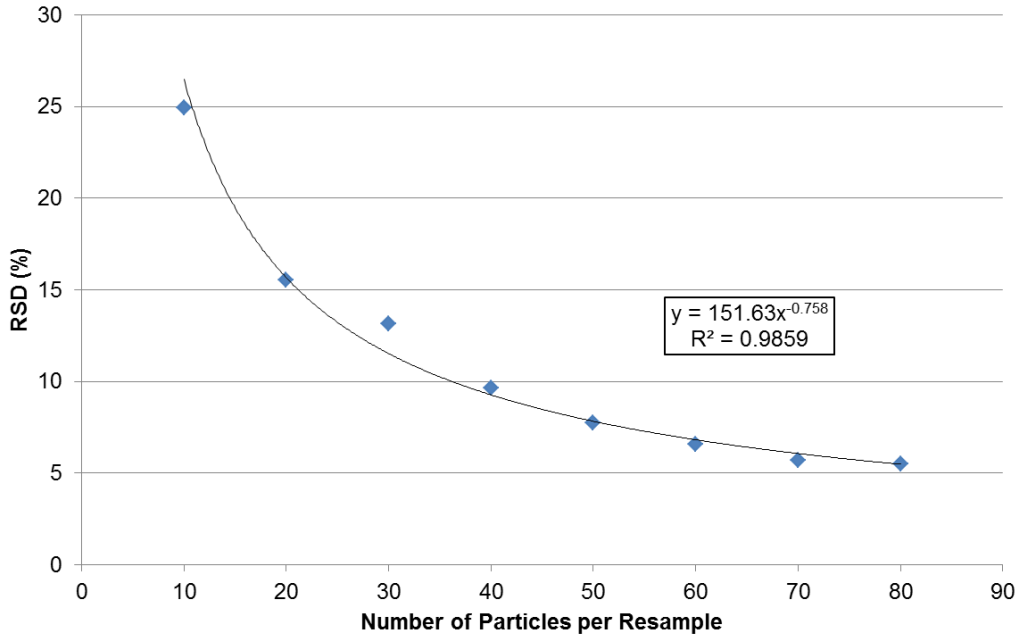

Figure 48: Regression curve for the Cu grade determined using the hand-held XRF.

4.2.3.5 Proxy Elements for Copper Grade

The copper grade was compared with the elemental composition to assess if there are any proxy elements that correlate with the copper content. The measurement of proxy element compositions could potentially be used to sort the ore. The copper grade is compared with the iron and sulphur content in Figure 49 whilst the silicon and aluminium content is compared in Figure 50. It was determined, based on the elements analysed, that there are no robust proxies for copper grade that could be used to sort the ore.

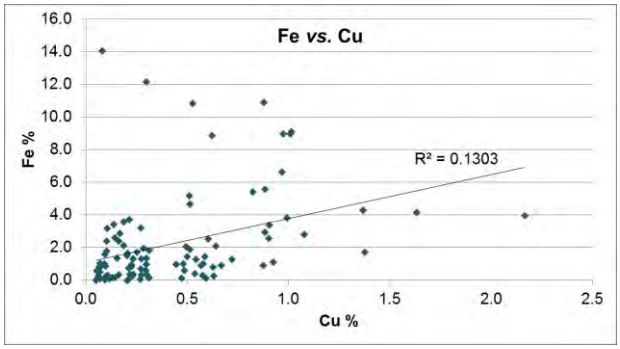

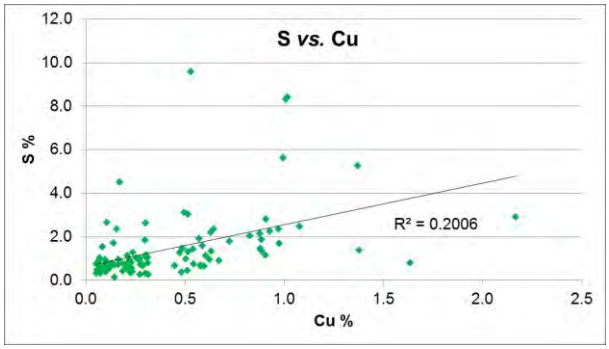

Figure 49: Cu grade vs. *Fe, and S composition.*

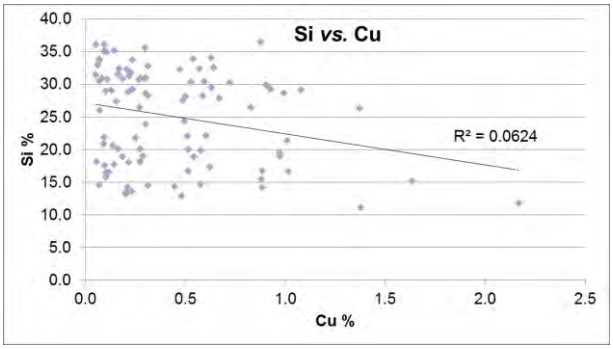

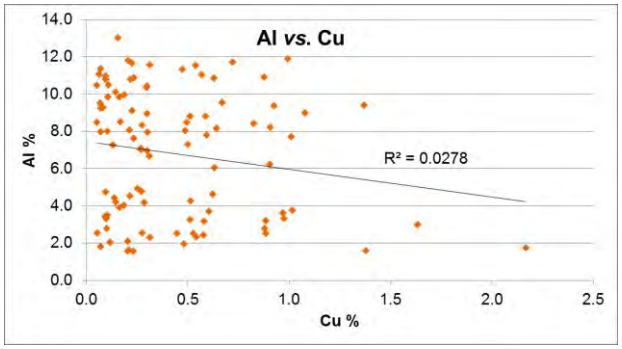

Figure 50: Cu grade vs. *Si and Al composition.*

4.3 Intrinsic sortability

The intrinsic sortability was determined using the methods described in Section 3.4. The pebbles were divided into two size classes (+40 mm and -40 mm) based on their ESD for the analysis to determine if the sortability differed based on size. The size distribution indicated that there was a 50 % split between the selected fractions. The intrinsic sortability was determined on an overall and size-by-size basis using the copper grades and masses of each pebble.

The data was processed in five successive simulated separation tests. For Tests 1 to 5, the pebbles were grouped by copper grade into five grade thresholds: 1.0 %, 0.8 %, 0.6 %, 0.4 % and 0.2 % Cu respectively. Figure 51 presents a flow diagram of the test procedure. The discrete and cumulative grade, recovery and mass rejection data was calculated based on the intrinsic particle properties. Cumulative recovery and mass rejection data per copper grade threshold was plotted along with cumulative grade-recovery curves to assess the data.

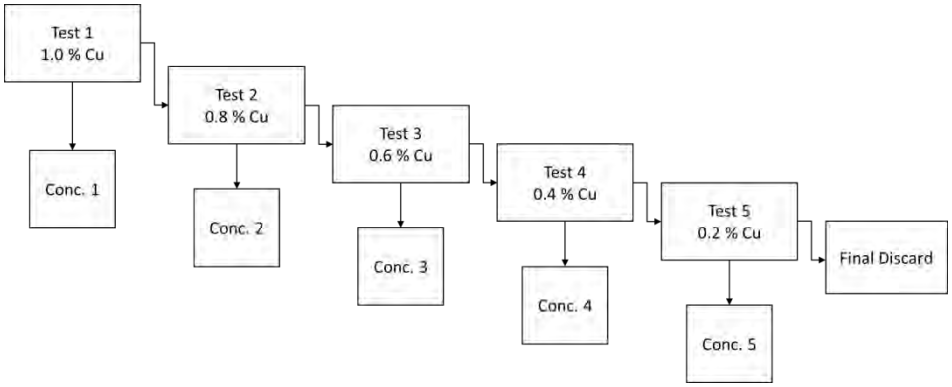

Figure 51: Intrinsic sortability tests.

The economic impact of implementing ore sorting was assessed using the methods described in Section 3.4.2 using the different Cu cut-off grades from each test described in Figure 51. The operational data used to assess the economic impact represents that of a typical copper operation.

4.4 Ore Sorting Amenability Tests

The amenability of the 100 pebble sample to physical and sensor-based ore sorting was determined using the techniques described in Section 4.4.1 and 4.4.2 respectively.

4.4.1 Amenability to Physical Sorting

The size (ESD) and density of each pebble was compared with the copper grade to determine if pebbles were amenable to sorting by size classification or gravity separation techniques.

4.4.2 Amenability to Sensor-Based Sorting

The sensor selection for the case study is discussed in Section 4.4.2.1 and the ideal laboratory-scale sensor analysis parameters are described in Section 4.4.2.2.

4.4.2.1 Sensor Selection

The selection of sensors for the case study was based on the description of the Los Bronces deposit (Warnaars, 1985). The sensor potential for each of the selected sensors for the case study is detailed in Table 8.

Table 8: Comparison of sensor type, properties measured and potential to sort Los Bronces ore.

Sensor	Properties measured	Sensor potential for Los Bronces
Colour	Colour	Colour may correlate to grade based on the alteration mineral content (*i.e.* black tourmaline may correlate with copper grade)
EM	Magnetic susceptibility	The samples contain iron oxides that are potentially ferromagnetic, could relate to copper grade
XRT	Atomic density	BMS rich pebbles may be more dense, BMS content could relate to grade
NIR	Absorption	Alteration silicate content, determined by the NIR sensor, could be indicative of grade
XRF	Elemental composition	Copper content could potentially be measured as well as possible proxy elements

4.4.2.2 Sensor Response Measurements

The one hundred pebble set was submitted to Tomra, an ore sorting sensor supplier, to determine the amenability of the ore to various ore sorting sensors on a laboratory-scale under ideal conditions. Sensors included optical, EM, NIR, XRF, XRT. The sensor measurement parameters are described in Table 9.

Table 9: Laboratory-scale sensor response parameters for the amenability tests using NIR, XRT, XRF, optical and EM sensors.

Sensor	Area measured	Number of measurements	Number of sides measured
Optical	Entire surface	2	2
EM	20-30 mm spot	2	2
NIR	Single surface	1	1
XRF	~10 mm spot	2	2
XRT	Entire volume	1	-

4.4.2.2.1 Optical Sensor Response

The optical sensor collected particle images in YUV colour space, images were collected on two sides of each pebble. The pixels were classified as either white, black, grey or brown. The area percent of each colour was calculated for each pebble.

4.4.2.2.2 Electromagnetic Sensor Response

The electromagnetic sensor determined the magnetic susceptibility for each pebble on a 20-30 mm spot on two sides of each pebble. The technique measures minerals that are ferromagnetic. The Los Bronces pebbles did not show any response with the EM sensor as the iron oxide present in the pebbles was hematite, as confirmed by XRD, which is not ferromagnetic.

4.4.2.2.3 Near-Infrared Sensor Response

The NIR sensor was used to analyse the infrared absorption between 800 nm and 2780 nm of the electromagnetic spectrum. The absorption of radiation in the NIR spectrum is dominated by OH, H_2O, CO_3 and NH_4. The technique could not be used for the Los Bronces case study as the base-metals were below the detection limit for the technique. In order to use the NIR sensor for the Los Bronces case study, there needed to be a correlation between the alteration silicate and copper content. The NIR spectra for the pebbles were very similar and it was not possible to estimate the alteration silicate content.

4.4.2.2.4 X-Ray Fluorescence Sensor Response

The XRF sensor was used to analyse the pebbles on two sides using a relative large spot size of ~10 mm. The X-ray counts for copper were recorded and the number of copper counts per area was calculated.

4.4.2.2.5 X-Ray Transmission Sensor Response

The XRT sensor measured the X-ray attenuation across the entire volume of each pebble and projection images were collected in grey-scale. The grey level intensity is indicative of density. The grey level images were converted to binary images and the amount of low-density and high-density material was calculated.

4.5 Laboratory-Scale Sensor Sortability

The sensors that were amenable to sorting of the Los Bronces pebbles (XRF and XRT) were further assessed in this section to assess the sortability of the ore. The sortability of the one hundred pebble sample was first calculated using ideal XRF and XRT sensor measurement parameters as described in Section 4.5.1. The laboratory-scale sensor response was then calculated using sensor measurement parameters that would be used on industrial-scale XRF ore sorting system as discussed in Section 4.5.2.

4.5.1 Ideal Laboratory-Scale Sortability

The aim was to determine the potential of the ore sorting sensors without taking into account the throughput of material that would be necessary for actual ore sorting operations. If the sortability is poor using ideal sensor response then it will not work on an industrial-scale. The sensor response categories selected for the XRF and XRT are described in Section 4.5.1.1. The means to determine the grade recovery relationship are presented in 4.5.1.2.

For the case study, all of the one hundred pebbles were analysed during the amenability test work phase. This section therefore describes the methods to calculate the grade recovery relationship based on the results for the XRF and XRT ore sorting sensors analysed in Section 4.4.2.

4.5.1.1 Sensor Response Categories

The sensor response categories used to calculate the grade recovery relationship for the XRF and XRT sensors are presented in Table 10.

Table 10: XRF and XRT sensor response categories.

Sorting Test Number	Sensor Response Category	
	XRF - CPA Cu	XRT - % high density
1	>=0.0020	>30%
2	>=0.0016-0.0019	20-30 %
3	>=0.0012-0.0015	10-20 %
4	>=0.0008-0.0011	5-10 %
5	>=0.0004<0.0008	3-5 %
Discard	<0.0002	<3 %

4.5.1.2 Data Processing and Grade-Recovery Relationship

Using a similar approach to determining the intrinsic sortability, the pebble data was processed based on the XRF and XRT sensor response categories instead of copper grade. Using the XRF and XRT sensor response categories and the particle characterisation data, five successive simulated separation tests for each sensor were calculated. Figures 52 and 53 present the simulated separation tests for the XRF and XRT sorting tests respectively.

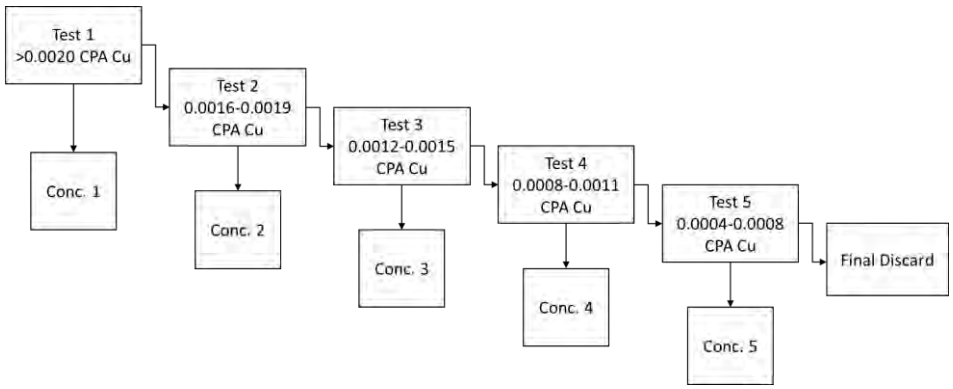

Figure 52: Simulated sorting tests for the ideal laboratory-scale sorting tests indicating the sensor response categories.

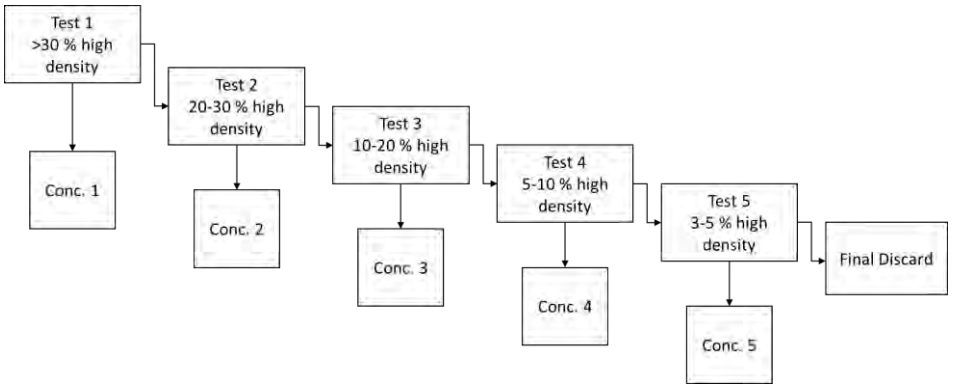

Figure 53: Simulated sorting tests for the ideal laboratory-scale sorting tests indicating the sensor response categories.

4.5.1.3 Economic Impact Based on Ideal Sensor Response

The economic impact of implementing ore sorting was assessed using the methods described in Section 3.4.2 using the various sorting criteria for the XRF and XRT sensors as described in Figure 52 and 53.

4.5.2 Industrial-Scale Sortability

Based on the ideal laboratory-scale sorting tests, the XRF was selected for further assessment by determining the sortability based on the industrial scale sensor response. A set of Los Bronces pebbles for algorithm development as well as the 100 pebbles from the case study were submitted to Rados to assess their XRF sensor. Rados conducted amenability tests using their XRF sensor and established that an algorithm needed to be developed, the algorithm development and amenability tests are discussed in Section 4.5.2.1. The sensor measurements are discussed in 4.5.2.2 and the procedures to assess grade recovery relationship are described in Section

4.5.2.3. The economic impact of industrial-scale sorting are discussed in Section 4.5.2.4

4.5.2.1 Algorithm Development

Rados developed a sorting algorithm using 27 Los Bronces SAG-mill oversize pebbles. The pebbles were crushed and milled and a portion of the milled material was split out and submitted for chemical analysis. Approximately 100 g of the remaining pulp was combined with ~30 g of resin and hardener to create a briquette of homogenised material of known grade.

Each briquette was then analysed using the XRF sensor that measures the number of fluorescent photons (counts) for the element of interest (β) and the number of backscattered X-rays (N_s). The ratio for $100*(\beta_{Cu}/N_s)$ was calculated to be directly proportional to the copper composition determined by chemical assay. The sensor response *vs.* copper assay results for each briquette were plotted to determine the calibration factor (cf. Figure 54) to estimate the copper content from the sensor response. The estimated copper content based on the sensor response is calculated using Equation 14.

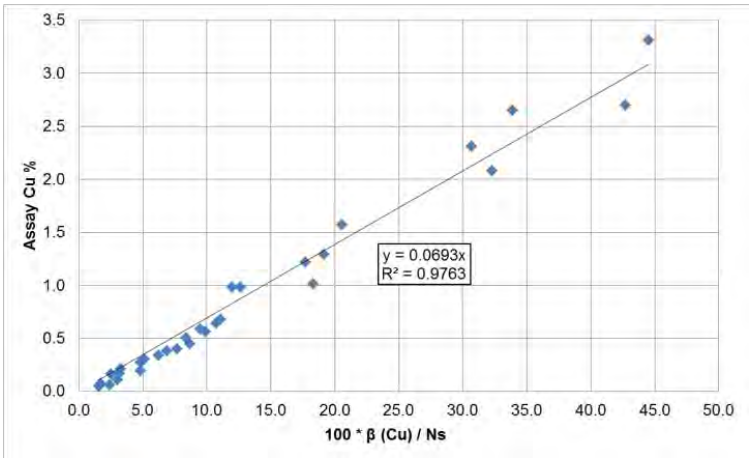

Figure 54: Copper content determined by assay vs. *the XRF sensor response ($100*\beta_{Cu}/N_s$). The linear trend line equation represents the calibration factor to estimate copper content based on the XRF sensor response.*

$$Estimated\ Cu\ content = \left(100 \times {}^{\beta_{Cu}}/_{N_S}\right) \times 0.0693 \qquad [14]$$

4.5.2.2 Industrial Sensor Response

The 100 pebble set was analysed using the Rados XRF sensor using industrial-scale sensor analysis parameters similar to those used for the algorithm development. Pebbles were fed from a vibratory feeder and were individually analysed as they fell past the XRF sensors. The analysis time ranged from 20 to 84 milliseconds. The estimated copper content was calculated using Equation 2 and was compared to the copper grade determined during the particle characterisation phase of the protocol.

4.5.2.3 Data Processing and Grade-Recovery Relationship

A similar approach used in Section 4.3 to assess the intrinsic grade recovery relationship was used to assess the sortability of the 100 Los Bronces pebbles using industrial-scale parameters.

The pebbles were grouped by copper grade into five grade thresholds based on the calculated copper grade from the XRF sensor; groups included 0.2 %, 0.4 %, 0.6 %, 0.8 % and 1.0 % calculated copper. The data was then processed based on the calculated grade thresholds in five successive simulated separation tests using a similar approach as described in Figure 51.

4.5.2.4 Economic Impact Based on Industrial Sensor Response

The economic impact of implementing ore sorting was assessed using the methods described in Section 3.4.2 using the XRF sorting criteria (0.2 %, 0.4 %, 0.6 %, 0.8 % and 1.0 % calculated copper).

4.6 Summary

The 100 pebble ore sample was selected based on visual appearance as to include a wide range of grades and pebble sizes. Only the +20 mm size range of the material was considered for the protocol development.

The physical properties including density, mass and volume were calculated using Archimedes' method. The total mass of the 100 pebble sample was ~8.6 kg. The density of the particles ranged from 2.48 to 3.28 g/cm^3. The particle size was determined based on the volume by calculating the ESD of each particle. The ESD for the 100 pebbles ranged from 27 mm to 49 mm.

The XMT was used to characterise the Los Bronces pebbles in terms of the volumetric and surface mineralogy. The results indicated that the surface and volumetric mineralisation showed a good correlation

It was decided that the pebbles would be characterised by measuring the surface chemical composition by XRF. A statistically accurate method was developed to determine the surface chemical composition. It was found that the copper grade ranged between ~0.1 % and ~2.2 % Cu. The overall grade of the sample was 0.44 % Cu. The error in copper content when analysing 100 pebbles was ~5 % RSD. The copper grade was also compared to the Fe, S, Si and Al content to establish if proxy elements could be used to assess the sorting potential. No proxy elements for Cu grade were established.

The intrinsic sortability and economic impact were established for the Los Bronces case study at different cut-off grades using the methods described in Section 3.4.2.

Ore sorting sensor amenability tests were conducted using colour, EM, XRT, NIR and XRF sensors. Only the XRT and XRF sensors showed a good correlation with Cu grade.

The XRF and XRT sensors were used in the next stage of the protocol to establish the sorting potential based on ideal laboratory-scale sensor responses. The economic impact was established for the ideal sensor response categories.

The XRF sensor was then selected for further assessment by determining the sorting potential based on laboratory-scale sensor response tests using measurement parameters similar to industrial-scale ore sorting. The economic impact was established for the industrial sensor response categories.

Chapter 5

Results and Discussion

This chapter presents the results of the ore sortability tests for the Los Bronces case study. The particle-by-particle characterisation and laboratory-scale sensor response data was used to determine the sortability results. The sortability was assessed by calculating the economic impact of implementing ore sorting on the Los Bronces operation at differing cut-off grades/ sensor response categories.

As the pebble sample is not representative, the results presented in this chapter are used as a demonstration of the protocol and are not an estimation of the actual mass pull achievable for the Los Bronces ore using sorting.

The intrinsic sortability results are presented in Section 5.1. Ore sorting amenability test results are given in Section 5.2. The laboratory-scale ore sorting test results are discussed in Section 5.3.

5.1 Intrinsic Sortability

The intrinsic grade-recovery relationship is presented in Section 5.1.1 and the economic impact of implementing ore sorting based is discussed in Section 5.1.2.

5.1.1 Intrinsic Grade-Recovery Relationship

The intrinsic grade-recovery relationship was calculated on an overall and size-by-size basis using the ore characterisation data in a series of simulated separation tests as described in Section 4.3. The ore sample was split into two size fractions for the analysis (+40 mm and -40 mm fractions). The aim was to determine the ideal grade-recovery relationship if a perfect separator existed and whether or not the relationship varied at different size fractions. The overall intrinsic grade-recovery relationship is presented in Table 11 whilst Figure 55 graphically presents the cumulative grade-recovery curves based on the overall and size-by-size results.

Table 11 presents the feed and concentrate data for each simulated separation test as well as the cumulative grade, recovery and mass rejection data at varying cut-off grades. The feed grade for the Los Bronces pebbles is 0.44 % Cu and the target cut-off grade for the pebble crusher stream is 0.4 % Cu in the case study. The results in Table 11 indicate that, at a cut-off grade of 0.4 % Cu, the copper grade increases to ~0.79 % Cu with a recovery of ~78 %. The results indicate that ~57 % of the mass can be rejected from the pebble crusher stream at a cut-off grade of 0.4 % Cu. The grade recovery curves for both the +40 mm and -40 mm fractions are very similar where recovery is 50 % or more. The slope of the +40 mm grade recovery curve is steeper than the -40 mm curve where recoveries are below 50 %. A coarse higher grade particle (~2 % Cu) occurs in the +40 mm size fraction and resulting in a slight nugget effect on the data.

Table 11: Overall intrinsic sortability results.

Product	Mass %	Cu Grade %	Cu Distribution %
Test 1 Feed	100.00	0.44	100.00
Conc. 1	8.01	1.44	26.01
Test 2 Feed	91.99	0.36	73.99
Conc. 2	8.82	0.91	18.13
Test 3 Feed	83.18	0.30	55.86
Conc. 3	6.86	0.65	10.03
Test 4 Feed	76.31	0.27	45.83
Conc. 4	19.74	0.53	23.48
Test 5 Feed	56.57	0.17	22.35
Conc. 5	25.85	0.25	14.78
Discard	30.72	0.11	7.57
Threshold Cu %	Cumulative %		
	Cu Recovery	Conc. Grade Cu	Mass Rejected
1.0	26.01	1.44	91.99
0.8	44.14	1.16	83.18
0.6	54.17	1.01	76.31
0.4	77.65	0.79	56.57
0.2	92.43	0.59	30.72

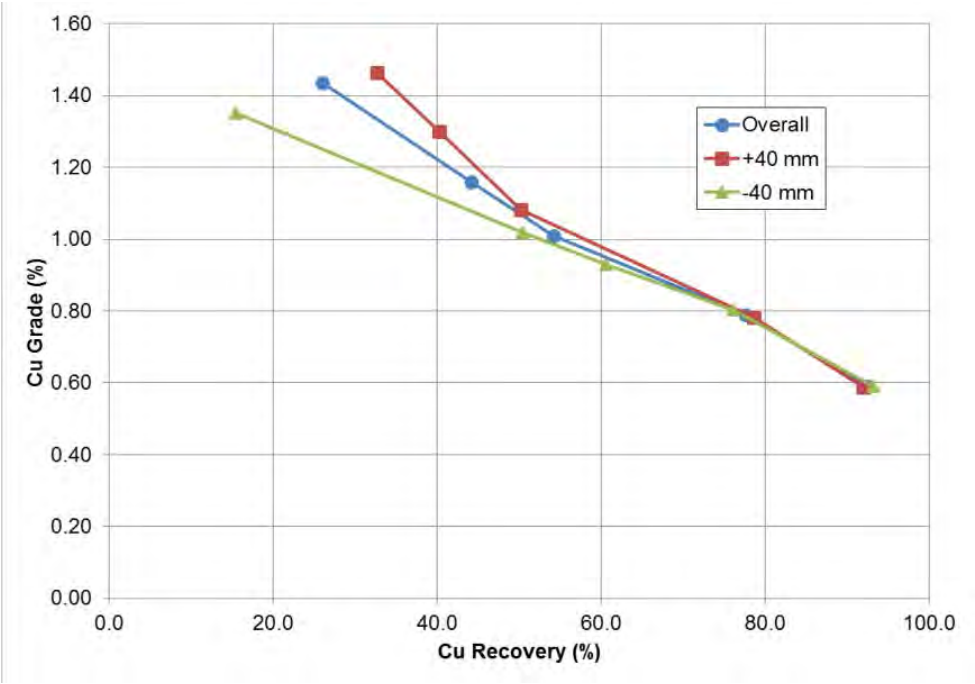

Figure 55: Cumulative grade-recovery curves for the overall sample as well as the +40 mm and -40 mm size fractions.

Generally, the aim of implementing ore sorting is to remove low-grade/ barren particles prior to downstream processing. Therefore the aim of sorting is to reject as much waste material from the process without impacting too heavily on the recovery.

The sorting opportunity identified for Los Bronces was to remove hard, low-grade pebbles at a cut-off grade of 0.4 % Cu. The overall results for the case study indicate that the ore shows the potential for ore sorting as a large proportion of waste can be rejected from the process without losing too much copper to the waste stream. The upgrading ratio, which is the ratio of the concentrate to feed grade (Neethling *et al.*, 2008), is not expected to be high for ore sorting but is used in the case study to compare the efficiencies of the different ore sortability tests. An upgrading ratio of ~1.8 could potentially be achieved at a cut-off grade of 0.4 % Cu for the Los Bronces pebbles. In a similar study by Tong (2012), an upgrading ratio of ~2.1 could be achieved when implementing ore sorting on a lead-zinc ore. Similar upgrading ratios were observed in the sized fractions and therefore the case study focusses on the unsized Los Bronces material.

5.1.2 Economic Impact

The economic impact of implementing ore sorting was assessed based on the intrinsic grade-recovery relationship as well as operational data for a typical copper operation similar to Los Bronces and is summarized in Table 12. The additional revenue/ profit is determined at each copper grade threshold (cf. Table 11).

The mill operational data (cf. Table 12) used for the base-line operation without ore sorting assumes a ROM feed rate of 3000 tph. The SAG screen oversize material reports to the pebble circuit and a pebble generation rate of 20 % was used. As the ore sorter rejects more waste, the ROM throughput must increase so that a constant feed to flotation is achieved. The pebble circuit operational data includes the tonnages around the pebble circuit based on the rejection rate of the sorter (cf. Table 13). The flotation operating data includes the differences in grades around the SAG mill, pebble circuit and flotation plant. The pebble feed to SAG grade and sorter waste was determined based on the intrinsic sortability results. The overall circuit recovery is kept constant at 80 %, however, rejection of waste material prior to flotation would probably have a slight impact on the recovery. The additional copper revenue, total additional costs and copper value in the waste at the different cut-off grades is calculated for the circuit based on the copper spot price on the 19th of January 2016. The mining, waste disposal, flotation and sorter costs at the varying cut-off grades are described in the operating cost section. The milling cost remains constant as no additional material reports to the mill. Lastly, the additional profit is presented which takes the copper value reporting to the waste into account to give the overall additional profit per day and per year.

Table 12: Economic impact of sorting determined based on different cut-off grades.

Cost/ operational data	Baseline - No sorting	Intrinsic sortability thresholds (Cut-off grade % Cu)				
		0.2	0.4	0.6	0.8	1
Mill operational data						
ROM feed (tph)	3000	3184	3339	3458	3499	3552
Pebble circuit SAG feed (tph)	600	416	261	142	101	48
Total SAG feed (tph)	3600	3600	3600	3600	3600	3600
SAG screen oversize (%)	20	20	20	20	20	20
Oversize to pebble circuit (tph)	300	300	300	300	300	300
Undersize to Sag (tph)	3000	3000	3000	3000	3000	3000
Pebble circuit operational data						
Sorter Feed (tph)		600	600	600	600	600
Sorter Rejection as waste (%)		31	57	76	83	92
Waste (tph)		184	339	458	499	552
Pebble (tph)	600	416	261	142	101	48
Crusher feed (tph)	600	416	261	142	101	48
Flotation operational data						
Feed grade to flotation (%Cu)	0.76	0.78	0.80	0.81	0.81	0.82
Pebble feed to SAG grade (%Cu)	0.44	0.59	0.79	1.01	1.16	1.44
Flotation circuit recovery (%)	80	80	80	80	80	80
Sorter waste grade (%Cu)		0.11	0.17	0.27	0.30	0.36
Value of Cu conc ($/ ton Cu)	4441	4441	4441	4441	4441	4441
Additional Cu in feed (t/day)		35	65	89	98	108
Additional Cu in waste (t/day)		5	14	29	36	47
Additional Cu recovered (t/day)		24	41	48	50	49
Additional Cu revenue ($/day)		105720	180788	212753	220249	216301
Cu value in waste ($/day)		17105	50526	103609	126274	167256
Operating costs						
Mining costs ($/t)	3	3	3	3	3	3
Mining costs ($/day)		13272	24439	32967	35932	39741
Waste disposal cost ($/t)	1	1	1	1	1	1
Waste disposal cost ($/day)		4424	8146	10989	11977	13247
Milling cost ($/t)	4	4	4	4	4	4
Milling cost ($/day)		0	0	0	0	0
Sorting cost ($/t)		2	2	2	2	2
Sorting cost ($/day)		8848	16293	21978	23954	26494
Additional revenue ($/day)		105720	180788	212753	220249	216301
Total additional costs ($/day)		26544	48879	65935	71863	79482
Additional Profit						
Additional profit ($/day)		62072	81384	43209	22112	-30436
Additional profit ($/year)		22671644	29725347	15781906	8076289	-11116825

In an example from Lessard *et al.* (2015), the economic impact of implementing ore sorting was calculated based on hypothetical sorter rejection rates for a copper operation similar to Los Bronces. It was found that an additional ~$7 million profit per year could be achieved if the ore sorter could reject 60 % of the ore through sorting. The increase in profit that could be achieved indicated that the ore had the potential to be sorted pending on a feasibility study to determine the actual economic impact.

The results for the case study indicate that there is potential to implement ore sorting at cut-off grades below 1 % Cu as an increase in profit could be achieved. The best-case sorting potential occurs at a cut-off grade of 0.4 % Cu where an additional profit of ~$30 million could be achieved. The increase in profitability indicates that the ore is potentially sortable therefore the next stage in the protocol was initiated. Note that this additional "profit" excludes the capital and operational expenditure required to implement ore sorting. The actual profitability of ore sorting would need to be investigated to determine the financial viability. The positive "profit" indicates that there is at least the potential that ore sorting could be implemented.

5.2 Ore Sorting Amenability

There are various methods to sort an ore based on physical/ measured particle properties including gravity, electrostatic, magnetic and dense medium separation as well as sensor based ore sorting. The aim of the current research is to establish the sortability of an ore based on sensor-based sorting. As part of establishing ore sortability, it is useful to determine if there are any other means to sort an ore based on physical properties. Section 5.2.1 discusses two examples of assessing the amenability of an ore to physical sorting based on size and density. The amenability of the ore to sensor-based ore sorting is presented on Section 5.2.2.

5.2.1 Amenability to Physical Sorting

The comparison of the pebble size (ESD) and density with the copper grade is presented in Figure 56 to establish if the ore is amenable to physical sorting. The comparison of the size and grade of the pebbles shows a weak negative correlation indicating that the grade increases slightly with a decrease in size which is expected. The comparison of density with grade indicates that there is a weak positive correlation between copper grade and density. Three distinct groups of low (<0.4), medium (~0.5 - 0.8 % Cu) and high grade (>0.8 % Cu) pebbles were observed that correlate with differing densities.

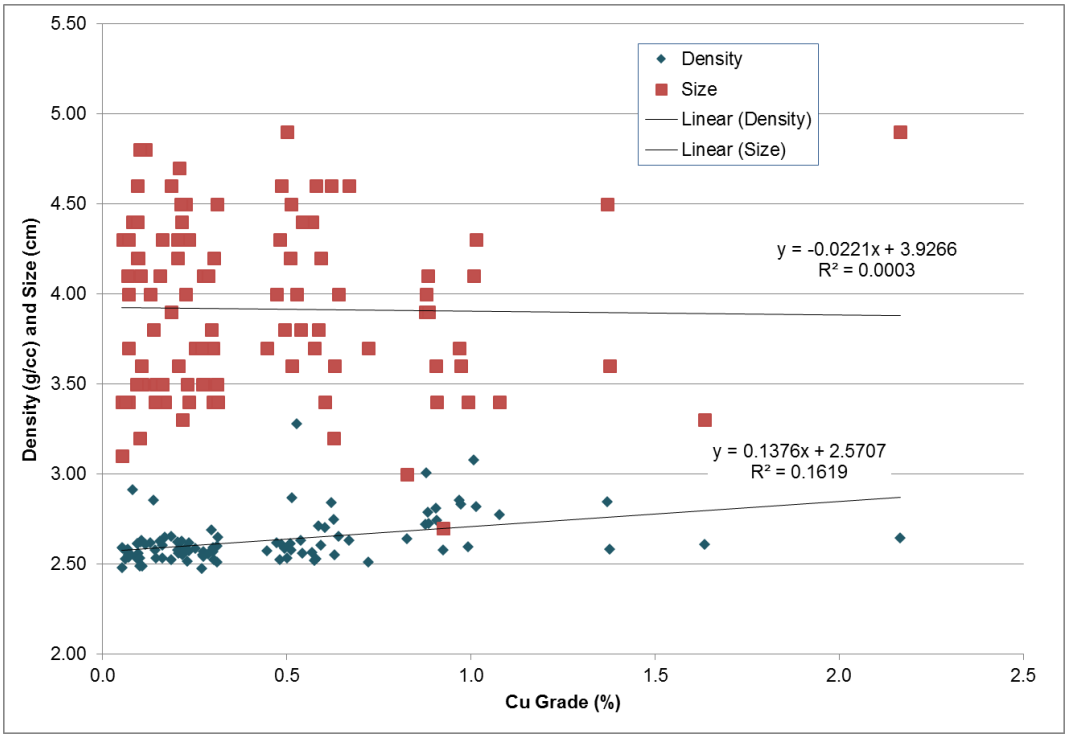

Figure 56: Size (ESD) and density vs. *copper grade for the 100 Los Bronces pebbles.*

The ore may not be sortable by size classification but the spread in results indicates that there are pebbles of differing grade that are of similar size. This indicates that the ore has potential to be sorted into streams of differing grade.

Gravity separation, specifically jigging, can be applied to sort coarse ore particles based on density, the technique requires that there is a sufficient difference in density of ore from waste. Jigging has been successfully applied to separate fluorite (CaF_2) from quartz (SiO_2) which have specific gravities of 3.2 and 2.7 respectively (Wills, 2006). The Los Bronces ore could potentially be sorted by gravity separation as there are distinct groups of particles with differing grades that correlate with different densities. Ore sorting sensors that measure density, such as the XRT, could potentially be used to sort the Los Bronces pebbles and is investigated further in Section 5.2.2.

5.2.2 Amenability to Sensor Based Sorting

The physical particle properties that were measured using various electronic sensors, including XRT, XRF and NIR, are compared with the copper grade in Figures 56 to 58. The aim was to determine which sensors could discriminate between particles of differing grades based on measured physical properties.

The XRF sensor response is a measure of the copper counts per area and is compared with the copper grade of each pebble determined by XRF during the ore characterisation stage. A positive correlation was observed between the sensor response and the grade (cf. Figure 57). Some particles were misidentified by the sensor as the XRF sensor only analyses a small portion of the surface of the particles. The area measured may not be representative of the particle grade as copper may not be fully disseminated in these particles.

The XRT sensor measured the area percent of high density material, based on the average atomic number, within the pebbles and was compared with the grade of each pebble in Figure 58. The results indicate that there is a weak positive correlation between the sensor response and grade. There are, however, particles that show a high XRT sensor response but are of low grade and vice versa. The particles that have been misidentified as the pebbles comprise a large proportion of minerals with a similar density to the copper bearing phases (hematite (Fe_2O_3) and/ or pyrite (FeS_2)) but the particles contain little chalcopyrite ($CuFeS_2$). Other particles were identified as low density but were of high grade, the mineralisation in these particles was too fine to be detected by the sensor.

The NIR sensor response is compared with the grade of the Los Bronces pebbles in Figure 59. A weak positive correlation was observed but the spread in results indicates that there is no direct correlation between the sensor response and grade.

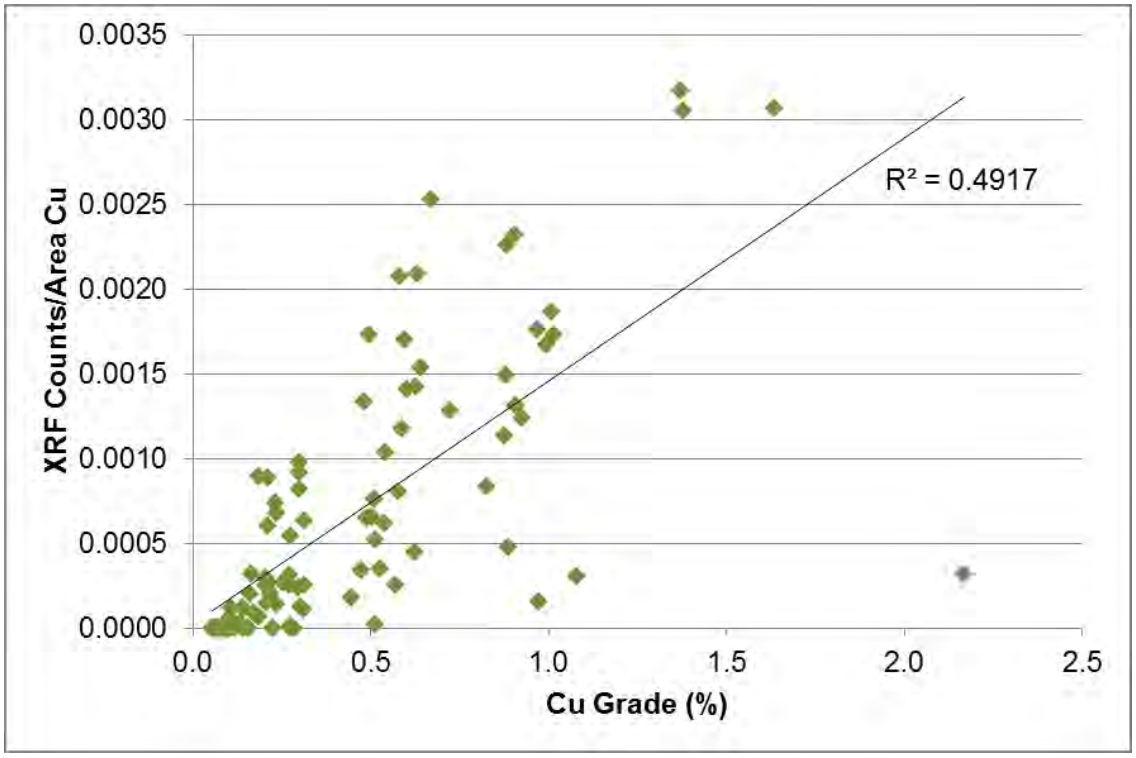

Figure 57: Tomra XRF sensor response (CPA Cu) vs. copper content indicating a good correlation.

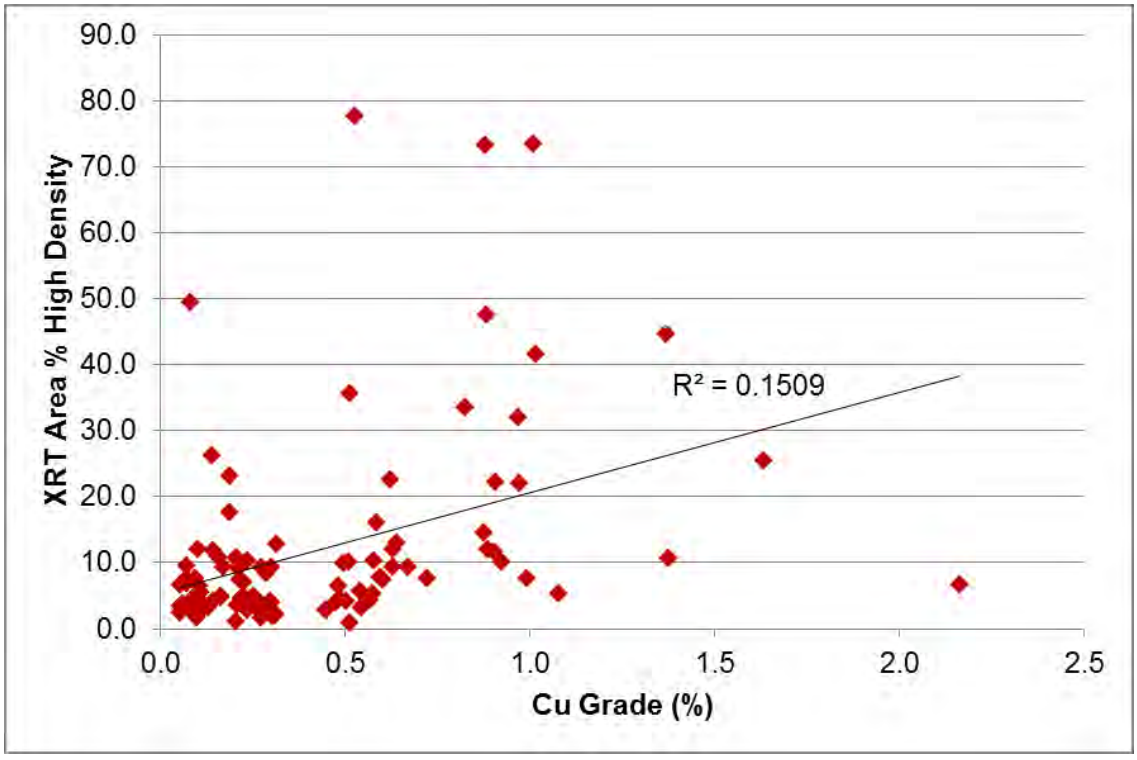

Figure 58: Tomra XRT sensor response (% high density) vs. copper content indicating a fair correlation.

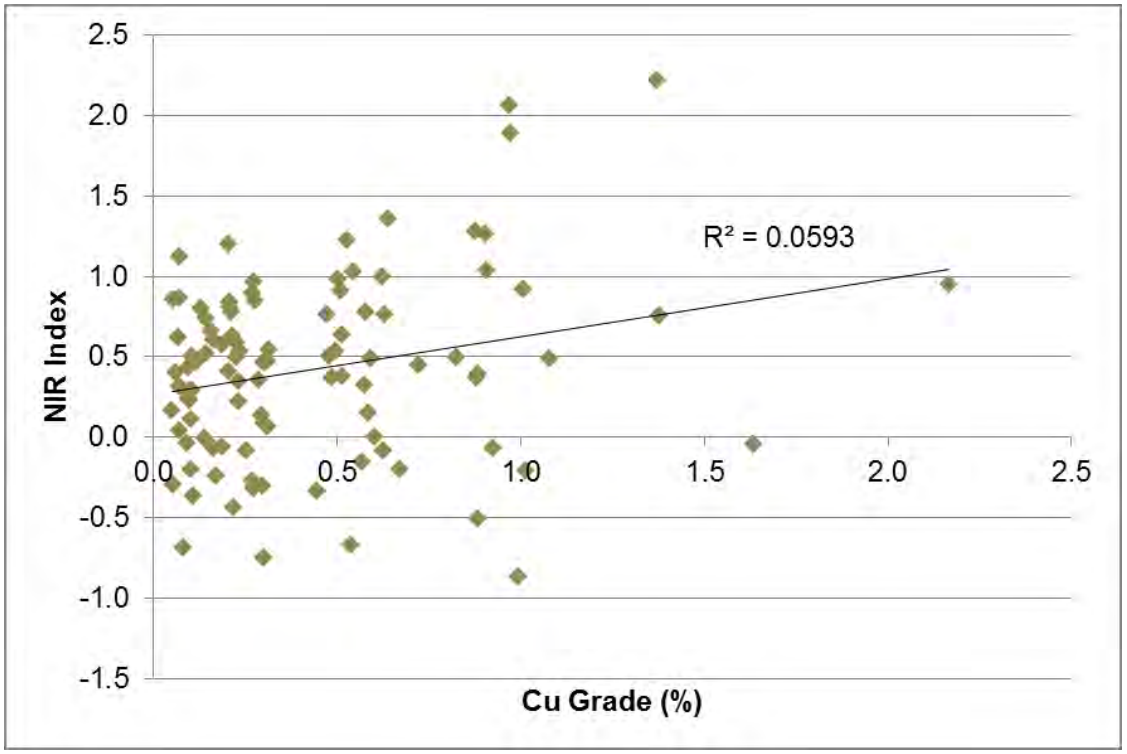

Figure 59: Tomra NIR sensor response (NIR index value) vs. copper content indicating a poor correlation.

Tong (2012) compared the XRF sensor response on a laboratory-scale with the grade determined by chemistry for a lead-zinc ore. The sensor response correlated well with both the lead and zinc assay results with a goodness of fit of >95 %. The grade of the Los Bronces pebbles is much lower than the grades in the example from Tong (2012) and as a result the sensor is more likely to misidentify particles that are close to the detection limit of the XRF sensor. The result of the increased number of misidentified particles is a lower goodness of fit when comparing the XRF sensor response and grade for the case study. The correlation is fairly good considering these lower grades. The XRF sensor was therefore considered for the laboratory-scale sortability tests in the next stage of the protocol.

Strydom (2010) investigated the use of the DE-XRT ore sorting sensor to separate torbanite (oil-shale) from coal. The differences in atomic number, due to the differences in mineral content, measured by DE-XRT between the coal and torbanite particles could be used to separate the components of the ore effectively; a good correlation between the XRT sensor response and grade (calorific value) was observed. The correlation between XRT sensor response and grade indicates that the Los Bronces pebbles have potential to be sorted the using XRT. Therefore the sensor is further investigated in the next stage of the protocol to determine the sortability.

A previous study on the applicability of NIR sensor based ore sorting of the Los Bronces SAG mill oversize pebbles (Dalm, 2011) found that there was no direct correlation between the copper grade and the NIR sensor response. The results from the current study on the Los Bronces pebbles confirm the findings of Dalm (2011). The NIR sensor has the potential to discriminate between particles based on different alteration minerals present that produce characteristic absorption spectra. The correlation between the copper grade and the degree of alteration is yet to be established for the Los Bronces ore. The sensor was not considered for the next stage of the protocol.

Based on the amenability test results, the XRF and XRT sensors were selected for the next stage of the protocol as there was a direct correlation between the grade and sensor response.

5.3 Laboratory-Scale Sensor Sorting Tests

The laboratory-scale sortability tests, based on the ideal and industrial-scale sensor responses, is presented in Section 5.3.1 and 5.3.2 respectively.

5.3.1 Sortability Based on Ideal XRF and XRT Sensor Response

The grade-recovery relationship based on the laboratory-scale XRF and XRT sensor sortability tests is presented in Section 5.3.1.1 and the economic impact of implementing ore sorting based on the grade-recovery relationship is discussed in Section 5.3.1.2.

5.3.1.1 Grade-Recovery Relationship

The grade-recovery relationship is calculated using a similar approach to assess the intrinsic sortability, the results are calculated based on differing sensor response thresholds instead of cut-off grades in this section. The grade-recovery relationships based on the ideal laboratory-scale XRF and XRT sensor response thresholds are presented in Tables 13 and 14. The cumulative grade recovery curves based on the ideal sensor response categories are compared with the intrinsic grade-recovery in Figure 60. The intrinsic grade-recovery curve represents the limit of separation efficiency for the Los Bronces ore based on mineralogical characteristics. The grade

and recovery of actual separation processes can only fall on or below this curve. The range in cumulative copper concentrate grades is fairly low compared to the intrinsic sortability results for both the XRF and XRT sensor ranging from 0.62 % to 0.95 % Cu for the XRF and 0.47 % to 0.81 % Cu for the XRT. It was observed that the XRF and XRT grade-recovery curves fall below the intrinsic curve in Figure 60. These results indicate that lower upgrading ratios are expected compared to the intrinsic sortability results.

Table 13: Grade-recovery relationship for the ideal laboratory-scale XRF sensor.

Product	Mass %	Cu Grade %	Cu Distribution %
Test 1 Feed	100.00	0.44	100.00
Conc. 1	8.46	0.95	18.25
Test 2 Feed	91.54	0.39	81.75
Conc. 2	6.11	0.85	11.82
Test 3 Feed	85.43	0.36	69.93
Conc. 3	7.19	0.69	11.17
Test 4 Feed	78.25	0.33	58.76
Conc. 4	9.50	0.44	9.47
Test 5 Feed	68.75	0.32	49.29
Conc. 5	30.39	0.52	35.78
Discard	38.36	0.16	13.50
Threshold sensor response (CPA Cu)	Cumulative %		
	Cu Recovery	Conc. Grade Cu	Mass Rejected
>=0.0020	18.25	0.95	91.54
>=0.0016-0.0019	30.07	0.91	85.43
>=0.0012-0.0015	41.24	0.84	78.25
>=0.0008-0.0011	50.71	0.72	68.75
>=0.0002<0.0008	86.50	0.62	38.36

Table 14: Grade-recovery relationship for the ideal laboratory-scale XRT sensor.

Product	Mass %	Cu Grade %	Cu Distribution %
Test 1 Feed	100.0	0.44	100.0
Conc. 1	11.4	0.81	21.0
Test 2 Feed	88.6	0.39	79.0
Conc. 2	6.2	0.61	8.5
Test 3 Feed	82.5	0.38	70.5
Conc. 3	17.1	0.48	18.6
Test 4 Feed	65.3	0.35	51.9
Conc. 4	26.3	0.48	28.7
Test 5 Feed	39.0	0.26	23.2
Conc. 5	24.9	0.27	15.3
Discard	14.1	0.25	7.9
Threshold sensor response (% high density)	Cumulative %		
	Cu Recovery	Conc. Grade Cu	Mass Rejected
>30%	20.96	0.81	88.63
20-30 %	29.45	0.74	82.46
10-20 %	48.08	0.61	65.32
5-10 %	76.77	0.56	38.98
3-5 %	92.11	0.47	14.09

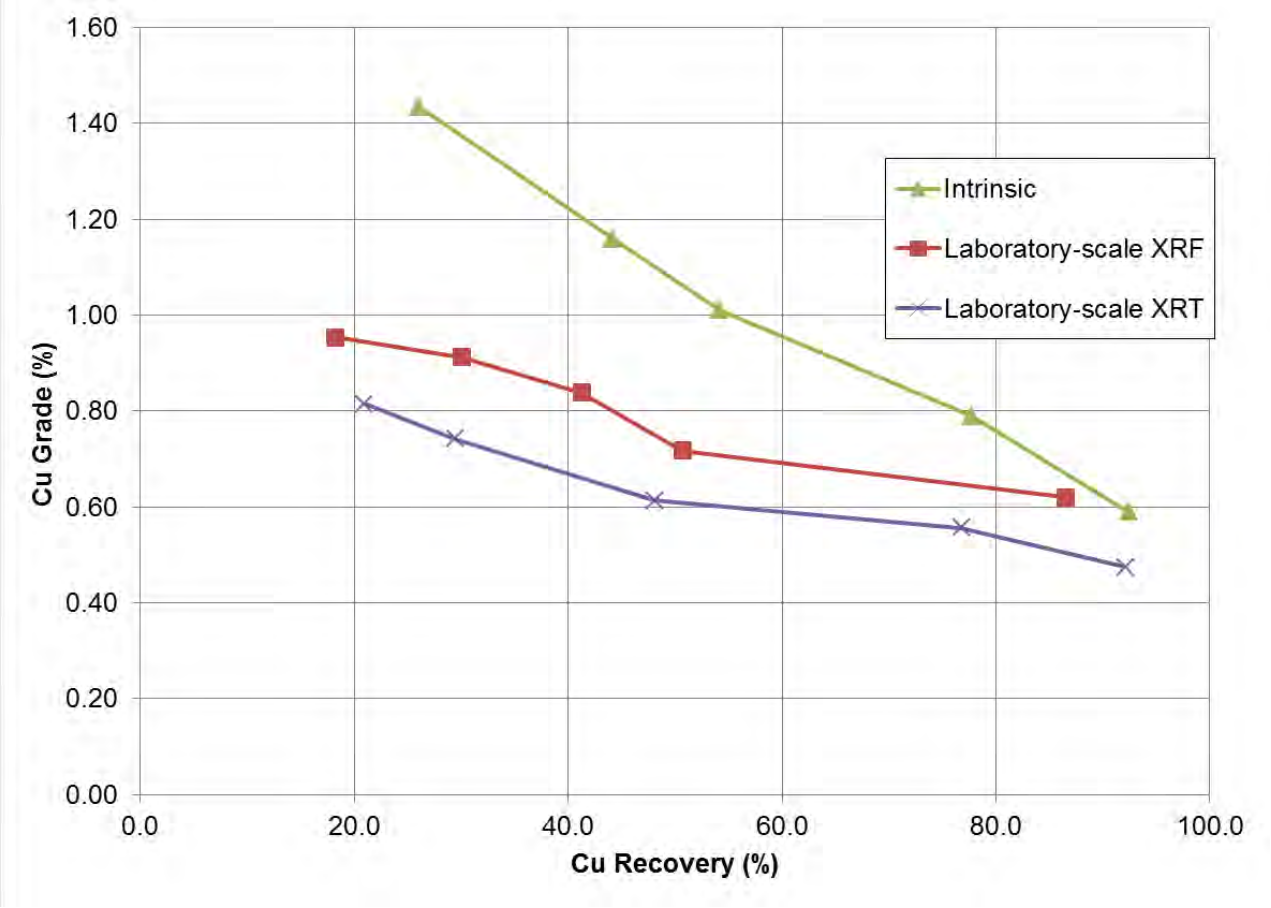

Figure 60: Cumulative grade-recovery relationship based on intrinsic and ideal laboratory scale sorting tests using the XRT and XRF sensor.

In a previous study on ore sorting by Tong (2012) where the sortability of an ore was determined based on various ore sorting sensor tests, the best case sorting was achieved with an XRF sensor. Approximately 47 % of the mass could be rejected as waste at a cut-off grade of 5 % zinc using the XRF sensor. The results indicated that the ore had the potential to be sorted as good recoveries (>95 %) could be achieved whilst rejecting a large amount of low grade waste from the process. The upgrading ratio achieved for the lead-zinc ore was ~1.8. In the study, the upgrading ratios were compared based on various ore sorting sensor tests to assess differences in sorting efficiency between the different sensors.

The upgrading ratio, where sufficient copper recovery was achieved, for the XRF and XRT sensors is slightly lower than in the example (Tong, 2012) at ~1.4 and ~1.3 respectively. Although the upgrading ratios are low, the results indicate that there is potential to sort the ore using the selected sensors as ~40 % mass can be rejected as waste whilst recoveries above 75 % can be achieved for the XRF and XRT sensors.

5.3.1.2 Economic impact

The economic potential was determined for the XRF and XRT sensors based on the grade-recovery relationship using varying sensor response thresholds and the additional profit at each threshold is presented in Table 15. The complete financial model results for the XRF and XRT sensors can be found in Appendices D.1 and D.2. The additional profit was calculated using the same operational and cost data used to establish the economic impact based on the intrinsic sortability data.

Table 15: Additional profit for the Los Bronces operation when implementing the XRF and XRT sensor at differing levels of performance.

Additional profit	XRF sensor thresholds (CPA Cu)				
	>=0.0004<0.0008	>=0.0008-0.0012	>=0.0012-0.0015	>=0.0015-0.0020	>=0.0020
Additional profit ($/day)	58169	-4499	-10994	-37498	-68522
Additional profit ($/year)	21246202	-1643271	-4015568	-13696325	-25027602
	XRT sensor thresholds (% high density)				
	3-5 %	5-10 %	10-20 %	20-30 %	>30%
Additional profit ($/day)	7325	18642	-25859	-55057	-67418
Additional profit ($/year)	2675542	6809019	-9445041	-20109540	-24624422

The optimal sensor response categories would improve the profit of the operation by an additional ~$21 million and ~$7 million when implementing sorting using the XRF and XRT sensors respectively. This indicates that there is a potential to implement ore sorting using these sensors. The XRF sensor showed the highest potential based on the results and was further investigated in the next stage of the protocol where the industrial-scale sensor response is used to assess the sortability.

5.3.2 Sortability Based on Industrial-Scale XRF Sensor Response

The grade-recovery relationship based on the industrial-scale XRF sensor sortability tests is presented on Section 5.3.2.1 and the economic impact of implementing ore sorting based on the grade-recovery is discussed in Section 5.3.2.2.

5.3.2.1 Grade-Recovery Relationship

The grade-recovery relationship using XRF sensor measurement parameters that would be used for actual ore sorting (industrial-scale) was determined and is presented in Table 16. The cumulative grade recovery curves for the intrinsic, ideal

and industrial-scale XRF sorting tests are presented in Figure 61. The range in cumulative concentrate grades is lower than those observed for the ideal XRF sensor tests (0.49 % to 0.82 % Cu), the cumulative grade recovery curve also falls well below the ideal XRF curve.

Table 16: Grade-recovery relationship for the industrial-scale XRF sorting tests.

Product	Mass %	Cu Grade %	Cu Distribution %
Test 1 Feed	100.00	0.44	100.00
Conc. 1	10.04	0.82	18.66
Test 2 Feed	89.96	0.40	81.34
Conc. 2	6.84	0.54	8.29
Test 3 Feed	83.12	0.39	73.05
Conc. 3	9.96	0.54	12.15
Test 4 Feed	73.15	0.37	60.90
Conc. 4	14.94	0.53	17.75
Test 5 Feed	58.22	0.33	43.15
Conc. 5	29.94	0.34	23.36
Discard	28.28	0.31	19.79
Threshold Cu %	Cumulative %		
	Cu Recovery	Conc. Grade Cu	Mass Rejected
1.0	18.66	0.82	89.96
0.8	26.95	0.71	83.12
0.6	39.10	0.64	73.15
0.4	56.85	0.60	58.22
0.2	80.21	0.49	28.28

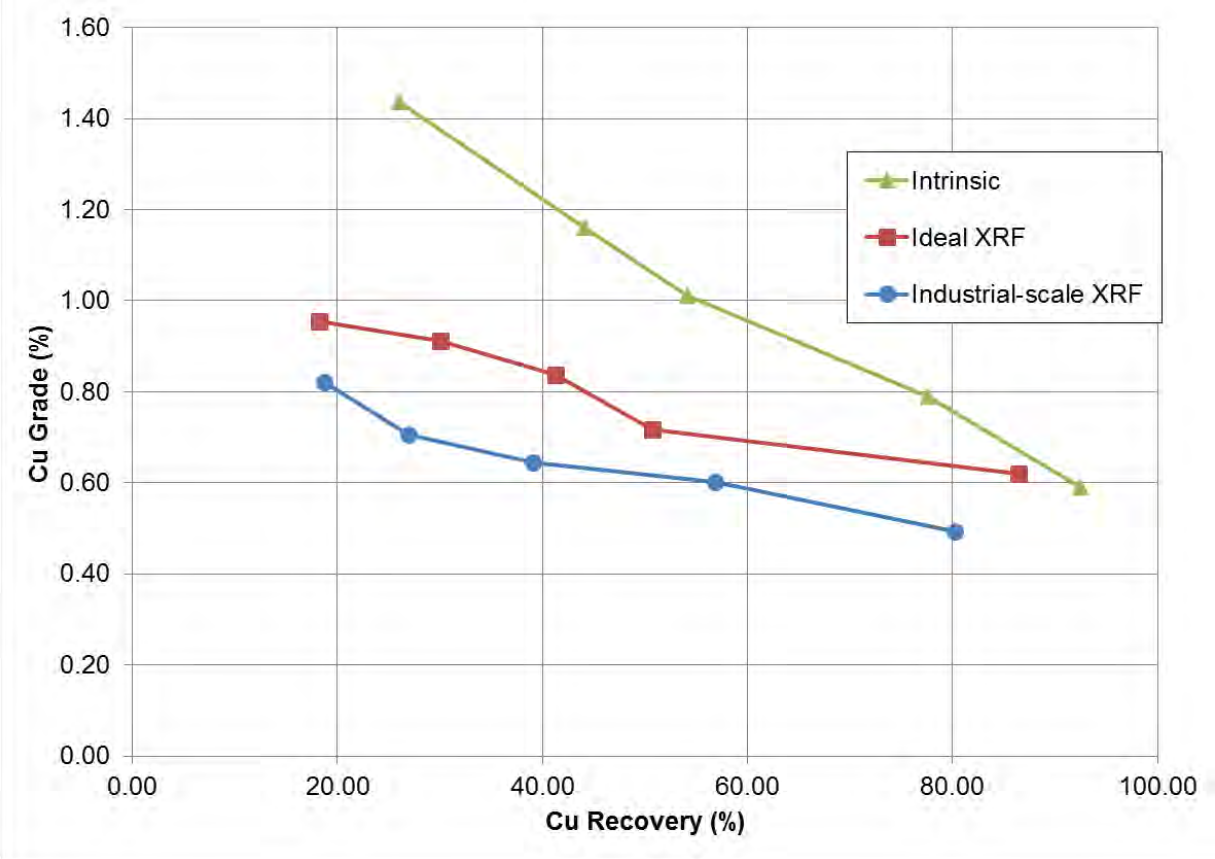

Figure 61: Comparison of grade-recovery curves based on intrinsic, ideal and industrial XRF sensor sorting tests.

The best case sortability where sufficient copper recovery (>75 %) was achieved at a sensor cut-off grade of 0.2 % Cu where 28 % of the mass could be rejected as waste with 80 % recovery. The upgrading ratio was only ~1.1 which is lower than the ideal XRF sensor sortability tests (~1.4). This indicates that the industrial XRF sensor cannot discriminate between particles of differing grade as effectively as the ideal XRF sensor when analysed at an industrial-scale. The XRF analysis period may be too short to accurately analyse for copper.

5.3.2.2 Economic Impact

The additional profit was calculated for the industrial-scale XRF sensor response categories and is presented in Table 17. The complete financial model results for the industrial XRF sensor can be found in Appendix D.3. The results show that no additional profit could be achieved across the entire range of sensor response thresholds.

Table 17: Financial model for the Los Bronces operation for the implementation of the industrial-scale XRF sensor at differing levels of performance.

Additional profit	XRF sensor thresholds (Calculated % Cu)				
	0.2	0.4	0.6	0.8	1.0
Additional profit ($/day)	-1837	-11772	-42912	-64270	-77568
Additional profit ($/year)	-670889	-4299887	-15673748	-23474682	-28331582

Based on the economic impact results, there is no potential for industrial-scale XRF sorting with the current sensor as it was found that the operation would make a net loss if ore sorting was implemented using the industrial-scale XRF sensor.

5.4 Summary of Results

A comparison between the best-case intrinsic and laboratory-scale sorting test results are compared in Table 18. The recovery, concentrate grade, mass rejection and additional profit are compared.

The upgrading ratio for the various sortability tests is used to compare the efficiency of sorting. The upgrading ratio for the ideal laboratory-scale tests is lower than the intrinsic upgrading ratio. This is expected as perfect separation of the ore is not practically possible. The upgrading ratio for industrial XRF sensor is lower than the ideal XRF sensor indicating that sorting using the industrial scale sensor is not as

efficient. The best case sortability of the ore with a perfect separator would result in $30 million of additional profit. Sorting of the ore at the optimum sorter performance for the ideal XRF and XRT sensor would result in ~$21 million and ~$7 million of additional profit per year respectively. As discussed in Section 5.1, the additional "profit" does not include the capital and operating expenditure of ore sorting. The positive "profit' indicates that there is the potential to implement ore sorting. Implementing industrial-scale sorting using the XRF sensor would result in a loss of ~$7 million.

Table 18: Grade-recovery relationship and increased profitability at the optimum cut-off grade/ or sorter performance for the intrinsic and laboratory-scale sorting tests.

	Property/ Sensor	Cu Recovery (%)	Concentrate Cu Grade (%)	Mass Rejected (%)	Upgrading Ratio	Additional Profit ($/year)
Intrinsic sortability	Cu %	77.6	0.79	56.6	1.8	30 million
Laboratory-scale sorting tests	Ideal XRF	86.5	0.62	38.4	1.4	21 million
	Ideal XRT	76.8	0.56	39.0	1.3	7 million
	Industrial XRF	80.2	0.49	28.3	1.1	-7 million

The Los Bronces ore has shown the potential to be sorted based on the intrinsic as well as the ideal laboratory-scale sortability results. The results of the industrial scale sensor tests indicate that there is no potential to sort the ore with the current XRF sensor.

5.5 Conclusions

This chapter demonstrated the use of the protocol developed during the current research using the Los Bronces case study. The sample used for the case study is not representative of the Los Bronces ore as particles were hand-picked to incorporate a wide range of particle sizes and grades. Therefore the case study is used to demonstrate the protocol should a representative sample have been taken. In Section 5.1, the intrinsic sortability was assessed at different size fractions and it was found that the ore sortability was similar at all sizes. The economic impact based on the overall intrinsic sortability indicated that there is potential for sorting which would need to be confirmed by establishing the financial viability.

In Section 5.2, the amenability of the ore to sorting using XRF, XRT and NIR ore sorting sensors on an ideal laboratory-scale was assessed. The XRF and XRT sensor response data showed a correlation with the grade of the pebbles and the sortability

of the ore using these sensors was further assessed in the next stage of the protocol. The NIR sensor response was found to have no correlation with the grade of the pebbles and was ruled for the sortability tests.

In Section 5.3, the laboratory-scale sortability of the ore was determined based on the sensor response tests. Firstly, the XRF and XRT sensors were assessed based on the ideal sensor response. The sensors both showed that there is the potential to sort the ore with both the XRT and, more so, the XRF sensor. Ore sorting tests were then carried out for the XRF sensor using industrial-scale measurement parameters. The results indicated that there was no potential to sort the ore using industrial-scale XRF sorting.

Based on the results it can be concluded that the Los Bronces ore sample for the case study has the potential to be sorted based on the intrinsic sortability. The ideal XRF and, to a lesser extent, XRT sensors both showed potential to be used for sorting. The industrial-scale XRF was shown to have no potential to be used for sorting. Therefore, bulk sorting tests would not be considered for the ore using the current XRF sensor.

Chapter 6

Conclusions and Recommendations

The objective of this research was to develop a protocol/ methodology to determine the potential for an ore to be sorted using sensor-based sorting. The research builds upon previous methodologies in literature to determine ore sortability as well as methods to establish the economic impact of ore sorting on an operation. The first attempt to create a standard methodology to assess the amenability of an ore to sorting at a pilot-scale was established by Fitzpatrick (2008). Tong (2012) developed a methodology to assess the amenability of an ore to sensor-based sorting on an ideal laboratory-scale. Methods were developed by Lessard *et al.* (2015) to assess the economic impact of ore sorting on an operation.

The conclusions from this thesis for the protocol and the Los Bronces case study as well as recommendations for future research are discussed in Section 6.1, 6.2 and 6.3 respectively.

6.1 The Protocol

A protocol was developed during the current research to determine the ore sortability based on intrinsic/ measured particle properties. The protocol is used to determine the potential ore sortability based, firstly, on intrinsic particle properties. These results represent the ideal/ best-case sortability if a perfect separator existed and are calculated based on particle-by-particle ore characterisation.

Ore that is intrinsically sortable is further assessed based on ideal laboratory-scale sensor sortability tests using selected sensors. Ore sorting sensors that show good potential based the ideal sensor tests are further assessed by determining the sortability of the ore using sensor measurement parameters similar to those used on industrial-scale ore sorting machines.

The sortability is assessed at each stage of the protocol by estimating the overall economic impact of implementing ore sorting on an operation. The protocol follows a

stepwise process where the project only progresses to the next stage if the economic potential warrants it, therefore avoiding unnecessary test work. The economic impact established in the protocol does not include the capital and operating expenditure required to implement ore sorting and is used to determine if there is any potential for sorting *i.e.* a positive economic impact indicates the potential to implement ore sorting.

6.2 Los Bronces Case Study

The protocol was applied to a case study from the Los Bronces operation. The Los Bronces case study was used to demonstrate the protocol developed during the current research and the results do not represent the actual sorting potential of the ore.

It was shown that the ore had potential to be sorted based on the intrinsic sortability results. It was also found that the ore had the potential for sorting using the XRF and, to a lesser extent, XRT sensors based on the ideal sensor sortability tests. The XRF sensor was selected for further investigation using industrial-scale measurement parameters. It was determined that the XRF sensor under industrial conditions would be ineffective for sorting as a net loss for the operation would be incurred if industrial-scale XRF sorting was to be implemented. Bulk sorting tests would therefore not be considered with the current XRF sensor technology.

6.3 Recommendations for Future Research

Further research should focus on improving the techniques, such as the XMT, available to characterise coarse (>10 mm) particles for the purpose estimating ore sortability. Research into improving the sensitivity/ resolution of ore sorting sensors as well as the throughput of automated sorting machines will open up further opportunities to implement ore sorting.

The protocol developed has the potential to be used for *any* particulate material. Further research into the use of the protocol in the recycling, food and/ or pharmaceutical industries would be required to assess the suitability of the protocol in assessing the sorting potential of different particle systems.

References

Afewu, K. I., Lewis, G. O., 1998. Sampling of run-of-mine mill feed – A practical approach. The Journal of the Southern African Institute of Mining and Metallurgy 115, 557-561.

Agus, A. J. L., 2011. Mapping white mica in milled porphyry copper pebbles using hyperspectral imagery: An exploratory study. Master's thesis, University of Twente, Faculty of Geo-Information Science and Earth Observation, Enschede.

Al-Thyabat, S., Miles, N. J., Koh, T. S., 2007. Estimation of the size distribution of particles moving on a conveyor belt. Minerals Engineering 20, 72-83.

AMIRA P754, 2007. Metal Accounting and Reconciliation. Code Release 3: 20070291

AMIRA P902, 2005. Dry Processing of Minerals. Final Report.

Assibey-bonsu, W., 1996. Summary of present knowledge on the representative sampling of ore in the mining industry. The Journal of the Southern African Institute of Mining and Metallurgy (November), 289–296.

Bamber, A. S., 2008. Integrated mining, pre-concentration and waste disposal systems for the increased sustainability of hard rock metal mining. Ph. D. thesis, University of British Columbia, Department of Mining Engineering, Vancouver.

Bennett, D., Miljak, D., Khachan, J., 2007. Quantitative measurement of copper mineralogy using magnetic resonance. Minerals Engineering 20, 1344-1350.

Bennett, D., Miljak, D. & Khachan, J. 2009. The measurement of chalcopyrite content in rocks and slurries using magnetic resonance. Minerals Engineering 22 (9-10), 821-825.

Blasco, J., Aleixos, N., Gómez, J., Moltó, E., 2007. Citrus sorting by identification of the most common defects using multispectral computer vision. Journal of Food Engineering 83 (3), 384-393.

Burt, R., 1999. The role of gravity concentration in modern processing plants. Minerals Engineering 12 (11), 1291-1300.

Cnudde, V., Boone, M.N., 2013. High-resolution x-ray computed tomography in geosciences: A review of the current technology and applications. Earth-Science Reviews 123, 1–17.

Corrans, I. J., Levin, J., 1979. Wet high-intensity magnetic separation for the concentration of Witwatersrand gold-uranium ores and residues. Journal of the South African Institute of Mining and Metallurgy 79, 210-228.

Cui, J., Forssberg, E., 2003. Mechanical recycling of waste electric and electronic equipment: A review. Journal of Hazardous Materials 99 (3), 243-263.

Cutmore, N. G., Middleton, A. G., 1998. On-line ore characterisation and sorting. Minerals Engineering 11 (9), 843-847.

Dalm, M., 2011. Applicability of Near-Infrared Spectroscopy for Sensor Based Sorting of Mill pebbles from the Los Bronces Copper Mine, Chile. Master's thesis, Delft University of Technology, Department of Geotechnology, Delft.

Dalm, M., Buxton, M. W, N., van Ruitenbeek, F. J. A., Voncken, J. H. L., 2014. Application of near-infrared spectroscopy to sensor based sorting of a porphyry popper ore. Minerals Engineering 58, 7-16.

Demir, F., Budak, G., Baydaş, E., Şahin, Y., 2006. Standard deviations of the error effects in preparing pellet samples for WDXRF spectroscopy. Nuclear Instruments and Methods in Physics Research Section B: Beam Interactions with Materials and Atoms, 243(2), pp.423–428.

Death, D., 2005. Chapter 3: Review of Sensing Technologies for Ore Sorting, In: AMIRA P902 Dry Processing of Minerals.

Dobbins, M., Domenico, J., Dunn, P., 2007 A discussion of magnetic separation techniques for concentrating ilmenite and chromite ores. International Heavy Minerals Conference, The Journal of the Southern African Institute of Mining and Metallurgy.

Drzymala, J., Kowalczuk P. B., Oteng-Peprah, M., Foszcz, D., Muszer, A., Hencd, T. & Luszczkiewicz, A., 2013. Application of the grade-recovery curve in the batch flotation of polish copper ore. Minerals Engineering 49, 17-23.

Drzymala, J., 2007. Mineral Processing, Foundations of Theory and Practice of Minerallurgy. University of Technology Press, Wroclaw.

Drzymala, J., 2003. Sorting as a procedure of evaluating and comparing separation results. Physicochemical Problems of Mineral Processing 37, 19-26.

Esbensen, K.H., 2004. 50 years of Pierre Gy's "Theory of Sampling". Chemometrics and Intelligent Laboratory Systems 74 (1), 3-6. Special Issue: 50 years of Pierre Gy's Theory of Sampling Proceedings: First World Conference on Sampling and Blending (WCSB1).

Evans, C. L., Napier-Munn, T. J., 2013. Estimating error in measurements of mineral grain size distribution. Minerals Engineering 52, 198-203.

Fandrich, R., Gu, Y., Burrows, D., Moeller, K., 2007. Modern SEM-based mineral liberation analysis. International Journal of Mineral Processing 84 (1-4), 310-320.

Feng, J., Rivard, B, Gallie E. A., Sanchez, A., 2006. Quantifying total sulfide content of cores and cut-rock surfaces using thermal infrared reflectance. Geophysics 71 (3), M1–M9.

Fitzpatrick, R., 2008. The development of a methodology for automated sorting in the minerals industry. Ph. D. Thesis, University of Exeter.

François-Bongarçon, D., 2004. Theory of Sampling and geostatistics: an intimate link. Chemometrics and Intelligent Laboratory Systems 74 (1), 143-148.

Gallie, E. A., McArdle, S., Rivard, B., Francis, H., 2002. Estimating sulphide ore grade in broken rock using visible/infrared hyperspectral reflectance spectra. International Journal of Remote Sensing 23 (11), 2229-2246.

Geelhoed, B., 2011. Is Gy's formula for the fundamental sampling error accurate? Experimental evidence. Minerals Engineering 24 (2), 169-173.

Ghorbani, Y. Becker, M., Petersen, J., Morar, S. H., Mainza, A., Franzidis, J. P., 2011. Use of X-ray computed tomography to investigate crack distribution and mineral dissemination in sphalerite ore particles. Minerals Engineering 24 (12), 1249-1257.

Gupta, A., Yan, D., 2006. Minerals Processing Design and Operation. Elsevier Science.

Hoal, K. O., Stammer, J. G., Appleby, S. K., Botha, J., Ross, J. K., Botha P. W., 2009. Research in quantitative mineralogy : examples from diverse applications. Minerals Engineering 22 (4), 402-408.

Hsieh, C. -H., 2012. Procedure and Analysis of Mineral Samples Using High Resolution X-ray Micro Tomography. Master's thesis, University of Utah, Department of Metallurgical Engineering, Utah.

Huang, W. -L., Lin, D. -H., Chang, N. -B., Lin, K. -S., 2002. Recycling of construction and demolition waste via a mechanical sorting process. Resources, Conservation and Recycling 37 (1), 23-37.

Jones, M.P., 1987. Applied Mineralogy: A Quantitative Approach, Graham & Trotman, London

Kelly, E. G., Spottiswood, D. J., 1982. Introduction to mineral processing, Wiley.

Lessard, J., de Bakker, J., McHugh, L., 2014 Development of ore sorting and its impact on mineral processing economics. Minerals Engineering 65, 88-97.

Lessard, J., Sweetser, W., Bartram, K., Figueroa, J., McHugh, L., 2015. Bridging the gap: Understanding the economic impact of ore sorting on a mineral processing circuit. Minerals Engineering, doi:10.1016/j.mineng.2015.08.019

Lin, C. L., Hsieh, C. -H., Tserendagva, T. -A., Miller, J. D., 2013. Dual energy rapid scan radiography for geometallurgy evaluation and isolation of trace mineral particles. Minerals Engineering 40, 30-37.

Lyman, G., 1986. Application of Gy's sampling theory to coal: a simplified explanation and illustration of some basic aspects. International Journal of Mineral Processing 17, 1-22.

Lyman, G., van Tonder, E. & Schouwstra, R., 2013. Best practice in quality assurance : determination of the sampling fundamental error. Sampling and Analysis: Best Practice in African mining, The Journal of the Southern African Institute of Mining and Metallurgy, 1-9.

Lyman, G. J., 2014. Determination of the complete sampling distribution for a particulate material. In Sampling 2014, 17–24.

Lyman, G. J., 2012. In-situ and Particulate Material Heterogeneity. In: 5th international conference on sampling and blending.

Lyman, G. J., Schouwstra, R., 2011. Use of the scanning electron microscope to determine the sampling constant and liberation factor for fine minerals. In: 5th international conference on sampling and blending, 89–104.

Miller, J. D., Lin, C. L., Hupka, L., Al-Wakeel, M. I., 2009. Liberation-limited grade/recovery curves from X-ray micro CT analysis of feed material for the evaluation of separation efficiency. International Journal of Mineral Processing 93 (1), 48-53.

Minkkinen, P., 2004. Practical applications of sampling theory. Chemometrics and Intelligent Laboratory Systems 74, 85-94.

Minnitt, R. C. A., Assibey-Bonsu, W., 2010. A comparison between the duplicate series analysis method and the heterogeneity test as methods for calculating the sampling constants , K and alpha. The Journal of the Southern African Institute of Mining and Metallurgy 110, 21-23.

Minnitt, R. C. A., Rice, P. M., Spangenberg, C., 2007a. Part 1: Understanding the components of the fundamental sampling error : a key to good sampling practice. The Journal of the Southern African Institute of Mining and Metallurgy 107, 505-511.

Minnitt, R. C. A., Rice, P. M. Spangenberg, C., 2007b. Part 2: Experimental calibration of sampling parameters K and alpha for Gy's formula by the sampling tree method. The Journal of the Southern African Institute of Mining and Metallurgy 107, 513-518.

Murphy, B., van Zyl, J., Domingo, G., 2012. Underground Preconcentration by Ore Sorting and Coarse Gravity Separation. In: Narrow vein mining conference, 26-27, Perth.

Neethling, S. J., Cilliers, J. J., 2008. Predicting and correcting grade-recovery curves: Theoretical aspects. International Journal of Mineral Processing 89, 17-22.

Pascoe, R. D., Power, M. R., Simpson, B., 2007. QEMSCAN analysis as a tool for improved understanding of gravity separator performance. Minerals Engineering 20, 487-495.

Petersen, L., Minkkinen, P., Esbensen, K. H., 2005. Representative sampling for reliable data analysis: Theory of Sampling. Chemometrics and Intelligent Laboratory Systems 77 (1-2), 261-277.

Schouwstra, R. P. & Smit, A. J., 2011. Developments in mineralogical techniques – What about mineralogists? Minerals Engineering 24 (12), 1224–1228.

Strydom, H., 2010. The application of dual energy X-ray transmission sorting to the separation of coal from torbanite. Master's thesis, University of Johannesburg, Faculty of Engineering and the Built Environment, Johannesburg.

Tessier, J., Duchesne, C., Bartolacci, G., 2007. A machine vision approach to on-line estimation of run-of-mine ore composition on conveyor belts. Minerals Engineering 20, 1129–1144.

Tong, Y., 2012. Technical amenability study of laboratory-scale sensor-based ore sorting on a Mississippi Valley type lead-zinc ore. Master's thesis, University of British Columbia, Department of Mining Engineering, Vancouver

Warnaars, F. W., 1985. Porphyry Copper and Tourmaline Breccias at Los Bronces-Rio Blanco, Chile. Economic Geology 80, 1544-1565.

Wills, B. A., Napier-munn, T., 2006. Mineral Processing Technology, Elsevier.

Wood, M., 2011, Making Sense of Statistics: A Non-mathematical Approach. Palgrave Macmillan, London.

Xradia, 2013, VersaXMT User's Guide, XRadia, 2013.

Appendix A: Los Bronces Pebble Characterisation Data

A.1: Mass, Density, Volume and Particle Size (ESD)

Pebble Number	Mass (g)	Density (g/cc)	Volume (cm^3)	ESD (cm)	Pebble Number	Mass (g)	Density (g/cc)	Volume (cm^3)	ESD (cm)
1	59.0	2.60	22.7	3.5	51	48.0	2.61	18.4	3.3
2	108.0	3.28	32.9	4.0	52	110.0	2.56	43.0	4.3
3	88.0	2.55	34.5	4.0	53	63.0	2.58	24.4	3.6
4	99.0	2.61	37.9	4.2	54	106.0	2.63	40.4	4.3
5	96.0	2.62	36.6	4.1	55	142.0	2.56	55.4	4.7
6	57.0	2.74	20.8	3.4	56	68.0	2.52	27.0	3.7
7	111.0	2.62	42.4	4.3	57	57.0	2.55	22.4	3.5
8	52.0	2.59	20.1	3.4	58	101.0	2.56	39.5	4.2
9	83.0	2.72	30.5	3.9	59	164.0	2.65	62.0	4.9
10	48.0	2.75	17.5	3.2	60	76.0	2.86	26.6	3.7
11	118.0	2.57	46.0	4.4	61	42.0	2.53	16.6	3.2
12	26.0	2.58	10.1	2.7	62	147.0	2.49	59.1	4.8
13	69.0	2.83	24.4	3.6	63	54.0	2.57	21.0	3.4
14	126.0	2.91	43.3	4.4	64	131.0	2.65	49.4	4.6
15	147.0	2.84	51.7	4.6	65	121.0	2.82	42.9	4.3
16	90.0	2.62	34.4	4.0	66	79.0	2.71	29.1	3.8
17	94.0	2.57	36.6	4.1	67	99.0	2.58	38.4	4.2
18	78.0	2.69	29.0	3.8	68	102.0	2.53	40.4	4.3
19	56.0	2.77	20.2	3.4	69	70.0	2.81	24.9	3.6
20	106.0	2.60	40.7	4.3	70	108.0	3.08	35.1	4.1
21	119.0	2.51	47.4	4.5	71	61.0	2.55	23.9	3.6
22	120.0	2.59	46.4	4.5	72	87.0	2.72	31.9	3.9
23	57.0	2.49	22.9	3.5	73	70.0	2.87	24.4	3.6
24	59.0	2.55	23.1	3.5	74	124.0	2.58	48.0	4.5
25	56.0	2.53	22.1	3.5	75	133.0	2.61	51.0	4.6
26	102.0	3.01	33.9	4.0	76	66.0	2.57	25.6	3.7
27	94.0	2.58	36.4	4.1	77	40.0	2.48	16.1	3.1
28	89.0	2.62	34.0	4.0	78	66.0	2.54	26.0	3.7
29	66.0	2.63	25.1	3.6	79	56.0	2.70	20.7	3.4
30	50.0	2.54	19.7	3.4	80	72.0	2.59	27.8	3.8
31	132.0	2.85	46.4	4.5	81	53.0	2.58	20.6	3.4
32	69.0	2.59	26.6	3.7	82	67.0	2.58	26.0	3.7
33	126.0	2.53	49.8	4.6	83	39.0	2.64	14.8	3.0
34	53.0	2.57	20.6	3.4	84	48.0	2.55	18.8	3.3
35	57.0	2.65	21.5	3.4	85	66.0	2.48	26.6	3.7
36	57.0	2.65	21.5	3.4	86	87.0	2.58	33.7	4.0
37	54.0	2.53	21.4	3.4	87	79.0	2.53	31.3	3.9
38	69.0	2.57	26.9	3.7	88	76.0	2.63	28.9	3.8
39	154.0	2.61	59.0	4.8	89	99.0	2.61	38.0	4.2
40	106.0	2.59	41.0	4.3	90	90.0	2.55	35.2	4.1
41	59.0	2.55	23.2	3.5	91	101.0	2.79	36.2	4.1
42	81.0	2.86	28.4	3.8	92	130.0	2.63	49.4	4.6
43	126.0	2.53	49.8	4.6	93	86.0	2.66	32.4	4.0
44	71.0	2.59	27.4	3.7	94	94.0	2.63	35.8	4.1
45	120.0	2.63	45.7	4.4	95	158.0	2.53	62.4	4.9
46	58.0	2.54	22.9	3.5	96	103.0	2.62	39.4	4.2
47	118.0	2.56	46.1	4.4	97	97.0	2.53	38.4	4.2
48	52.0	2.60	20.0	3.4	98	120.0	2.58	46.6	4.5
49	63.0	2.56	24.6	3.6	99	65.0	2.51	25.9	3.7
50	58.0	2.52	23.1	3.5	100	115.0	2.61	44.0	4.4

A.2: XMT Volumetric and Surface Mineral Composition

Pebble ID	XMT mineral volume %	Total volume (mm^3)	XMT mineral surface area %	Total area (mm^2)
18	1.1	36104.0	1.1	5602.0
19	4.0	20234.7	2.5	3872.2
23	0.7	17835.2	1.4	3285.7
59	0.1	26926.8	0.5	5001.7
68	7.2	45051.2	13.9	6143.8
102	1.5	43831.9	2.0	6244.1
121	0.1	34635.9	0.2	4959.3
132	0.2	22122.9	0.5	4218.3
133	0.0	41108.2	0.0	6335.4
144	0.3	21758.5	0.5	3902.2
146	0.2	21923.5	0.4	3799.7
161	1.4	26823.8	1.7	4518.4
168	0.1	29974.3	0.2	5107.8
183	0.2	26591.9	0.7	4256.3
192	0.3	19006.4	0.3	3245.2
198	0.0	26903.6	0.0	5080.9
202	0.9	20221.4	1.3	3581.9
239	0.8	42439.4	0.9	5730.9
249	0.6	22289.6	1.0	3792.4
285	0.3	21224.3	0.4	3613.1
287	0.7	20109.7	0.7	3555.4
335	2.4	42504.7	6.8	6049.7
358	2.0	21422.7	2.1	5597.7
361	0.5	37018.7	1.2	6022.1
363	0.2	25944.9	0.6	4390.5
364	0.5	25553.4	1.0	4409.0
387	0.3	25109.8	2.8	4163.4
396	0.6	32057.7	1.5	4539.1
436	0.6	19944.4	1.2	4105.5
440	5.0	36095.2	6.3	5432.2
447	1.5	22852.4	2.4	3993.5
474	1.8	24105.6	1.9	4601.3
482	0.5	19232.6	0.7	3597.4
496	0.9	25768.0	1.1	3970.3

A.3: XRF Results

Pebble Number	Cu	Fe	S	Si	Al	Pebble Number	Cu	Fe	S	Si	Al
1	0.31	0.15	1.05	32.83	11.57	51	1.63	4.14	0.82	15.20	2.99
2	0.53	10.84	9.61	30.35	2.51	52	0.07	0.49	0.65	14.63	1.80
3	0.07	1.03	0.31	26.05	9.26	53	1.38	1.71	1.38	11.20	1.61
4	0.09	1.58	0.97	21.95	4.74	54	0.20	1.51	0.72	13.55	2.11
5	0.10	1.77	0.43	29.00	8.01	55	0.21	0.02	0.71	14.26	1.63
6	0.91	3.37	2.83	29.87	8.22	56	0.58	0.29	0.68	14.70	2.44
7	0.23	1.30	0.40	33.81	10.88	57	0.27	0.71	0.88	26.51	7.02
8	0.05	0.00	0.76	36.11	8.49	58	0.10	0.87	0.39	17.62	3.32
9	0.88	0.89	2.15	36.58	10.92	59	2.17	3.96	2.91	11.80	1.75
10	0.63	0.81	2.21	34.09	10.86	60	0.97	6.64	2.36	19.56	3.62
11	0.57	0.89	1.92	32.39	11.03	61	0.10	0.24	0.86	15.82	2.79
12	0.93	1.12	2.25	29.30	9.36	62	0.10	2.39	0.44	16.51	3.50
13	0.97	8.98	1.69	19.07	3.32	63	0.23	0.36	1.29	29.30	7.63
14	0.08	14.06	1.54	30.97	9.28	64	0.19	2.12	0.78	30.87	9.95
15	0.62	8.88	0.95	17.36	4.63	65	1.02	9.11	8.43	16.63	3.78
16	0.47	0.11	1.26	32.29	11.34	66	0.59	1.44	1.60	28.27	8.81
17	0.27	1.30	0.73	18.19	2.54	67	0.20	0.00	0.64	13.20	1.58
18	0.30	0.59	1.86	30.93	10.36	68	0.48	1.01	0.37	12.97	1.95
19	1.08	2.79	2.48	29.16	8.98	69	0.90	2.56	1.16	29.96	6.23
20	0.16	2.40	0.73	20.16	3.92	70	1.01	8.98	8.34	21.40	7.70
21	0.31	0.14	0.80	28.33	6.68	71	0.63	0.25	1.34	29.57	6.05
22	0.22	0.82	0.36	31.76	11.66	72	0.89	2.94	1.37	14.23	2.52
23	0.11	0.29	0.70	30.77	10.51	73	0.51	4.68	3.05	20.08	4.26
24	0.28	0.34	0.72	30.99	8.34	74	0.21	0.73	0.49	28.83	8.07
25	0.14	0.14	0.72	35.21	10.11	75	0.49	0.61	1.47	27.62	8.02
26	0.88	10.89	1.47	15.46	2.80	76	0.45	0.95	0.68	14.36	2.51
27	0.07	0.82	1.04	33.83	9.52	77	0.05	0.00	0.32	31.53	10.46
28	0.13	0.17	0.77	29.11	7.26	78	0.27	3.21	0.27	20.10	4.77
29	0.11	3.17	2.66	34.94	9.84	79	0.60	2.53	1.14	22.14	3.72
30	0.07	0.79	0.36	33.68	11.36	80	0.50	2.04	3.12	24.35	8.49
31	1.37	4.29	5.27	26.37	9.39	81	0.14	2.60	0.15	17.81	4.22
32	0.30	12.16	0.33	23.93	6.96	82	0.30	1.33	2.64	35.68	8.97
33	0.09	0.12	0.71	35.15	10.80	83	0.83	5.42	2.05	26.52	8.41
34	0.30	0.95	1.08	28.63	10.43	84	0.22	0.37	0.93	31.32	10.79
35	0.17	2.88	4.51	32.40	8.53	85	0.27	0.04	1.01	30.81	7.10
36	0.31	1.81	0.28	14.55	2.31	86	0.23	0.95	0.80	31.85	9.11
37	0.06	0.24	0.88	33.03	11.07	87	0.19	3.57	0.43	18.91	4.05
38	0.07	0.07	0.63	30.57	7.98	88	0.54	0.40	1.45	33.96	11.53
39	0.12	0.09	0.55	16.62	2.06	89	0.59	0.11	0.66	30.44	7.81
40	0.05	0.57	0.48	18.18	2.57	90	0.29	1.95	0.69	19.01	4.19
41	0.09	0.99	0.46	20.90	3.43	91	0.88	5.57	1.87	16.76	3.20
42	0.14	3.42	1.73	20.61	4.41	92	0.67	0.88	0.90	27.94	9.56
43	0.58	1.01	0.69	19.86	3.18	93	0.64	2.08	2.35	32.59	8.15
44	0.25	1.72	1.02	21.87	4.92	94	0.16	1.32	2.36	27.38	13.02
45	0.22	3.70	0.55	18.14	4.54	95	0.50	1.45	1.00	28.19	7.30
46	0.16	0.31	0.97	31.57	9.84	96	0.51	5.16	0.46	22.05	8.80
47	0.54	1.28	0.75	18.97	2.33	97	0.30	0.33	1.16	31.04	7.96
48	0.99	3.83	5.62	28.73	11.88	98	0.51	1.88	1.30	16.78	3.27
49	0.21	1.64	1.13	32.37	11.80	99	0.72	1.27	1.81	30.34	11.72
50	0.23	0.27	0.54	13.59	1.58	100	0.09	0.03	0.56	36.15	10.99

Appendix B: Intrinsic Sortability +40 mm and -40 mm Sized Fractions

B.1: +40 mm Intrinsic Sortability

Product	Mass %	Cu Grade %	Cu Distribution %
Test 1 Feed	100.0	0.4	100.0
Conc. 1	9.6	1.5	32.6
Test 2 Feed	90.4	0.3	67.4
Conc. 2	3.7	0.9	7.6
Test 3 Feed	86.7	0.3	59.8
Conc. 3	6.7	0.6	9.9
Test 4 Feed	80.0	0.3	49.8
Conc. 4	23.4	0.5	28.5
Test 5 Feed	56.6	0.2	21.4
Conc. 5	24.0	0.2	13.3
Discard	32.7	0.1	8.0
Threshold Cu	Cumulative %		
%	Cu Recovery	Conc. Grade Cu	Mass Rejected
1.0	32.6	1.46	90.4
0.8	40.2	1.30	86.7
0.6	50.2	1.08	80.0
0.4	78.6	0.78	56.6
0.2	92.0	0.59	32.7

B.1: -40 mm Intrinsic Sortability

Product	Mass %	Cu Grade %	Cu Distribution %
Test 1 Feed	100.0	0.5	100.0
Conc. 1	5.2	1.4	15.4
Test 2 Feed	94.8	0.4	84.6
Conc. 2	17.6	0.9	35.0
Test 3 Feed	77.2	0.3	49.6
Conc. 3	7.2	0.6	10.2
Test 4 Feed	70.0	0.3	39.4
Conc. 4	13.5	0.5	15.5
Test 5 Feed	56.5	0.2	23.9
Conc. 5	29.0	0.3	17.1
Discard	27.4	0.1	6.8
Threshold Cu	Cumulative %		
%	Cu Recovery	Conc. Grade Cu	Mass Rejected
1.0	15.4	1.35	94.8
0.8	50.4	1.02	77.2
0.6	60.6	0.93	70.0
0.4	76.1	0.80	56.5
0.2	93.2	0.59	27.4

Appendix C: Ore Sorting Sensor Response Data

Pebble Number	Sensor data								
	Rados XRF (Calc. Cu %)	Tomra XRF (CPA Cu)	Tomra XRT (% high density)	Tomra NIR (Cu Index)	Tomra EM (Mag.Susc.)	Tomra Optical (% colour)			
						Black	Grey	Brown	White
1	0.44	0.0002	2.3	0.1	0.0	8.6	80.1	1.5	9.7
2	0.19	0.0003	77.6	1.2	10.0	48.0	49.1	0.0	2.9
3	0.31	0.0000	6.9	0.3	0.0	8.2	76.6	0.1	15.0
4	0.29	0.0000	7.6	0.2	0.0	22.8	60.3	1.8	15.1
5	0.63	0.0001	3.9	0.3	0.0	1.3	42.4	0.0	56.3
6	0.00	0.0013	22.1	1.0	0.0	41.1	54.9	0.5	3.3
7	0.22	0.0007	10.4	0.3	0.0	16.4	51.4	3.3	28.8
8	0.96	0.0000	2.4	0.9	0.0	0.9	33.3	0.0	65.8
9	0.46	0.0011	14.5	1.3	0.0	9.4	82.9	0.0	7.6
10	0.44	0.0014	12.0	-0.1	0.0	16.0	77.0	3.8	3.1
11	0.90	0.0003	4.3	-0.2	0.0	15.5	75.2	0.4	8.9
12	0.59	0.0012	10.2	-0.1	0.0	29.4	69.3	0.2	1.1
13	0.29	0.0002	22.1	1.9	0.0	92.9	5.3	1.4	0.0
14	0.16	0.0000	49.4	-0.7	0.0	7.5	78.7	0.1	13.7
15	0.15	0.0004	22.6	1.0	8.0	23.8	48.6	20.0	7.5
16	0.84	0.0003	3.9	0.8	0.0	2.5	62.1	0.0	35.4
17	0.19	0.0000	1.7	-0.3	3.0	15.9	75.5	6.3	2.3
18	0.30	0.0002	4.1	0.1	0.0	1.8	78.3	0.0	19.9
19	1.22	0.0003	5.4	0.5	0.0	43.7	55.4	0.1	0.9
20	0.34	0.0002	4.8	-0.1	0.0	3.5	57.9	0.0	38.6
21	0.35	0.0001	2.0	0.5	0.0	4.0	63.3	0.1	32.6
22	0.23	0.0000	7.0	0.6	0.0	23.0	66.1	0.6	10.4
23	0.14	0.0001	5.5	-0.4	0.0	2.5	68.9	2.0	26.6
24	0.15	0.0000	2.8	0.8	0.0	14.8	77.9	0.6	6.7
25	0.18	0.0000	4.1	0.7	0.0	16.7	81.0	0.0	2.3
26	0.48	0.0015	73.2	0.4	9.5	84.5	14.6	0.7	0.2
27	0.10	0.0000	3.2	0.6	0.0	4.8	78.3	0.8	16.1
28	0.24	0.0000	3.3	0.8	0.0	8.1	71.3	9.4	11.2
29	0.10	0.0000	6.4	0.5	0.0	26.3	62.4	1.1	10.1
30	0.20	0.0000	7.0	0.9	0.0	9.3	78.3	0.4	12.0
31	0.19	0.0032	44.7	2.2	0.0	8.4	76.5	3.5	11.6
32	0.60	0.0008	4.0	0.1	0.0	13.9	63.4	0.1	22.6
33	0.16	0.0000	2.4	0.4	0.0	4.6	75.9	1.1	18.4
34	0.31	0.0009	9.3	-0.7	0.0	2.1	59.2	0.0	38.7
35	0.35	0.0001	9.4	-0.2	0.0	29.4	69.4	0.0	1.1
36	5.04	0.0006	12.7	0.5	0.0	40.2	51.8	0.8	7.3
37	0.30	0.0000	3.8	0.4	0.0	2.0	67.4	0.7	29.9
38	0.16	0.0000	7.6	1.1	0.0	7.6	79.1	0.2	13.0
39	0.24	0.0000	3.3	0.5	0.0	9.7	85.7	0.3	4.3
40	0.19	0.0000	6.6	-0.3	0.0	9.7	87.2	0.0	3.1

Appendix C (continued): Ore Sorting Sensor Response Data

Pebble Number	Sensor data								
	Rados XRF (Calc. Cu %)	Tomra XRF (CPA Cu)	Tomra XRT (% high density)	Tomra NIR (Cu Index)	Tomra EM (Mag.Susc.)	Tomra Optical (% colour)			
						Black	Grey	Brown	White
41	0.18	0.0000	4.8	0.0	0.0	4.2	63.6	14.9	17.4
42	0.14	0.0001	26.3	0.0	0.0	26.8	69.6	2.5	1.1
43	0.27	0.0021	10.4	0.8	3.5	3.9	74.1	0.2	21.8
44	0.61	0.0003	4.8	-0.1	0.0	3.0	87.6	0.0	9.4
45	0.04	0.0003	7.5	0.6	0.0	33.5	58.1	8.0	0.5
46	0.41	0.0003	4.9	0.6	0.0	2.0	54.2	2.0	41.8
47	0.19	0.0010	3.2	1.0	0.0	21.1	74.4	2.9	1.5
48	0.53	0.0017	7.6	-0.9	0.0	1.5	75.4	0.0	23.2
49	0.78	0.0001	10.6	0.8	0.0	7.0	72.7	8.4	11.9
50	0.46	0.0007	3.4	0.2	0.0	3.2	56.8	0.9	39.1
51	2.47	0.0031	25.4	0.0	0.0	24.7	17.6	56.9	0.8
52	1.44	0.0000	9.6	0.0	0.0	12.6	79.2	3.5	4.8
53	0.23	0.0030	10.7	0.8	0.0	17.2	50.7	29.1	3.1
54	1.06	0.0003	10.6	0.4	0.0	32.2	52.4	14.0	1.4
55	1.09	0.0009	3.6	0.8	0.0	0.7	34.8	0.0	64.5
56	0.41	0.0008	5.4	0.3	0.0	1.5	86.8	0.0	11.7
57	0.32	0.0003	2.6	-0.3	0.0	7.0	79.3	0.6	13.1
58	0.10	0.0000	1.6	0.2	0.0	0.9	39.3	2.3	57.5
59	1.05	0.0003	6.7	0.9	0.0	39.4	56.4	1.1	3.1
60	1.06	0.0018	32.0	2.1	0.0	17.8	63.4	15.3	3.5
61	0.27	0.0000	4.4	-0.2	0.0	6.9	73.7	5.4	13.9
62	0.18	0.0000	12.1	0.1	10.0	5.4	76.9	0.5	17.2
63	0.27	0.0001	2.7	0.5	0.0	1.1	70.9	1.9	26.1
64	0.15	0.0001	23.1	0.6	10.0	6.1	79.7	0.0	14.2
65	0.21	0.0017	41.7	-0.2	16.0	4.8	78.7	1.2	15.3
66	0.55	0.0012	16.0	0.2	0.0	18.7	78.3	0.0	3.0
67	0.34	0.0003	1.0	1.2	0.0	0.7	57.5	0.0	41.8
68	0.22	0.0013	6.5	0.5	0.0	5.9	43.7	0.0	50.3
69	0.78	0.0023	11.7	1.3	0.0	65.6	30.9	0.0	3.5
70	0.76	0.0019	73.3	0.9	0.0	49.0	44.5	5.3	1.3
71	0.60	0.0021	9.3	0.8	0.0	5.1	78.8	0.7	15.3
72	0.30	0.0005	12.0	-0.5	0.0	35.1	61.7	2.3	1.0
73	1.60	0.0005	35.6	0.6	0.0	16.2	80.8	0.1	2.9
74	0.57	0.0006	9.0	0.8	10.0	9.8	83.9	1.5	4.8
75	0.23	0.0006	4.5	0.4	0.0	28.3	68.6	2.8	0.3
76	0.43	0.0002	2.8	-0.3	0.0	5.7	59.7	3.2	31.4
77	0.15	0.0000	3.4	0.2	0.0	0.5	42.7	0.0	56.8
78	0.28	0.0005	9.3	1.0	0.0	9.7	62.3	0.1	27.8
79	0.67	0.0014	7.4	0.0	0.0	52.7	41.9	5.0	0.4
80	0.98	0.0017	9.9	0.5	0.0	36.5	60.0	1.0	2.4

Appendix C (continued): Ore Sorting Sensor Response Data

Pebble Number	Sensor data								
	Rados XRF (Calc. Cu %)	Tomra XRF (CPA Cu)	Tomra XRT (% high density)	Tomra NIR (Cu Index)	Tomra EM (Mag.Susc.)	Tomra Optical (% colour)			
						Black	Grey	Brown	White
81	0.14	0.0001	11.9	0.5	11.0	42.0	52.3	2.6	3.0
82	0.32	0.0010	3.8	-0.3	0.0	0.9	83.0	0.2	15.9
83	1.62	0.0008	33.6	0.5	0.0	81.7	15.0	2.9	0.4
84	0.30	0.0002	4.5	-0.4	0.0	8.5	81.7	1.2	8.6
85	0.29	0.0002	3.9	0.9	0.0	1.0	62.9	2.1	34.0
86	0.09	0.0000	4.9	0.5	0.0	3.4	88.1	0.1	8.4
87	0.52	0.0009	17.6	-0.1	0.0	6.3	76.4	0.2	17.0
88	0.53	0.0006	5.7	-0.7	0.0	12.4	79.2	1.8	6.6
89	0.62	0.0017	7.8	0.5	0.0	11.9	71.5	0.1	16.4
90	0.11	0.0000	8.3	0.4	0.0	8.4	64.1	20.4	7.1
91	0.90	0.0023	47.6	0.4	0.0	10.9	81.8	1.1	6.2
92	0.53	0.0025	9.4	-0.2	0.0	60.8	35.4	2.8	1.0
93	0.46	0.0015	12.9	1.4	0.0	30.5	54.8	0.8	14.0
94	0.35	0.0000	10.9	0.7	0.0	1.2	52.8	5.6	40.5
95	0.87	0.0007	4.1	1.0	0.0	6.1	55.3	0.0	38.6
96	0.77	0.0008	10.1	0.9	0.0	40.9	53.5	1.6	4.1
97	0.53	0.0001	1.8	0.5	0.0	6.5	71.4	0.5	21.7
98	0.19	0.0000	0.9	0.4	0.0	11.6	73.2	11.5	3.7
99	0.73	0.0013	7.7	0.4	0.0	9.4	56.1	32.3	2.1
100	0.21	0.0000	2.0	0.3	0.0	6.3	82.4	2.1	9.2

Appendix D: Economic Impact for the Laboratory-Scale Sensor Sortability Tests

D.1: Economic Impact based on the Ideal XRF Sortability Tests

Cost/ operational data	Baseline - No sorting	XRF sensor thresholds (CPA Cu)				
		>=0.0004 <0.0008	>=0.0008 <0.0012	>=0.0012 <0.0015	>=0.0015 <0.0020	>=0.0020
Mill						
ROM feed (tph)	3000	3230	3412	3469	3513	3549
Pebble circuit SAG feed (tph)	600	370	188	131	87	51
Total SAG feed (tph)	3600	3600	3600	3600	3600	3600
SAG screen oversize (%)	20	20	20	20	20	20
Oversize to pebble circuit (tph)	300	300	300	300	300	300
Undersize to Sag (tph)	3000	3000	3000	3000	3000	3000
Pebble circuit						
Sorter Feed (tph)		600	600	600	600	600
Sorter Rejection as waste (%)		38	69	78	85	92
Waste (tph)		230	412	469	513	549
Pebble (tph)	600	370	188	131	87	51
Crusher feed (tph)	600	370	188	131	87	51
Operating data						
Feed grade to flotation (%Cu)	0.76	0.79	0.80	0.80	0.80	0.80
Pebble feed to SAG grade (%Cu)	0.44	0.62	0.72	0.84	0.91	0.95
Circuit recovery (%)	80	80	80	80	80	80
Sorter waste grade (%Cu)		0.16	0.32	0.33	0.36	0.39
Value of Cu conc ($/ ton Cu)	4441	4441	4441	4441	4441	4441
Additional Cu in feed (t/day)		43	79	90	99	106
Additional Cu in waste (t/day)		9	32	37	44	51
Additional Cu recovered (t/day)		28	38	42	44	44
Additional Cu revenue ($/day)		122708	167431	188699	193644	193199
Cu value in waste ($/day)		31396	112534	132088	157330	182630
Operating costs						
Mining costs ($/t)	3	3	3	3	3	3
Mining costs ($/day)		16571	29698	33802	36906	39546
Waste disposal cost ($/t)	1	1	1	1	1	1
Waste disposal cost ($/day)		5524	9899	11267	12302	13182
Milling cost ($/t)	4	4	4	4	4	4
Milling cost ($/day)		0	0	0	0	0
Sorting cost ($/t)		2	2	2	2	2
Sorting cost ($/day)		11047	19799	22535	24604	26364
Additional Cu revenue ($/day)		122708	167431	188699	193644	193199
Total additional costs ($/day)		33142	59396	67604	73813	79092
Additional Profit						
Additional profit ($/day)		58169	-4499	-10994	-37498	-68522
Additional profit ($/year)		21246202	-1643271	-4015568	-13696325	-25027602

D.2: Economic Impact based on the Ideal XRT Sortability Tests

Cost/ operational data	Baseline - No sorting	XRT sensor thresholds (% high density)				
		3-5 %	5-10 %	10-20 %	20-30 %	>30%
Mill						
ROM feed (tph)	3000	3085	3234	3392	3495	3532
Pebble circuit SAG feed (tph)	600	515	366	208	105	68
Total SAG feed (tph)	3600	3600	3600	3600	3600	3600
SAG screen oversize (%)	20	20	20	20	20	20
Oversize to pebble circuit (tph)	300	300	300	300	300	300
Undersize to Sag (tph)	3000	3000	3000	3000	3000	3000
Pebble circuit						
Sorter Feed (tph)		600	600	600	600	600
Sorter Rejection as waste (%)		14	39	65	82	89
Waste (tph)		85	234	392	495	532
Pebble (tph)	600	515	366	208	105	68
Crusher feed (tph)	600	515	366	208	105	68
Operating data						
Feed grade to flotation (%Cu)	0.76	0.77	0.78	0.79	0.80	0.80
Pebble feed to SAG grade (%Cu)	0.44	0.47	0.56	0.61	0.74	0.81
Circuit recovery (%)	80	80	80	80	80	80
Sorter waste grade (%Cu)		0.25	0.26	0.35	0.38	0.39
Value of Cu conc ($/ ton Cu)	4441	4441	4441	4441	4441	4441
Additional Cu in feed (t/day)		16	44	74	95	102
Additional Cu in waste (t/day)		5	15	33	45	50
Additional Cu recovered (t/day)		8	23	33	40	42
Additional Cu revenue ($/day)		37527	104174	147530	176476	185966
Cu value in waste ($/day)		18024	51850	116952	160289	176812
Operating costs						
Mining costs ($/t)	3	3	3	3	3	3
Mining costs ($/day)		6089	16841	28218	35622	38286
Waste disposal cost ($/t)	1	1	1	1	1	1
Waste disposal cost ($/day)		2030	5614	9406	11874	12762
Milling cost ($/t)	4	4	4	4	4	4
Milling cost ($/day)		0	0	0	0	0
Sorting cost ($/t)		2	2	2	2	2
Sorting cost ($/day)		4059	11227	18812	23748	25524
Additional Cu revenue ($/day)		37527	104174	147530	176476	185966
Total additional costs ($/day)		12177	33682	56437	71244	76572
Additional Profit						
Additional profit ($/day)		7325	18642	-25859	-55057	-67418
Additional profit ($/year)		2675542	6809019	-9445041	-20109540	-24624422

D.3: Economic Impact based on the Industrial-Scale XRF Sortability Tests

Cost/ operational data	Baseline - No sorting	XRF Cu% (Cut-off grade % Cu)				
		0.20	0.40	0.60	0.80	1.00
Mill						
ROM feed (tph)	3000	3170	3349	3439	3499	3540
Pebble circuit SAG feed (tph)	600	430	251	161	101	60
Total SAG feed (tph)	3600	3600	3600	3600	3600	3600
SAG screen oversize (%)	20	20	20	20	20	20
Oversize to pebble circuit (tph)	300	300	300	300	300	300
Undersize to Sag (tph)	3000	3000	3000	3000	3000	3000
Pebble circuit						
Sorter Feed (tph)		600	600	600	600	600
Sorter Rejection as waste (%)		28	58	73	83	90
Waste (tph)		170	349	439	499	540
Pebble (tph)	600	430	251	161	101	60
Crusher feed (tph)	600	430	251	161	101	60
Operating data						
Feed grade to flotation (%Cu)	0.80	0.78	0.79	0.79	0.80	0.80
Pebble feed to SAG grade (%Cu)	0.44	0.49	0.60	0.64	0.71	0.82
Circuit recovery (%)	80	80	80	80	80	80
Sorter waste grade (%Cu)		0.31	0.33	0.37	0.39	0.40
Value of Cu conc ($/ ton Cu)	4441	4441	4441	4441	4441	4441
Additional Cu in feed (t/day)		32	66	84	95	104
Additional Cu in waste (t/day)		13	28	39	47	52
Additional Cu recovered (t/day)		15	31	36	39	41
Additional Cu revenue ($/day)		67444	136812	158743	173374	184234
Cu value in waste ($/day)		44847	98282	138454	165829	184077
Operating costs						
Mining costs ($/t)	3	3	3	3	3	3
Mining costs ($/day)		12217	25151	31601	35908	38863
Waste disposal cost ($/t)	1	1	1	1	1	1
Waste disposal cost ($/day)		4072	8384	10534	11969	12954
Milling cost ($/t)	4	4	4	4	4	4
Milling cost ($/day)		0	0	0	0	0
Sorting cost ($/t)		2	2	2	2	2
Sorting cost ($/day)		8145	16767	21067	23939	25908
Additional Cu revenue ($/day)		67444	136812	158743	173374	184234
Total additional costs ($/day)		24434	50302	63202	71816	77725
Additional Profit						
Additional profit ($/day)		-1837	-11772	-42912	-64270	-77568
Additional profit ($/year)		-670889	-4299887	-15673748	-23474682	-28331582